1-1-2007

A quasi-2D finite element formulation of active constrained-layer functionally graded beam

Elena Miroshnichenko
Ryerson University

A QUASI-2D FINITE ELEMENT FORMULATION OF ACTIVE CONSTRAINED-LAYER FUNCTIONALLY GRADED BEAM

BY

ELENA MIROSHNICHENKO
B.ENG (AEROSPACE ENGINEERING),
RYERSON UNIVERSITY (CANADA), 2005.

A THESIS
PRESENTED TO RYERSON UNIVERSITY

IN PARTIAL FULFILMENT OF THE
REQUIREMENTS FOR THE DEGREE OF
MASTER OF APPLIED SCIENCE
IN THE PROGRAM OF
MECHANICAL ENGINEERING

TORONTO, ONTARIO, CANADA, 2007

Author's Declaration

I hereby declare that I am the sole author of this thesis.

I authorize Ryerson University to lend this thesis to other institutions or individuals for the purpose of scholarly research.

Elena Miroshnichenko

I further authorize Ryerson University to reproduce this thesis by photocopying or by other means, in total or in part, at the request of other institutions or individuals for the purpose of scholarly research.

Elena Miroshnichenko

Abstract

A QUASI-2D FINITE ELEMENT FORMULATION OF ACTIVE CONSTRAINED-LAYER FUNCTIONALLY GRADED BEAM

© Elena Miroshnichenko, 2007

Master of Applied Science

in the program of

Mechanical Engineering

Ryerson University

A functionally graded (FG) beam with an active constrained-layer damping (ACLD) treatment is modeled and analyzed. ACLD consists of a passive element, in the form of a viscoelastic layer bonded to the host structure, and an active constraining element which is represented by a piezoelectric fiber-reinforced composite (PFRC) laminate. It is assumed in the current formulation that the field variables are expressible as polynomials through the thickness of the beam and are cubically interpolated across the span. Hamilton's principle is used in the derivation of the equations of motion, which are solved using the Newmark time-integration method. The versatility of the formulation is demonstrated using different support mechanisms in the form of analysis of cantilevered, fixed-end partially-constrained and simply-supported beam cases. The effects of ply orientation in the PFRC laminate and varying elastic modulus in the FG beam are also examined.

Acknowledgements

I would like to express my sincere appreciation to my supervisor, Dr. Donatus Oguamanam, for all his guidance, support, and insight throughout my studies. Dr. Oguamanam, you helped me find the right path as you were the first professor who triggered my interest in structural mechanics and I am grateful to you for that.

Furthermore, I would like to thank my family and friends for being extremely patient with me during my thesis work. Your understanding, encouragement and support are greatly appreciated and will always be remembered. Special gratitude goes to my boyfriend, Drew, without whom I would not be able to accomplish this work in the first place.

Table of Contents

List of Figures

List of Tables

Nomenclature

VARIABLE	DEFINITION	UNITS
L	Length of host beam	m
b	Width of composite beam	m
h	Height of composite beam	m
h_i	Thickness coordinate	m
$()_b$	FGM beam subscript	--
$()_c$	Viscoelastic core subscript	--
$()_p$	PFRC laminate subscript	--
$\rho_{b,c,p}$	Density	$\mathrm{kg/m^3}$
v	Poisson's ratio	--
E	Young's modulus of elasticity	Pa
x, z	Beam coordinates	--
t	Temporal variable	s
Q	Elastic matrix	Pa
$\bar{Q}_p$	Top layer transformed matrix	Pa
$\tilde{Q}_p$	Top layer reduced matrix	Pa
C	Elastic stiffness matrix	Pa
$\tilde{C}_c$	Anelastic stiffness matrix	Pa
c_{ij}	Effective elastic coefficients	Pa
e_{ij}	Piezoelectric constants	$\mathrm{C/m^2}$
d_{ij}	Dielectric permittivity	F/m
D	Operator matrix	--
λ	Functional material gradient	$\mathrm{m^{-1}}$
α	Fractional derivative order	--

τ	Relaxation time	s
ω	Natural frequency	s^{-1}
E_0	Static elastic modulus	Pa
E_∞	Dynamic elastic modulus	Pa
$u_{b,c,p}$	Displacement vector	m
$\bar{u}_{b,c,p}$	Local displacement vector	m
$\hat{(\ )}$	Electrical component	--
$\tilde{(\ )}$	Viscoelastic component	--
I	Moment of inertia	m^2
k_s	Shear correction factor	--
$\varepsilon_i, \gamma_{ij}$	Strains	--
$\varepsilon_{b,c,p}$	Strain vectors	--
$\tilde{\varepsilon}_c$	Core anelastic strain vector	--
σ_i, τ_{ij}	Normal stress, shear stress	Pa
$\bar{\sigma}_c$	Core anelastic stress	Pa
V	Voltage	V
ψ	Electrical potential	V
E_z	Electrical field	V/m
D_z	Electrical displacement field	C/m^2
k	Ply number	--
θ	Ply orientation angle	deg
T_k	Transformation matrix	--
Δt	Time step	s
$u(x,z,t)$	Axial displacement	m
$w(x,z,t)$	Transverse displacement	m
$\tilde{u}_c$	Anelastic displacement vector	m

q_e	Element displacement vector	m
M	Mass matrix	kg
K	Stiffness matrix	N / m
K_c	Core elastic stiffness matrix	N / m
$\tilde{K}_c$	Core anelastic stiffness matrix	N / m
A_{ij}	Extensional stiffness component	N / m
B_{ij}	Coupling stiffness component	N m / m
D_{ij}	Bending stiffness component	N m
N_x^p	Electrical force resultant component	N / m
M_x^p	Electrical moment resultant component	N m / m
ξ	Local coordinate	--
N_j	Shape functions	--
J	Jacobian	--
$a_i, l_i, c_i, m_i, e_i, n_i$	Displacement field coefficients	--
δ	Variation function	--
T	Kinetic energy	J
U	Strain energy	J
$\tilde{U}_c$	Anelastic strain energy	J
W	Work	J
$\tilde{W}_c$	Work due to anelastic force	J
F	Force vector	N

Chapter 1 Introduction

Mechanical vibration and noise reduction is a crucial issue in many engineering systems, ranging from simple mechanism such as automobile parts to large-scale structures such as airplanes and spacecrafts. It is especially a concern in lightweight structures, wherein weight addition is not an option for suppressing vibration. Successful reduction of noise and vibration results in a higher performance and durability of the machines and structures, as well as creating an improved living/working environment.

A considerable amount of research has been done over the years with regard to the modeling and control of lightweight composite structures [1-3]. One of the most widely used conventional methods for suppressing vibrations and noise involves the addition of damping by bonding a viscoelastic layer to the host structure. This technique can be enhanced by the addition of an active element in the form of a piezoelectric material attached to the structure. The resulting configuration is known as 'smart' or 'intelligent' structure and it is emerging as a promising active-damping technique.

Direct and inverse effects of the piezoelectric materials allow them to be used in structural applications as sensors and actuators, respectively. The analysis of such structures requires accurate modeling that takes into account the electromechanical coupling of the structure. As observed by Stanway et al. [1], piezoelectric sensors and actuators are widely used in vibration and noise control of smart structures because of their excellent frequency characteristics and capability in reciprocal conversion between the electric and mechanical strain energy.

The assumptions which support the classical three-layer theory [4-7] are: 1) the host beam and the constraining layer deform as Euler-Bernoulli beams, that is, plane cross sections remain plane and perpendicular to the deflection curve of the deformed beam, 2) the viscoelastic core behaves as a Timoshenko beam and, consequently, shears, 3) the axial displacement field in each layer is linear through the thickness and the transverse displacement is constant throughout the thickness, 4) the core supports only shear load, 5) perfect bonding exists at the interfaces and no slip occurs between the layers, 6) in-plane inertia effects are ignored, and 7) small-displacement theory is used. To improve the model, one has to consider shear and longitudinal energy contributions of all three layers

and, consequently, allow for shear deformations in the facings and normal direct deformations in the core. The current formulation is based on a Timoshenko beam theory for each layer; however, for sufficiently thin beams it also captures the assumptions of Euler-Bernoulli hypothesis.

The present work extends the use of the quasi-two-dimensional finite element model developed by Bekuit [8] for the vibration analysis. In [8], the author assumed cubic axial deformation and quadratic transverse deformation along the thickness direction of the core only. As in [8], at each node of current formulation, through-the-thickness integration of field variables is carried out analytically, thus reducing what would have been a two-dimensional problem to a one-dimensional finite element procedure. Thereafter, a Gaussian quadrature is used to numerically integrate over the span for each element. This greatly increases efficiency of the computer program and saves computational time. However, unlike in Bekuit's three-layer model [8], both the host beam and middle layer axial displacements are modeled as cubic functions, while transverse displacements are quadratic functions with respect to z. The top layer employs a linear interpolation of the axial displacements and constant transverse displacement, as is common for the three-layer theory mentioned above. The "quasi" concept follows Nabarrete et al. [9] who developed a quasi-three-dimensional finite element formulation, where in-plane displacement characteristics are modeled after the bicubic trial functions and are interpolated through the thickness.

This thesis is concerned with utilizing the aforementioned active-passive damping technique in a three-layer quasi-two-dimensional finite element beam model. The beam is made of a functionally graded material (FGM). A viscoelastic material is sandwiched between the beam and a piezoelectric fiber-reinforced composite (PFRC) laminate constraining layer. The properties of these materials are discussed in Chapter two. The passive and active methods for controlling noise and vibration are presented in greater detail in the next section. In Chapter three, the mathematical formulation of the current quasi-two-dimensional beam model is presented. This includes the description of the system, kinematic assumptions, and constitutive equations. Chapter four discusses the process of developing a finite element model. The extended Hamilton's principle is used to derive the equation of motion, which is solved using the Newmark time-integration

method. The fifth chapter presents simulation results, and concluding remarks and suggestions for the future work are discussed in Chapter six.

1.1 Active Constrained-Layer Damping (ACLD)

The desire to reduce weight in machines and structures for economic benefits increases the need for vibration control of these structures. Their excitation responses are dominated by resonant modes that occur at low natural frequencies. These low frequency vibrations are difficult to control using conventional technologies, which are mainly passive and effective for high frequency vibration suppression. In these structures, a viscoelastic layer is often bonded to the host structure to increase the dissipation of energy. Viscoelastic materials contain long-chain molecules, which are effective at converting mechanical energy into heat under deformation [1]. When a second layer of metallic material is bonded on top of the viscoelastic layer, then a certain type of treatment is produced and is known as a passive constrained-layer damping (PCLD) treatment [1,2]. Stanway et al. [1] discussed the progression from such treatment to what is now known as active constrained-layer damping (ACLD), where a piezoelectric layer acts as the constraining layer. ACLD treatments significantly increase performance by enabling vibration control at low frequencies. With this upgrade from PCLD to ACLD, vibration control is possible at both the high modes due to the passive element and low modes due to active element. The components of ACLD complement each other in that the active elements allow structures to adapt to a changing environment and remain within weight and size constraints, while the passive elements provide a fail-safe control mechanism [1-3, 10-11]. Furthermore, these performance benefits are achieved without much consequence in terms of cost, weight and complexity.

The passive element, in the form of a viscoelastic damping layer added to one of the surfaces of the host structure, is subjected to both direct and shear strains upon the deformation of the beam. The damping layer is introduced to exploit the ability of one of the strains, mostly shear strain, to dissipate energy at particular areas [1]. The active element involves an actuator, usually in the form of a piezoelectric layer, which can increase the beam's deformation and thus enhance the damping capability of the viscoelastic layer. In [1], Stanway et al. emphasized practical applications in terms of

structural elements utilized in ACLD, other than the most common application to cantilevered beam. They also presented various actuator and sensor configurations that have been investigated by other researchers. The development of some modeling and control techniques were also discussed. Trindade et al. [2] similarly described various hybrid vibration damping treatments, modeling approaches and control algorithms used in the literature. A thorough comparative analysis has been done regarding the different hybrid active-passive damping configurations that already exist in literature. However, the authors presented all configurations known to the research world without distinguishing between the proposed simulated and experimentally investigated options. Balamurugan and Narayanan [3] highlighted the aforementioned advantages of the ACLD treatment in their development of a beam finite element model that has been partially covered with the constrained layer. Further, Gao et al. [10] analyzed a simply-supported beam using enhanced self-sensing ACL treatment that comprises edge elements connected to both host structure and piezoelectric layer for the purpose of transmissibility between actuator and sensor.

1.2 Piezoelectric Element as Actuator and Sensor

An advantage of the piezoelectric element that must be mentioned is its dual nature in being able to act as both an actuator and sensor. A piezoelectric element is able to convert mechanical energy into electrical energy and vice versa. The direct effect is defined as the generation of an electric charge in proportion to an applied force/pressure. The inverse effect, however, is the opposite and induces an expansion (contraction) of the piezoelectric ceramic/polymer under an applied electric field parallel to the polarization direction. Hence, this benefit results in a simplified ACLD configuration due to the piezoelectric element's dual nature as a 'self-sensing' actuator, whereby sensor and actuator are truly collocated, thus removing chances of instability [1, 2, 10].

Another configuration was noted by Stanway et al. [1] and Trindade et al. [2], which consisted only of the elastic beam with the viscoelastic core, the constraining layer in the form of a piezoelectric actuator and the sensor bonded beside the treatment. This results in the reduction of the structure to three layers. An ACLD arrangement that is used in this thesis work closely resembles this configuration presented in both [1] and [2],

where the piezoelectric element acts as an actuator while a sensor/accelerometer provides the input signal to the controller/amplifier of the system, which, in turn, sends the signal to excite the piezoelectric actuator. A schematic of the configuration is shown in **Fig. 1.1** below.

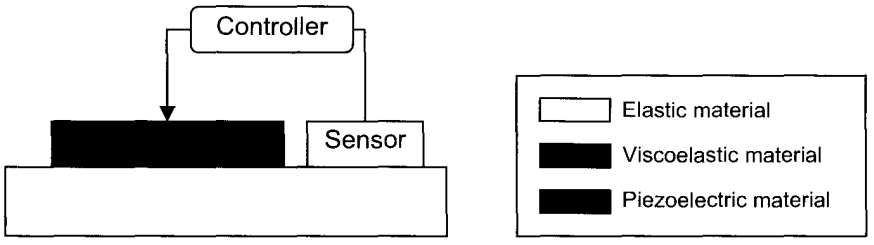

Figure 1.1: ACLD actuator/sensor configuration

Further simplification of this arrangement will result in the sensor/accelerometer being removed and the self-sensing piezoelectric actuator implemented, as was mentioned in the previous paragraph.

Many theoretical models have been proposed to describe the interaction between piezoelectric materials and host structures. Among them, Crawley and de Luis [12] introduced the fundamental concepts of using piezoelectric materials as actuators and sensors in 'intelligent' structures. Their paper also presented static and dynamic models of distributed piezoelectric actuators. From the amount of literature surveyed for this thesis, it is evident that a flurry of research activity continues to go on, validating the concept of intelligent structures, quantifying the effects of piezoelectric sensors and actuators, and analyzing the true feasibility of intelligent structures.

Chapter 2 Materials

As was mentioned in the preceding chapter, the system of interest consists of the host beam, made of FGM, with a bonded viscoelastic layer which is covered with piezoelectric fiber-reinforced composite (PFRC). The use of this combination of materials results in a strong, lightweight structure that is suitable for active control. The following describes each material and its properties.

2.1 Functionally Graded Material (FGM)

FGMs have recently emerged as a new class of materials that exhibit gradual spatial variation of material properties. Unlike laminated composites, they do not possess distinct interfaces across which properties abruptly change. In the case of laminates, the sudden change in properties causes large interlaminar shear stresses, which may give rise to delamination in the structure [13]. Such damage can be avoided if the properties vary smoothly across the thickness, as in the case of FGM.

During the past decade, this class of materials has been investigated by many researchers. Sankar [14], for instance, developed an exact elasticity solution for functionally graded (FG) beams subjected to transverse loads, where Young's modulus was assumed to vary exponentially through the thickness and the Poisson ratio was constant. Euler-Bernoulli beam theory was adapted to FGM beams and compared to the elasticity solutions. This was later extended by Sankar and Tzeng [15] by including a thermal gradient across the thickness of the beam. The authors were able to achieve a reduction in residual thermal stresses when the variation of thermoelastic constants was opposite in direction to that of the temperature distribution.

Ray and Sachade [13, 16] derived the exact solutions for the simply-supported FG plates with integrated layers of PFRC. They also developed a finite element model for the same composite plate. Liew et al. [17] also developed a finite element formulation for static and dynamic analysis and control of FGM plates subjected to a temperature gradient. The authors based their model on a first-order shear deformation theory to actively control FGM plates using distributed piezoelectric sensor/actuator pairs.

In this thesis, the Poisson ratio v is assumed to be constant because the effect of variation of Poisson's ratio on the deformation is much less than that of Young's modulus [18]. However, Young's modulus varies continuously through the thickness of the beam ($z-$axis), i.e., $E = E(z)$, according to the volume fraction of constituents defined by an exponential function. In [18], the exponential function was given as:

$$E(z) = E_2 e^{\lambda(z+h/2)} \tag{2.1}$$

where the functional material gradient is given as $\lambda = \frac{1}{h}\ln(E_1/E_2)$; E_1 and E_2 are the Young's moduli of the bottom ($z = h/2$) and top surfaces ($z = -h/2$) of the FGM plate, respectively; and h is the thickness of the plate.

2.2 *Viscoelastic Material*

As noted in the previous chapter, viscoelastic materials are often incorporated into structures to increase passive damping and largely reduce structural vibrations and noise. There are also a number of techniques associated with modeling a viscoelastic solid, which has a weak frequency dependence on its dynamic properties over an extensive frequency range [19]. Therefore, it is important to accurately describe the frequency dependence of the viscoelastic material. For instance, the frequency band chosen for applying the curve fitting technique of master curves can be the transition band or the region of maximum loss factor [20]. However, to use this technique, a number of additional material parameters are introduced, thus increasing computational effort. Some of the methods suggested for time-domain analysis of viscoelastic structures include the anelastic displacement fields (ADF) and Golla-Hughes-McTavish (GHM) models [3, 20, 21]. The Prony series is a classical time-based technique for fitting creep or relaxation data in the form of exponential functions and is compared to a fractional derivative model in [22]. The fractional derivative model is another time-domain method which is based on fractional calculus. In order to use more traditional Kelvin and Maxwell-based models, more parameters are required to represent viscoelastic material behavior than in the

fractional model [22]. The fractional derivative model, however, is not common in commercial finite element codes which mainly use the Prony series method.

One of the widely used fractional derivative methods is the four-parameter model, a dissipation model based on memory mechanism. Caputo and Mainardi developed the model for hysteretic response of metallic materials by generalizing the integer order derivatives in the standard solid model to fractional order [22]. This method has been successful in describing the weak frequency dependence mentioned above. The only disadvantage associated with using fractional derivative models is the added mathematical complexity of applying fractional calculus. However, it becomes relatively simple once the Fourier transform of the fractional derivative constitutive equation is taken and the expression of the elastic complex modulus in the frequency domain of ω is obtained as [19]:

$$E^*(\omega) = E'(\omega) + iE''(\omega) \tag{2.2}$$

where $E'(\omega)$ and $E''(\omega)$ are the storage and loss moduli, respectively, which can be used to plot and compare master curves to the experimental results.

In the study by Galucio et al. [19], the complex modulus for the one-dimensional model is shown as:

$$E^*(\omega) = \frac{\sigma^*(\omega)}{\varepsilon^*(\omega)} = \frac{E_0 + E_\infty(i\omega\tau)^\alpha}{1 + (i\omega\tau)^\alpha} \tag{2.3}$$

where σ^* and ε^* are the Fourier transforms of $\sigma(t)$ and $\varepsilon(t)$, respectively; E_0 represents the static modulus of elasticity or E^* at $\omega \to 0$; E_∞ is the dynamic modulus or E^* at $\omega \to \infty$; τ is the relaxation time; and α is the fractional derivative order. To satisfy the second law of thermodynamics, conditions such as: $0 < \alpha < 1$, $\tau > 0$ and $E_\infty > E_0$ must hold true.

2.3 *Piezoelectric Fiber-Reinforced Composite (PFRC)*

As mentioned in Chapter one, piezoelectric materials have been widely used as sensors and/or actuators when integrated into a high-performance lightweight smart structure to actively control its vibration. The performance of such structures highly depends on the magnitude of the piezoelectric stress/strain coefficients, which are quite low for the monolithic piezoelectric materials [23, 24]. Therefore, a significant amount of control voltage must be used to achieve a considerable amount of active damping. To avoid this, the piezoelectric stress/strain properties must be modified to further improve the damping characteristics of the smart structures [25]. Piezoelectric composites are effective in improving flexural vibration control if their fibers are orientated longitudinally to render a bending mode of actuators. It is also practical to apply a constant electric field across the thickness of the composite, that is, in a direction transverse to the fiber direction. The schematic diagram of a lamina of PFRC, which depicts a representative volume that includes both fiber and matrix, is shown in **Fig. 2.1** [25].

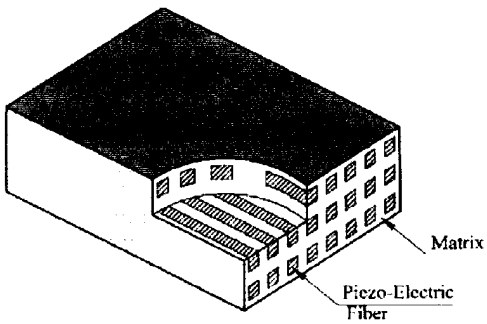

Figure 2.1: Schematic diagram of lamina of PFRC [25]

Recent investigations carried out regarding the implementation of PFRC in the lightweight high-performance flexible structures included the work of Ray and Mallik [23], and Ray and Sachade [16]. The earlier work by Mallik and Ray [25] showed that the effective PFRC coefficients are significantly larger than the corresponding piezoelectric material coefficients. Based on a certain fiber volume fraction, they were able to determine these effective coefficients of PFRC using a micromechanical analysis, which will not be discussed in this thesis. As mentioned previously, the fibers are made of piezoelectric material, which possesses anisotropic properties. In this thesis,

piezoceramics, such as lead-zirconate titanate (PZT), will be used for the role of actuator in the PFRC laminate layer. This material is usually polarized in the thickness direction and exhibits transversely isotropic properties in the *xy*-plane [26].

The authors in [23] developed a finite element model of the smart structure coupled with the patches of ACLD treatment. The active damping performance of PFRC layer has been researched for thin symmetric and anti-symmetric cross-ply, and anti-symmetric angle-ply laminated composite plates. The effect of variation of fiber orientation in the PFRC layer on the damping characteristics has been investigated and the fiber angle for which the control authority of the PFRC layer is maximum has also been determined. In [16], Ray and Sachade derived the exact solutions for the static analysis of FG plates integrated with a layer of PFRC material. They concluded that the activated PFRC layer is more effective in controlling vibration of the plates when it is attached to the surface of the FG plate of minimum stiffness rather than to that of maximum stiffness.

The constitutive equations including the inverse and direct piezoelectric effects of the PFRC layer, respectively, with respect to *xyz* (geometric) coordinates will be used in the following chapter and are given as [27]:

$$\begin{aligned} \{\sigma\}_k &= \left[\bar{Q}\right]_k \{\varepsilon\}_k - \left[\bar{e}\right]_k^T \{E\}_k \\ \{D\}_k &= \left[\bar{e}\right]_k \{\varepsilon\}_k - \left[\bar{d}\right]_k^T \{E\}_k \end{aligned} \tag{2.4}$$

where $\{D\}$, $\{E\}$, $\{\varepsilon\}$ and $\{\sigma\}$ are the electric displacement, electric field, strain and stress vectors, $\left[\bar{Q}\right]$, $\left[\bar{e}\right]$, and $\left[\bar{d}\right]$ are the elastic, piezoelectric and permittivity constant matrices, respectively, and k is the ply order in the laminate.

Chapter 3 Theoretical Formulation

3.1 System Description

The system of interest is a rectangular cross-sectioned three-layer composite beam. The host beam is made of FGM with varying modulus of elasticity. The beam is bonded to a viscoelastic layer, which, in turn, is covered with a PFRC laminate layer, as illustrated in **Fig. 3.1**. The ACLD configuration in this thesis is adopted from the work of Stanway et al. [1] and Trindade et al. [2], as was mentioned in Chapter one. **Fig. 3.1** shows a segment of the span (1) that is fully treated with the active-passive constraining layer and segment (2) which represents only the host beam.

The geometrical parameters of the beam are length L, width b, host beam height h_b, core height h_c, and top layer height h_p. The mid-surface ($z = 0$) of the composite beam structure is at $\frac{h}{2}$ distance away from the bottom of the beam, where $h = h_b + h_c + h_p$. The material properties of each layer are density ρ, Young's modulus of elasticity E, and Poisson's ratio v. The layers are assumed to have perfect bonding at the interfaces, and the adhesive material is thin with infinite stiffness.

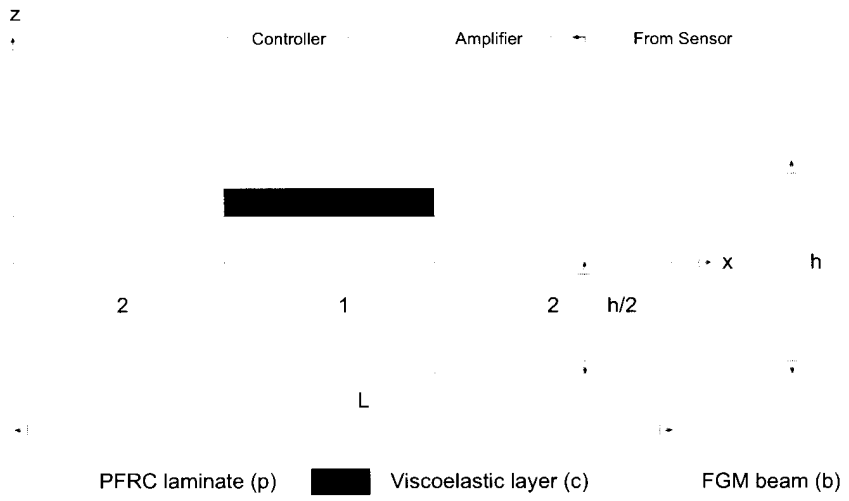

Figure 3.1: Schematic of the composite beam

3.2 FGM Beam (Bottom Layer)

The host beam, also referred to as the bottom layer, consists of the FGM and is identified by the subscript b in the following formulations. The material with varying elastic modulus or FGM was explained in Chapter two.

3.2.1 Kinematic Assumptions

The axial displacement is interpolated through the thickness by a cubic function, while the transverse displacement is quadratically interpolated. The displacement vector u_b is of the following form:

$$u_b = \begin{Bmatrix} u(x,z,t) \\ w(x,z,t) \end{Bmatrix} = \begin{Bmatrix} a_0 + a_1 z + a_2 z^2 + a_3 z^3 \\ l_0 + l_1 z + l_2 z^2 \end{Bmatrix} \tag{3.1}$$

where the coefficients a_0, a_1, a_2, a_3, l_0, l_1 and l_2 are functions of the spatial variable x and temporal variable t. A new vector $\{\overline{u}_b\}^T = \{a_0\ a_1\ a_2\ a_3\ l_0\ l_1\ l_2\}$ is introduced such that:

$$u_b = \begin{bmatrix} 1 & z & z^2 & z^3 & 0 & 0 & 0 \\ 0 & 0 & 0 & 0 & 1 & z & z^2 \end{bmatrix} \begin{Bmatrix} a_0 \\ a_1 \\ a_2 \\ a_3 \\ l_0 \\ l_1 \\ l_2 \end{Bmatrix} \equiv [Z_b]\{\overline{u}_b\} \tag{3.2}$$

Using linear strain-displacement relations [28] yields the following:

$$\begin{cases} \varepsilon_x = \dfrac{\partial u}{\partial x} = a_{0,x} + a_{1,x} z + a_{2,x} z^2 + a_{3,x} z^3 \\ \varepsilon_z = \dfrac{\partial w}{\partial z} = l_1 + 2 l_2 z \\ \gamma_{xz} = \dfrac{\partial u}{\partial z} + \dfrac{\partial w}{\partial x} = a_1 + 2 a_2 z + 3 a_3 z^2 + l_{0,x} + l_{1,x} z + l_{2,x} z^2 \end{cases} \tag{3.3}$$

In a compact matrix notation, the strain vector ε_b can be written as:

$$\varepsilon_b = \begin{Bmatrix} \varepsilon_x \\ \varepsilon_z \\ \gamma_{xz} \end{Bmatrix} = \begin{bmatrix} 0 & 0 & 0 & 1 & z & z^2 & z^3 & 0 & 0 & 0 & 0 & 0 \\ 0 & 0 & 0 & 0 & 0 & 0 & 0 & 1 & 2z & 0 & 0 & 0 \\ 1 & 2z & 3z^2 & 0 & 0 & 0 & 0 & 0 & 0 & 1 & z & z^2 \end{bmatrix} [D_b] \begin{Bmatrix} a_0 \\ a_1 \\ a_2 \\ a_3 \\ l_0 \\ l_1 \\ l_2 \end{Bmatrix} \equiv [\tilde{Z}_b][D_b]\{\overline{u}_b\} \tag{3.4}$$

where the derivative operator matrix $[D_b]$ is given as:

$$[D_b] = \begin{bmatrix} 0 & 1 & 0 & 0 & 0 & 0 & 0 \\ 0 & 0 & 1 & 0 & 0 & 0 & 0 \\ 0 & 0 & 0 & 1 & 0 & 0 & 0 \\ \partial/\partial x & 0 & 0 & 0 & 0 & 0 & 0 \\ 0 & \partial/\partial x & 0 & 0 & 0 & 0 & 0 \\ 0 & 0 & \partial/\partial x & 0 & 0 & 0 & 0 \\ 0 & 0 & 0 & \partial/\partial x & 0 & 0 & 0 \\ 0 & 0 & 0 & 0 & 0 & 1 & 0 \\ 0 & 0 & 0 & 0 & 0 & 0 & 1 \\ 0 & 0 & 0 & 0 & \partial/\partial x & 0 & 0 \\ 0 & 0 & 0 & 0 & 0 & \partial/\partial x & 0 \\ 0 & 0 & 0 & 0 & 0 & 0 & \partial/\partial x \end{bmatrix}$$

3.2.2 Constitutive Equations

For an orthotropic FGM where the principal material directions coincide with the x and z axes, the two dimensional stress-strain constitutive relations are:

$$\sigma_b = \begin{Bmatrix} \sigma_x \\ \sigma_z \\ \tau_{xz} \end{Bmatrix} = \begin{bmatrix} c_{11}(z) & c_{13}(z) & 0 \\ c_{13}(z) & c_{33}(z) & 0 \\ 0 & 0 & c_{55}(z) \end{bmatrix} \begin{Bmatrix} \varepsilon_x \\ \varepsilon_z \\ \gamma_{xz} \end{Bmatrix} \equiv [c(z)]\,\varepsilon_b \tag{3.5}$$

where σ_x and σ_z represent the normal stress in the x and z directions, respectively, and τ_{xz} is the shear stress in the xz plane. Given that the elastic stiffness coefficient c_{ij} varies exponentially in the z direction, the elasticity matrix may be written as:

$$[c(z)] = e^{\lambda(z+h/2)} \begin{bmatrix} c_{11}^0 & c_{13}^0 & 0 \\ c_{13}^0 & c_{33}^0 & 0 \\ 0 & 0 & c_{55}^0 \end{bmatrix} \equiv e^{\lambda(z+h/2)} \left[c_b^0\right] \tag{3.6}$$

where $\left[c_b^0\right]$ is the elastic coefficient matrix located at the bottom surface $(z = -h/2)$ of the beam and λ is a parameter describing the inhomogeneity of the FGM across the thickness.

If it is further assumed that the FGM is isotropic at every point and Poisson's ratio is a constant through the thickness, then the variation of Young's modulus is given by $E(z) = E_b^0 e^{\lambda(z+h/2)}$ with the functional gradient $\lambda = {}^{1}\!/_{h_b} \ln\left(E_b^1/E_b^0\right)$, where E_b^0 and E_b^1 correspond to the Young's moduli of the bottom and top surfaces of the FGM layer, respectively. Consequently, the elasticity matrix $\left[c_b^0\right]$ is related to the Young's modulus E_b^0 and Poisson's ratio v_b for plane strain assumption by the following expression:

$$\left[c_b^0\right] = \frac{E_b^0}{(1+v_b)(1-2v_b)} \begin{bmatrix} 1-v_b & v_b & 0 \\ v_b & 1-v_b & 0 \\ 0 & 0 & (1-2v_b)/2 \end{bmatrix} \tag{3.7}$$

Hence, the constitutive relation becomes:

$$\sigma_b = \left[c_b^0\right] e^{\lambda(z+h/2)}\, \varepsilon_b = \left[Q_b\right] e^{\lambda z}\, \varepsilon_b \tag{3.8}$$

where the elastic matrix $\left[Q_b\right]$ is given as:

$$\left[Q_b\right] = \left[c_b^0\right] e^{\lambda h/2}$$

3.2.3 Formulation using Variational Principle

The extended Hamilton's principle of variations of independent kinematic variables over time t is written as:

$$\int_t (\delta T - \delta U + \delta W)\, dt = 0 \tag{3.9}$$

where $\delta T = \delta T_b + \delta T_c + \delta T_p$ and $\delta U = \delta U_b + \delta U_c + \delta U_p$ are the variations of the kinetic energy and strain energy, respectively, and δW is the virtual work done by external forces on the system.

Kinetic Energy

For the FGM beam the first variation of kinetic energy is:

$$\delta T_b = \int_\upsilon \rho_b \delta u_b \ddot{u}_b\, d\upsilon \tag{3.10}$$

Substituting for u_b from **Eq. (3.2)** yields:

$$\delta T_b = \rho_b \int_x \int_y \left\{\delta \overline{u}_b\right\}^T \left[I_b\right] \left\{\ddot{\overline{u}}_b\right\} dy dx = \rho_b b \int_x \left\{\delta \overline{u}_b\right\}^T \left[I_b\right] \left\{\ddot{\overline{u}}_b\right\} dx \tag{3.11}$$

where the inertia matrix $[I_b]$ is given by:

$$[I_b] = \int_z \left([Z_b]^T [Z_b] \right) dz = \int_z \begin{bmatrix} 1 & z & z^2 & z^3 & 0 & 0 & 0 \\ z & z^2 & z^3 & z^4 & 0 & 0 & 0 \\ z^2 & z^3 & z^4 & z^5 & 0 & 0 & 0 \\ z^3 & z^4 & z^5 & z^6 & 0 & 0 & 0 \\ 0 & 0 & 0 & 0 & 1 & z & z^2 \\ 0 & 0 & 0 & 0 & z & z^2 & z^3 \\ 0 & 0 & 0 & 0 & z^2 & z^3 & z^4 \end{bmatrix} dz$$

Strain Energy

The variational strain energy is:

$$\delta U_b = \int_\upsilon \sigma_b \delta \varepsilon_b \, d\upsilon \tag{3.12}$$

Substituting for σ_b from **Eq. (3.8)** yields:

$$\delta U_b = \int_\upsilon [Q_b] e^{\lambda z} \varepsilon_b \delta \varepsilon_b \, d\upsilon \tag{3.13}$$

and using ε_b from **Eq. (3.4)**, the final expression of the variational strain energy may be written as:

$$\delta U_b = b \int_x \{\delta \overline{u}_b\}^T [D_b]^T [C_b][D_b]\{\overline{u}_b\} dx \tag{3.14}$$

where the stiffness matrix $[C_b]$ is written as:

$$[C_b] = \int_z \left(\left[\tilde{Z}_b \right]^T [Q_b] \left[\tilde{Z}_b \right] \right) e^{\lambda z} \, dz$$

3.3 *Viscoelastic Layer (Core)*

The core, or the middle layer, is made of viscoelastic material and is distinguished by the subscript c.

3.3.1 Kinematic Assumptions

Identical to the mechanical assumptions of the FGM beam, the axial and transverse displacement fields of the viscoelastic core are interpolated through the thickness by cubic and quadratic functions, respectively. The displacement vector u_c is of the following form:

$$u_c = \begin{Bmatrix} u(x,z,t) \\ w(x,z,t) \end{Bmatrix} = \begin{Bmatrix} c_0 + c_1 z + c_2 z^2 + c_3 z^3 \\ m_0 + m_1 z + m_2 z^2 \end{Bmatrix} \tag{3.15}$$

where, as in the previous section, the coefficients c_0, c_1, c_2, c_3, m_0, m_1 and m_2 are functions of the spatial variable x and temporal variable t. Establishing a new vector $\{\overline{u}_c\}^T = \{c_0\ c_1\ c_2\ c_3\ m_0\ m_1\ m_2\}$ permits the re-write of **Eq. (3.15)** as:

$$u_c = \begin{bmatrix} 1 & z & z^2 & z^3 & 0 & 0 & 0 \\ 0 & 0 & 0 & 0 & 1 & z & z^2 \end{bmatrix} \begin{Bmatrix} c_0 \\ c_1 \\ c_2 \\ c_3 \\ m_0 \\ m_1 \\ m_2 \end{Bmatrix} \equiv [Z_c]\{\overline{u}_c\} \tag{3.16}$$

The corresponding strain-displacement components are given as:

$$\begin{cases} \varepsilon_x = \dfrac{\partial u}{\partial x} = c_{0,x} + c_{1,x} z + c_{2,x} z^2 + c_{3,x} z^3 \\ \varepsilon_z = \dfrac{\partial w}{\partial z} = m_1 + 2m_2 z \\ \gamma_{xz} = \dfrac{\partial u}{\partial z} + \dfrac{\partial w}{\partial x} = c_1 + 2c_2 z + 3c_3 z^2 + m_{0,x} + m_{1,x} z + m_{2,x} z^2 \end{cases} \tag{3.17}$$

The strain vector ε_c takes the following form:

$$\varepsilon_c = \begin{Bmatrix} \varepsilon_x \\ \varepsilon_z \\ \gamma_{xz} \end{Bmatrix} = \begin{bmatrix} 0 & 0 & 0 & 1 & z & z^2 & z^3 & 0 & 0 & 0 & 0 & 0 \\ 0 & 0 & 0 & 0 & 0 & 0 & 0 & 1 & 2z & 0 & 0 & 0 \\ 1 & 2z & 3z^2 & 0 & 0 & 0 & 0 & 0 & 0 & 1 & z & z^2 \end{bmatrix} [D_c] \begin{Bmatrix} c_0 \\ c_1 \\ c_2 \\ c_3 \\ m_0 \\ m_1 \\ m_2 \end{Bmatrix} \equiv [\tilde{Z}_c][D_c]\{\overline{u}_c\} \tag{3.18}$$

where the matrix $[D_c]$ is expressed as:

$$[D_c] = \begin{bmatrix} 0 & 1 & 0 & 0 & 0 & 0 & 0 \\ 0 & 0 & 1 & 0 & 0 & 0 & 0 \\ 0 & 0 & 0 & 1 & 0 & 0 & 0 \\ \partial/\partial x & 0 & 0 & 0 & 0 & 0 & 0 \\ 0 & \partial/\partial x & 0 & 0 & 0 & 0 & 0 \\ 0 & 0 & \partial/\partial x & 0 & 0 & 0 & 0 \\ 0 & 0 & 0 & \partial/\partial x & 0 & 0 & 0 \\ 0 & 0 & 0 & 0 & 0 & 1 & 0 \\ 0 & 0 & 0 & 0 & 0 & 0 & 1 \\ 0 & 0 & 0 & 0 & \partial/\partial x & 0 & 0 \\ 0 & 0 & 0 & 0 & 0 & \partial/\partial x & 0 \\ 0 & 0 & 0 & 0 & 0 & 0 & \partial/\partial x \end{bmatrix}$$

3.3.2 Constitutive Equations

Elastic Properties

The two-dimensional stress-strain constitutive relation in the xz plane for an orthotropic material is given as:

$$\sigma_c = \begin{Bmatrix} \sigma_x \\ \sigma_z \\ \tau_{xz} \end{Bmatrix} = \begin{bmatrix} c_{11} & c_{13} & 0 \\ c_{13} & c_{33} & 0 \\ 0 & 0 & c_{55} \end{bmatrix} \begin{Bmatrix} \varepsilon_x \\ \varepsilon_z \\ \gamma_{xz} \end{Bmatrix} = [Q_c]\,\varepsilon_c \tag{3.19}$$

where, for an isotropic material and under plane strain assumptions, $[Q_c]$ becomes:

$$[Q_c] = \frac{E_c}{(1+\nu_c)(1-2\nu_c)} \begin{bmatrix} 1-\nu_c & \nu_c & 0 \\ \nu_c & 1-\nu_c & 0 \\ 0 & 0 & (1-2\nu_c)/2 \end{bmatrix} \tag{3.20}$$

Viscoelastic Properties

As mentioned previously in Chapter two, the behavior of the viscoelastic material at a given time depends not only on a current state of stress or strain, but also on the material's history. This behavior is mathematically described by Galucio et al. in [19] by a four-parameter fractional derivative model as:

$$\bar{\sigma}_c(t) + \tau^\alpha \frac{d^\alpha \bar{\sigma}_c(t)}{dt^\alpha} = E_0[\zeta]\varepsilon_c(t) + \tau^\alpha E_\infty[\zeta]\frac{d^\alpha \varepsilon_c(t)}{dt^\alpha} \tag{3.21}$$

The above equation represents two-dimensional constitutive relation of the viscoelastic core with $[\zeta] = \frac{1}{(1+\nu_c)(1-2\nu_c)} \begin{bmatrix} 1-\nu_c & \nu_c & 0 \\ \nu_c & 1-\nu_c & 0 \\ 0 & 0 & (1-2\nu_c)/2 \end{bmatrix}$. The fractional derivative operator $\frac{d^\alpha}{dt^\alpha}$ is approximated by the Grünwald definition as:

$$\frac{d^\alpha f(t)}{dt^\alpha} \approx \Delta t^{-\alpha} \sum_{j=0}^{N_t} A_{j+1} f(t - j\Delta t) \tag{3.22}$$

where $\Delta t = \frac{t}{N}$ is the time step increment, N_t is the maximum number of terms of the Grünwald approximation ($N_t < N$), and A_{j+1} represents Grünwald coefficients given by the recurrence formula:

$$A_{j+1} = \frac{j-\alpha-1}{j} A_j = \prod_{p=1}^{j} \frac{p-\alpha-1}{p} \tag{3.23}$$

An anelastic strain $\tilde{\varepsilon}_c$ at a given time t can be introduced as:

$$\tilde{\varepsilon}_c(t) = \varepsilon_c(t) - [\zeta]^{-1} \frac{\bar{\sigma}_c(t)}{E_\infty} \tag{3.24}$$

This permits the re-write of **Eq. (3.21)** as:

$$\tilde{\varepsilon}_c(t) + \tau^\alpha \frac{d^\alpha \tilde{\varepsilon}_c(t)}{dt^\alpha} = \frac{E_\infty - E_0}{E_\infty} \varepsilon_c(t) \tag{3.25}$$

This variable change reduced the number of fractional derivative terms from two to one, thus simplifying the equation.

Using the Grünwald approximation from **Eq. (3.22)** with $A_1 = 1$ at $j = 0$, Galucio et al. [19] show that **Eq. (3.25)** takes the following form:

$$\tilde{\varepsilon}_c(t) = (1-\eta)\frac{E_\infty - E_0}{E_\infty} \varepsilon_c(t) - \eta \sum_{j=1}^{N_t} \left(\prod_{p=1}^{j} \frac{p-\alpha-1}{p} \right) \tilde{\varepsilon}_c(t - j\Delta t) \tag{3.26}$$

where the dimensionless constant $\eta = \frac{\tau^\alpha}{\tau^\alpha + \Delta t^\alpha}$.

To be consistent with the typical form of a compact matrix notation taken for the strain vector of the FGM beam, a fictitious anelastic displacement vector $\{\tilde{u}_c(t)\}$, which depends on the displacement history, is defined such that the anelastic strain can be written as:

$$\tilde{\varepsilon}_c(t) = \left[\tilde{Z}_c\right]\left[D_c\right]\{\tilde{u}_c(t)\} \tag{3.27}$$

Following Galucio et al. [19], and substituting for $\varepsilon_c(t)$ from **Eq. (3.18)** and $\tilde{\varepsilon}_c(t)$ from **Eq. (3.27)** at a given time t into **Eq. (3.26)**, the displacement $\{\tilde{u}_c(t)\}$ is expressed as:

$$\{\tilde{u}_c(t)\} = (1-\eta)\frac{E_\infty - E_0}{E_\infty}\{\bar{u}_c(t)\} - \eta\sum_{j=1}^{N_t}\left(\prod_{p=1}^{j}\frac{p-\alpha-1}{p}\right)\{\tilde{u}_c(t-j\Delta t)\} \tag{3.28}$$

Rearranging **Eq. (3.24)** for $\bar{\sigma}_c(t)$ yields:

$$\bar{\sigma}_c(t) = E_\infty\left[\zeta\right]\left(\varepsilon_c(t) - \tilde{\varepsilon}_c(t)\right) \tag{3.29}$$

Replacing $\tilde{\varepsilon}_c(t)$ in **Eq. (3.29)** with **Eq. (3.26)** results in the updated expression of $\bar{\sigma}_c(t)$ at a given time t:

$$\bar{\sigma}_c(t) = E_0\left[\zeta\right]\left[\left(1+\eta\frac{E_\infty - E_0}{E_0}\right)\varepsilon_c(t) + \eta\frac{E_\infty}{E_0}\sum_{j=1}^{N_t}\left(\prod_{p=1}^{j}\frac{p-\alpha-1}{p}\right)\tilde{\varepsilon}_c(t-j\Delta t)\right] \tag{3.30}$$

For an elastic material, $\eta = 0$ and $E_0 = E_c$ and **Eq. (3.30)** is reduced to $\bar{\sigma}_c(t) = E_0\left[\zeta\right]\varepsilon_c(t) \equiv \left[Q_c\right]\varepsilon_c(t)$. Hence, the constitutive relation of the viscoelastic core is:

$$\bar{\sigma}_c(t) = [Q_c]\left[\left(1+\eta\frac{E_\infty - E_0}{E_0}\right)\varepsilon_c(t) + \eta\frac{E_\infty}{E_0}\sum_{j=1}^{N_t}\left(\prod_{p=1}^{j}\frac{p-\alpha-1}{p}\right)\tilde{\varepsilon}_c(t-j\Delta t)\right] \quad \textbf{(3.31)}$$

3.3.3 Formulation using Variational Principle

Kinetic Energy

Similar to the formulation of the FGM beam, for the viscoelastic layer the first variation of kinetic energy is:

$$\delta T_c = \int_\upsilon \rho_c \delta u_c \ddot{u}_c \, d\upsilon \quad \textbf{(3.32)}$$

Substituting for u_c from **Eq. (3.16)** yields:

$$\delta T_c = \rho_c \int_x \int_y \{\delta \bar{u}_c\}^T [I_c]\{\ddot{\bar{u}}_c\} dy dx = \rho_c b \int_x \{\delta \bar{u}_c\}^T [I_c]\{\ddot{\bar{u}}_c\} dx \quad \textbf{(3.33)}$$

where the inertia matrix $[I_c]$ is identified as:

$$[I_c] = \int_z \left([Z_c]^T [Z_c]\right) dz = \int_z \begin{bmatrix} 1 & z & z^2 & z^3 & 0 & 0 & 0 \\ z & z^2 & z^3 & z^4 & 0 & 0 & 0 \\ z^2 & z^3 & z^4 & z^5 & 0 & 0 & 0 \\ z^3 & z^4 & z^5 & z^6 & 0 & 0 & 0 \\ 0 & 0 & 0 & 0 & 1 & z & z^2 \\ 0 & 0 & 0 & 0 & z & z^2 & z^3 \\ 0 & 0 & 0 & 0 & z^2 & z^3 & z^4 \end{bmatrix} dz$$

Strain Energy

The variational strain energy of the core at a given time t is:

$$\delta U_c(t) = \int_{\upsilon} \bar{\sigma}_c(t)\delta\varepsilon_c \, d\upsilon \tag{3.34}$$

Substituting for $\bar{\sigma}_c(t)$ from **Eq. (3.31)** results in the modified equation:

$$\begin{aligned}\delta U_c(t) = & \int_{\upsilon} [Q_c]\varepsilon_c(t)\delta\varepsilon_c \, d\upsilon + \int_{\upsilon} [\tilde{Q}_c]\varepsilon_c(t)\delta\varepsilon_c \, d\upsilon + \\ & + \eta \frac{E_\infty}{E_0} \sum_{j=1}^{N_t} \left(\prod_{p=1}^{j} \frac{p-\alpha-1}{p} \right) \times \int_{\upsilon} [Q_c]\tilde{\varepsilon}_c(t - j\Delta t)\delta\varepsilon_c \, d\upsilon\end{aligned} \tag{3.35}$$

where $[\tilde{Q}_c] = \eta \frac{E_\infty - E_0}{E_0} [Q_c]$.

The above variation of the total viscoelastic strain energy can be rewritten as:

$$\delta U_c(t) = \delta \bar{U}_c(t) + \delta \tilde{U}_c(t) + \delta \tilde{W}_c(t) \tag{3.36}$$

where $\delta \bar{U}_c(t)$ represents the variation of the elastic strain energy, $\delta \tilde{U}_c(t)$ is the variational form of the anelastic strain energy, and $\delta \tilde{W}_c(t)$ is the virtual work done by the induced force acting in the viscoelastic layer.

Substituting for ε_c from **Eq. (3.18)** yields:

$$\delta \bar{U}_c(t) = b \int_x \{\delta \bar{u}_c\}^T [D_c]^T [C_c][D_c]\{\bar{u}_c(t)\} dx \tag{3.37}$$

where the elastic stiffness matrix $[C_c]$ is written as:

$$[C_c] = \int_z \left([\tilde{Z}_c]^T [Q_c][\tilde{Z}_c] \right) dz$$

Similarly, the variation of anelastic strain energy $\delta\tilde{U}_c(t)$ is expresses as:

$$\delta\tilde{U}_c(t) = b\int_x \{\delta\overline{u}_c\}^T [D_c]^T \left[\tilde{C}_c\right][D_c]\{\overline{u}_c(t)\}dx \tag{3.38}$$

where the anelastic stiffness matrix $\left[\tilde{C}_c\right]$ is given by:

$$\left[\tilde{C}_c\right] = \eta\frac{E_\infty - E_0}{E_0}[C_c]$$

and the virtual work $\delta\tilde{W}_c(t)$ is given as:

$$\delta\tilde{W}_c(t) = \eta\frac{E_\infty}{E_0}\sum_{j=1}^{N_t}\left(\prod_{p=1}^{j}\frac{p-\alpha-1}{p}\right)\times b\int_x \{\delta\overline{u}_c\}^T [D_c]^T [C_c][D_c]\{\tilde{u}_c(t-j\Delta t)\}dx \tag{3.39}$$

3.4 PFRC Laminate (Top Layer)

The PFRC laminate, or the top layer, is made of piezoelectric fiber-reinforced composite, as previously explained in Chapter two, and is identified by the subscript p. The piezoelectric fibers in PFRC are considered to act as the actuator of the beam. The fibers in each PFRC ply are horizontally reinforced and are aligned at orientation angle θ with respect to the reference plane. There are n number of plies in the laminate.

3.4.1 Kinematic Assumptions

Mechanical Field Assumptions

Here, unlike in the preceding subsections, the axial displacement is linearly interpolated through the thickness and the transverse displacement is constant. The displacement vector u_p, with the coefficients e_0, e_1, and n_0 as functions of the spatial variable x and temporal variable t, is of the form:

$$u_p = \begin{Bmatrix} u(x,z,t) \\ w(x,z,t) \end{Bmatrix} = \begin{Bmatrix} e_0 + e_1 z \\ n_0 \end{Bmatrix} \tag{3.40}$$

Defining a new vector $\{\overline{u}_p\}^T = \{e_0 \; e_1 \; n_0\}$ yields the modified u_p vector:

$$u_p = \begin{bmatrix} 1 & z & 0 \\ 0 & 0 & 1 \end{bmatrix} \begin{Bmatrix} e_0 \\ e_1 \\ n_0 \end{Bmatrix} \equiv [Z_p]\{\overline{u}_p\} \tag{3.41}$$

The equivalent strain-displacement relations are:

$$\begin{cases} \varepsilon_x = \dfrac{\partial u}{\partial x} = e_{0,x} + e_{1,x} z \\ \gamma_{xz} = \dfrac{\partial u}{\partial z} + \dfrac{\partial w}{\partial x} = e_1 + n_{0,x} \end{cases} \tag{3.42}$$

The strain vector ε_p takes the following form:

$$\varepsilon_p = \begin{Bmatrix} \varepsilon_x \\ \gamma_{xz} \end{Bmatrix} = \begin{Bmatrix} e_{0,x} \\ e_1 + n_{0,x} \end{Bmatrix} + z \begin{Bmatrix} e_{1,x} \\ 0 \end{Bmatrix} = \begin{Bmatrix} \varepsilon_x^0 \\ \gamma_{xz}^0 \end{Bmatrix} + z \begin{Bmatrix} \kappa_x \\ \kappa_{xz} \end{Bmatrix} \equiv \varepsilon_0 + z\kappa \tag{3.43}$$

The above equation is then converted into the following matrix notation:

$$\varepsilon_p = [1 \quad z] \begin{Bmatrix} \varepsilon_0 \\ \kappa \end{Bmatrix} = [1 \quad z] \begin{bmatrix} D_p^0 \\ D_p^1 \end{bmatrix} \{\overline{u}_p\} \tag{3.44}$$

where the derivative operator matrices $\left[D_p^0\right]$ and $\left[D_p^1\right]$ are expressed as:

$$[D_p^0]=\begin{bmatrix} \partial/\partial x & 0 & 0 \\ 0 & 1 & \partial/\partial x \end{bmatrix} \qquad [D_p^1]=\begin{bmatrix} 0 & \partial/\partial x & 0 \\ 0 & 0 & 0 \end{bmatrix}$$

Electrical Field Assumptions

Two electrostatic assumptions are consideration for the PFRC laminate. First, the electrical potential variable ψ_p is assumed linear within the thickness of the top layer and is of the following form:

$$\psi_p(x,z,t)=\psi_0(x,t)+z\frac{\partial\psi_p(x,z,t)}{\partial z} \tag{3.45}$$

where ψ_0 and $\frac{\partial\psi_p}{\partial z}$ are the electric potential and its gradient at the mid-plane of the PFRC laminate, respectively.

Second, the axial component of the electrical field is ignored (i.e., $E_x=0$), since its contribution to the electromechanical energy is negligible in comparison with that of the transverse component [20]. Also, since the thickness of the PFRC laminate is relatively thin, the voltage is assumed to be uniformly distributed through the thickness along the z direction.

Considering the above, the expression of the transverse component of the electrical field E_z then represents a constant field along the z axis as follows:

$$E_z=-\frac{\partial\psi_p}{\partial z}=-\frac{V}{h_p} \tag{3.46}$$

where V is the applied voltage in the beam and h_p is the thickness of the PFRC laminate.

3.4.2 Constitutive Equations

The piezoelectric fibers are continuous and longitudinal (x – axis) and subjected to a constant electric field acting in the direction transverse to the fiber direction or along the z axis, as was mentioned in the previous subsection. Note that the electric field is assumed to be the same in both the fibers and the surrounding matrix, where the matrix material is piezoelectrically inactive [25].

Mechanical Properties

The piezoelectric fibers are transversely isotropic in the 1-2 plane [26] and the constitutive relation for the PFRC in the principal 1-2-3 directions is of the following form:

$$\begin{Bmatrix} \sigma_1 \\ \sigma_2 \\ \sigma_3 \\ \tau_{23} \\ \tau_{13} \\ \tau_{12} \end{Bmatrix}_k = \begin{bmatrix} c_{11} & c_{12} & c_{13} & 0 & 0 & 0 \\ c_{12} & c_{22} & c_{23} & 0 & 0 & 0 \\ c_{13} & c_{23} & c_{33} & 0 & 0 & 0 \\ 0 & 0 & 0 & c_{44} & 0 & 0 \\ 0 & 0 & 0 & 0 & c_{55} & 0 \\ 0 & 0 & 0 & 0 & 0 & c_{66} \end{bmatrix}_k \begin{Bmatrix} \varepsilon_1 \\ \varepsilon_2 \\ \varepsilon_3 \\ \varepsilon_{23} \\ \varepsilon_{13} \\ \varepsilon_{12} \end{Bmatrix}_k - \begin{bmatrix} 0 & 0 & e_{31} \\ 0 & 0 & e_{31} \\ 0 & 0 & e_{33} \\ 0 & e_{15} & 0 \\ e_{15} & 0 & 0 \\ 0 & 0 & 0 \end{bmatrix}_k \begin{Bmatrix} E_1 \\ E_2 \\ E_3 \end{Bmatrix}_k \tag{3.47}$$

where for the k^{th} ply of the PFRC lamina and $i, j = 1,2,3$, σ_i, τ_{ij}, ε_i, ε_{ij} are the normal stress, shear stress, normal strain and shear strain components in the i^{th} direction, respectively; c_{ij} are the effective elastic coefficients derived by micromechanical analysis [25] at constant electric field; the constants e_{ij} denote piezoelectric coefficients; and E_i represents the electric field.

As the piezoelectric fibers are orientated longitudinally in the 1-2 plane, the transformation from the 1-2-3 coordinate system to a global xyz system must be performed through a counterclockwise rotation by an angle θ about the z axis. The transformation matrix of trigonometric functions of the mechanical aspect is written as [29, 30]:

$$[T]=\begin{bmatrix} \cos^2\theta & \sin^2\theta & 0 & 0 & 0 & 2\sin\theta\cos\theta \\ \sin^2\theta & \cos^2\theta & 0 & 0 & 0 & -2\sin\theta\cos\theta \\ 0 & 0 & 1 & 0 & 0 & 0 \\ 0 & 0 & 0 & \cos\theta & -\sin\theta & 0 \\ 0 & 0 & 0 & \sin\theta & \cos\theta & 0 \\ -\sin\theta\cos\theta & \sin\theta\cos\theta & 0 & 0 & 0 & \cos^2\theta-\sin^2\theta \end{bmatrix} \tag{3.48}$$

Similarly, for the electro-mechanical component in **Eq. (3.47)**, the transformation matrix is:

$$[T]^e=\begin{bmatrix} \cos\theta & -\sin\theta & 0 \\ \sin\theta & \cos\theta & 0 \\ 0 & 0 & 1 \end{bmatrix} \tag{3.49}$$

Hence, for the mechanical component, the stress-strain relation in the global coordinate system becomes:

$$\begin{Bmatrix} \sigma_x \\ \sigma_y \\ \sigma_z \\ \tau_{yz} \\ \tau_{xz} \\ \tau_{xy} \end{Bmatrix}^m_k = [T]_k^{-1}[C_p]_k[R][T]_k[R]^{-1}\begin{Bmatrix} \varepsilon_x \\ \varepsilon_y \\ \varepsilon_z \\ \gamma_{yz} \\ \gamma_{xz} \\ \gamma_{xy} \end{Bmatrix}_k \equiv [\bar{Q}_p]_k\begin{Bmatrix} \varepsilon_x \\ \varepsilon_y \\ \varepsilon_z \\ \gamma_{yz} \\ \gamma_{xz} \\ \gamma_{xy} \end{Bmatrix}_k \tag{3.50}$$

where $[R]=\begin{bmatrix} 1 & 0 & 0 & 0 & 0 & 0 \\ 0 & 1 & 0 & 0 & 0 & 0 \\ 0 & 0 & 1 & 0 & 0 & 0 \\ 0 & 0 & 0 & 2 & 0 & 0 \\ 0 & 0 & 0 & 0 & 2 & 0 \\ 0 & 0 & 0 & 0 & 0 & 2 \end{bmatrix}$ is used to account for the relationship between the

tensor shear strain ε and engineering shear strain γ and

$$\left[C_p\right]_k = \begin{bmatrix} c_{11} & c_{12} & c_{13} & 0 & 0 & 0 \\ c_{12} & c_{22} & c_{23} & 0 & 0 & 0 \\ c_{13} & c_{23} & c_{33} & 0 & 0 & 0 \\ 0 & 0 & 0 & c_{44} & 0 & 0 \\ 0 & 0 & 0 & 0 & c_{55} & 0 \\ 0 & 0 & 0 & 0 & 0 & c_{66} \end{bmatrix}_k$$ is the stiffness matrix from **Eq. (3.47)**;

σ_x, σ_y, and σ_z are the normal stresses in the x, y, and z directions, respectively; τ_{xz} and τ_{yz} are the transverse shear stresses; τ_{xy} is the in-plane shear stress; ε_x, ε_y, ε_z, γ_{yz}, γ_{xz}, and γ_{xy} are the corresponding strains.

In the same manner, the stress and electric field relation of **Eq. (3.47)** is expressed through the transformation as:

$$\begin{Bmatrix} \sigma_x \\ \sigma_y \\ \sigma_z \\ \tau_{yz} \\ \tau_{xz} \\ \tau_{xy} \end{Bmatrix}_k^e = \left[T\right]_k^{-1}\left[e\right]_k^T\left[T\right]_k^e \begin{Bmatrix} E_x \\ E_y \\ E_z \end{Bmatrix}_k \equiv \left[\bar{e}\right]_k^T \begin{Bmatrix} E_x \\ E_y \\ E_z \end{Bmatrix}_k \qquad \textbf{(3.51)}$$

where the piezoelectric coefficient matrix $\left[e\right]_k^T = \begin{bmatrix} 0 & 0 & e_{31} \\ 0 & 0 & e_{31} \\ 0 & 0 & e_{33} \\ 0 & e_{15} & 0 \\ e_{15} & 0 & 0 \\ 0 & 0 & 0 \end{bmatrix}_k$ is the transpose of $\left[e\right]_k$.

Following the paper by Sun and Huang [27], the assumptions regarding the reduction of the constitutive relations of **Eq. (3.47)** are used for the beam problem. After the stiffness matrix $\left[C_p\right]$ and the piezoelectric constant matrix $\left[e\right]_k^T$ are transformed into

the matrices $\left[\bar{Q}_p\right]_k$ and $\left[\bar{e}\right]_k^T$ by an angle θ in the xy plane, respectively, the assumption where $\sigma_z = \varepsilon_z = 0$ is used due to the negligible thickness of the PFRC layer. Once this modification is applied, the updated constitutive equation including the transformed matrices $\left[\bar{Q}_p\right]_k$ and $\left[\bar{e}\right]_k^T$ is expressed as:

$$\begin{Bmatrix} \sigma_x \\ \sigma_y \\ \tau_{yz} \\ \tau_{xz} \\ \tau_{xy} \end{Bmatrix}_k = \begin{bmatrix} \bar{Q}_{11} & \bar{Q}_{12} & 0 & 0 & \bar{Q}_{16} \\ \bar{Q}_{12} & \bar{Q}_{22} & 0 & 0 & \bar{Q}_{26} \\ 0 & 0 & \bar{Q}_{44} & \bar{Q}_{45} & 0 \\ 0 & 0 & \bar{Q}_{45} & \bar{Q}_{55} & 0 \\ \bar{Q}_{16} & \bar{Q}_{26} & 0 & 0 & \bar{Q}_{66} \end{bmatrix}_k \begin{Bmatrix} \varepsilon_x \\ \varepsilon_y \\ \gamma_{yz} \\ \gamma_{xz} \\ \gamma_{xy} \end{Bmatrix}_k - \begin{bmatrix} 0 & 0 & \bar{e}_{31} \\ 0 & 0 & \bar{e}_{31} \\ -\bar{e}_{25} & \bar{e}_{15} & 0 \\ \bar{e}_{15} & \bar{e}_{25} & 0 \\ 0 & 0 & 0 \end{bmatrix}_k \begin{Bmatrix} E_x \\ E_y \\ E_z \end{Bmatrix}_k \tag{3.52}$$

where $\bar{e}_{31} = e_{31}$, $\bar{e}_{15} = e_{15}(\cos^2\theta - \sin^2\theta)$ and $\bar{e}_{25} = -2e_{15}\sin\theta\cos\theta$; and

$$\bar{Q}_{11} = c_{11}\cos^4\theta + 2c_{12}\sin^2\theta\cos^2\theta + c_{22}\sin^4\theta + 4c_{66}\sin^2\theta\cos^2\theta$$
$$\bar{Q}_{12} = c_{11}\sin^2\theta\cos^2\theta + c_{12}\left(\sin^4\theta + \cos^4\theta\right) + c_{22}\sin^2\theta\cos^2\theta - 4c_{66}\sin^2\theta\cos^2\theta$$
$$\bar{Q}_{16} = \left[c_{11}\cos^2\theta + c_{12}\left(\sin^2\theta - \cos^2\theta\right) - c_{22}\sin^2\theta + 2c_{66}\left(\sin^2\theta - \cos^2\theta\right)\right]\sin\theta\cos\theta$$
$$\bar{Q}_{22} = c_{11}\sin^4\theta + 2c_{12}\sin^2\theta\cos^2\theta + c_{22}\cos^4\theta + 4c_{66}\sin^2\theta\cos^2\theta$$
$$\bar{Q}_{26} = \left[c_{11}\sin^2\theta - c_{12}\left(\sin^2\theta - \cos^2\theta\right) - c_{22}\cos^2\theta - 2c_{66}\left(\sin^2\theta - \cos^2\theta\right)\right]\sin\theta\cos\theta$$
$$\bar{Q}_{44} = c_{44}\cos^2\theta + c_{55}\sin^2\theta$$
$$\bar{Q}_{45} = -c_{44}\sin\theta\cos\theta + c_{55}\sin\theta\cos\theta$$
$$\bar{Q}_{55} = c_{44}\sin^2\theta + c_{55}\cos^2\theta$$
$$\bar{Q}_{66} = c_{11}\sin^2\theta\cos^2\theta - 2c_{12}\sin^2\theta\cos^2\theta + c_{22}\sin^2\theta\cos^2\theta + c_{66}\left(\sin^4\theta - 2\sin^2\theta\cos^2\theta + \cos^4\theta\right)$$

Another assumption from [27] is that $\sigma_y = \tau_{yz} = \tau_{xy} = 0$ while $\varepsilon_y \neq \gamma_{yz} \neq \gamma_{xy} \neq 0$. Since the piezoelectric fibers are polarized only in the thickness direction, as mentioned in the previous subsection, then $E_x = E_y = 0$. Hence, the final reduced constitutive equation of the k^{th} ply in the PFRC lamina from the transformed **Eq. (3.52)** is as follows:

$$\{\sigma_p\}_k = \begin{Bmatrix} \sigma_x \\ \tau_{xz} \end{Bmatrix}_k = \begin{bmatrix} \tilde{Q}_{11} & 0 \\ 0 & k_s \tilde{Q}_{55} \end{bmatrix}_k \begin{Bmatrix} \varepsilon_x \\ \gamma_{xz} \end{Bmatrix}_k - \begin{Bmatrix} \tilde{e}_{31} E_z \\ 0 \end{Bmatrix}_k \equiv \left[\tilde{Q}_p\right]_k \{\varepsilon_p\}_k - \begin{Bmatrix} \tilde{e}_{31} E_z \\ 0 \end{Bmatrix}_k \quad \textbf{(3.53)}$$

where,

$$\tilde{Q}_{11} = \bar{Q}_{11} + \frac{\bar{Q}_{16}\bar{Q}_{26} - \bar{Q}_{12}\bar{Q}_{66}}{\bar{Q}_{22}\bar{Q}_{66} - \bar{Q}_{26}^2}\bar{Q}_{12} + \frac{\bar{Q}_{12}\bar{Q}_{26} - \bar{Q}_{16}\bar{Q}_{22}}{\bar{Q}_{22}\bar{Q}_{66} - \bar{Q}_{26}^2}\bar{Q}_{16},$$

$$\tilde{Q}_{55} = \bar{Q}_{55} - \frac{\bar{Q}_{45}^2}{\bar{Q}_{44}},\ \tilde{e}_{31} = \left(1 - \frac{\bar{Q}_{12}\bar{Q}_{66} - \bar{Q}_{16}\bar{Q}_{26}}{\bar{Q}_{22}\bar{Q}_{66} - \bar{Q}_{26}^2}\right)\bar{e}_{31};\ \text{and}$$

$k_s = 5/6$ is the shear correction factor.

Electrical Properties

If modeling a self-sensing actuator, the direct piezoelectric effect would be taken into an account. For completeness, the electrical displacement field D_i is given by [26] and is shown in the principal 1-2-3 directions as:

$$\begin{Bmatrix} D_1 \\ D_2 \\ D_3 \end{Bmatrix}_k = \begin{bmatrix} 0 & 0 & 0 & 0 & e_{15} & 0 \\ 0 & 0 & 0 & e_{15} & 0 & 0 \\ e_{31} & e_{31} & e_{33} & 0 & 0 & 0 \end{bmatrix}_k \begin{Bmatrix} \varepsilon_1 \\ \varepsilon_2 \\ \varepsilon_3 \\ \gamma_{23} \\ \gamma_{13} \\ \gamma_{12} \end{Bmatrix}_k + \begin{bmatrix} d_{11} & 0 & 0 \\ 0 & d_{22} & 0 \\ 0 & 0 & d_{33} \end{bmatrix}_k \begin{Bmatrix} 0 \\ 0 \\ E_3 \end{Bmatrix}_k \quad \textbf{(3.54)}$$

where the coefficients d_{ij} represent the components of the dielectric permittivity tensor at constant strain.

The transformation of the permittivity constant matrix $[d]_k = \begin{bmatrix} d_{11} & 0 & 0 \\ 0 & d_{22} & 0 \\ 0 & 0 & d_{33} \end{bmatrix}_k$ is implemented in the same way as the above transformations, and results in the modified electrical displacement relation in the xyz coordinate system which is written as:

$$\begin{Bmatrix} D_x \\ D_y \\ D_z \end{Bmatrix}_k = \left([T]_k^e\right)^{-1}[e]_k[T]_k \begin{Bmatrix} \varepsilon_x \\ \varepsilon_y \\ \varepsilon_z \\ \gamma_{yz} \\ \gamma_{xz} \\ \gamma_{xy} \end{Bmatrix}_k + \left([T]_k^e\right)^{-1}[d]_k[T]_k^e \begin{Bmatrix} 0 \\ 0 \\ E_z \end{Bmatrix}_k \equiv [\bar{e}]_k \begin{Bmatrix} \varepsilon_x \\ \varepsilon_y \\ \varepsilon_z \\ \gamma_{yz} \\ \gamma_{xz} \\ \gamma_{xy} \end{Bmatrix}_k + [\bar{d}]_k \begin{Bmatrix} 0 \\ 0 \\ E_z \end{Bmatrix}_k \tag{3.55}$$

Applying the assumption $\varepsilon_z = 0$ yields the following updated constitutive relation from **Eq. (3.55):**

$$\begin{Bmatrix} D_x \\ D_y \\ D_z \end{Bmatrix}_k = \begin{bmatrix} 0 & 0 & -\bar{e}_{25} & \bar{e}_{15} & 0 \\ 0 & 0 & \bar{e}_{15} & \bar{e}_{25} & 0 \\ \bar{e}_{31} & \bar{e}_{31} & 0 & 0 & 0 \end{bmatrix}_k \begin{Bmatrix} \varepsilon_x \\ \varepsilon_y \\ \gamma_{yz} \\ \gamma_{xz} \\ \gamma_{xy} \end{Bmatrix}_k + \begin{bmatrix} \bar{d}_{11} & \bar{d}_{12} & 0 \\ \bar{d}_{12} & \bar{d}_{22} & 0 \\ 0 & 0 & \bar{d}_{33} \end{bmatrix}_k \begin{Bmatrix} 0 \\ 0 \\ E_z \end{Bmatrix}_k \tag{3.56}$$

where $\bar{d}_{11} = d_{11}\cos^2\theta + d_{22}\sin^2\theta$, $\bar{d}_{12} = (d_{22} - d_{11})\sin\theta\cos\theta$, $\bar{d}_{22} = d_{11}\sin^2\theta + d_{22}\cos^2\theta$, and $\bar{d}_{33} = d_{33}$.

For $D_x^k = D_y^k = 0$, the electrical displacement field D^k in the z direction becomes:

$$D_z^k = \bar{e}_{31}\varepsilon_x + \bar{e}_{31}\varepsilon_y + \bar{d}_{33}E_z^k \tag{3.57}$$

For the beam assumption of $\sigma_y = \tau_{yz} = \tau_{xy} = 0$, **Eq. (3.57)** is, as in the mechanical aspect of the constitutive relations, reduced to the following equation:

$$D_z^k = \tilde{e}_{31}\varepsilon_x + \tilde{d}_{33}E_z^k \tag{3.58}$$

where $\tilde{d}_{33} = \dfrac{\bar{Q}_{66}\bar{e}_{31}^2}{\bar{Q}_{22}\bar{Q}_{66} - \bar{Q}_{26}^2} + \bar{d}_{33}$.

3.4.2.1 Laminate Stiffness Matrix ABD

Mechanical

Using the classical lamination theory [29, 30], the resultant laminate stiffness matrix ABD can be determined by computing the force and moment resultants at the x-coordinate on the laminate reference plane (middle of the laminate). See **Fig. 3.2** below for the geometry of an n-layered laminate. The resultant forces and moments acting on the laminate are obtained by integrating the stresses and moments of the stresses in each ply through the thickness of the laminate [29, 30].

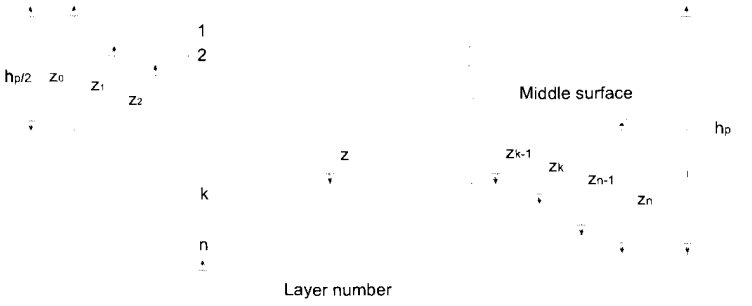

Figure 3.2: Geometry of an n-layered laminate.

The stress resultants in the x direction and in shear are the normal force resultant N_x and the shear force resultant N_{xz}, respectively, and are given by:

$$\begin{Bmatrix} N_x \\ N_{xz} \end{Bmatrix} = \int_{-h_p/2}^{h_p/2} \begin{Bmatrix} \sigma_x \\ \tau_{xz} \end{Bmatrix} dz = \sum_{k=1}^{n} \int_{z_{k-1}}^{z_k} \begin{Bmatrix} \sigma_x \\ \tau_{xz} \end{Bmatrix}_k dz \tag{3.59}$$

Note that the units of the stress resultants are force per unit length in the x direction.

Likewise, the bending moment resultant M_x and the twisting moment resultant M_{xz} are as follows:

$$\begin{Bmatrix} M_x \\ M_{xz} \end{Bmatrix} = \int_{-h_p/2}^{h_p/2} \begin{Bmatrix} \sigma_x \\ \tau_{xz} \end{Bmatrix} z dz = \sum_{k=1}^{n} \int_{z_{k-1}}^{z_k} \begin{Bmatrix} \sigma_x \\ \tau_{xz} \end{Bmatrix}_k z dz \tag{3.60}$$

where the units of the moment resultants are moment per unit length in the x direction.

In the above two expressions, the limits z_k and z_{k-1} are defined by the following transformation between the reference surface of the beam ($z = \frac{h}{2}$) and the PFRC laminate reference plane ($\overline{z} = \frac{h_p}{2}$):

$$z_k = \overline{z}_k + \frac{h}{2} - \frac{h_p}{2}; \qquad z_{k-1} = \overline{z}_{k-1} + \frac{h}{2} - \frac{h_p}{2} \tag{3.61}$$

Since the stiffness matrix from **Eq. 3.53** does not depend on z, that is, it is constant within each ply of the PFRC laminate, then the stiffness matrix can be placed outside the integration over each ply and still be within the summation of force and moment resultants of each layer. In addition, the strain vector $\begin{Bmatrix} \varepsilon_0 \\ \kappa \end{Bmatrix}$ from **Eq. 3.44** is not a function of z but is a middle surface value and, thus, can be removed from under both the integration and summation signs. Taking the above operations [29, 30] into an account and substituting the lamina constitutive relation from **Eq. 3.53**, the force and moment resultants can be expressed in the following matrix notation:

$$\begin{Bmatrix} N_x \\ N_{xz} \end{Bmatrix} = \begin{bmatrix} A_{11} & A_{12} \\ A_{12} & A_{22} \end{bmatrix} \begin{Bmatrix} \varepsilon_x^0 \\ \gamma_{xz}^0 \end{Bmatrix} + \begin{bmatrix} B_{11} & B_{12} \\ B_{12} & B_{22} \end{bmatrix} \begin{Bmatrix} \kappa_x \\ \kappa_{xz} \end{Bmatrix} - \begin{Bmatrix} N_x \\ 0 \end{Bmatrix}^p \tag{3.62}$$

and

$$\begin{Bmatrix} M_x \\ M_{xz} \end{Bmatrix} = \begin{bmatrix} B_{11} & B_{12} \\ B_{12} & B_{22} \end{bmatrix} \begin{Bmatrix} \varepsilon_x^0 \\ \gamma_{xz}^0 \end{Bmatrix} + \begin{bmatrix} D_{11} & D_{12} \\ D_{12} & D_{22} \end{bmatrix} \begin{Bmatrix} \kappa_x \\ \kappa_{xz} \end{Bmatrix} - \begin{Bmatrix} M_x \\ 0 \end{Bmatrix}^p \tag{3.63}$$

where

$$\begin{aligned} A_{ij} &= \sum_{k=1}^{n} \left(\tilde{Q}_{p_{ij}}\right)_k \left(z_k - z_{k-1}\right) \\ B_{ij} &= \tfrac{1}{2} \sum_{k=1}^{n} \left(\tilde{Q}_{p_{ij}}\right)_k \left(z_k^2 - z_{k-1}^2\right) \\ D_{ij} &= \tfrac{1}{3} \sum_{k=1}^{n} \left(\tilde{Q}_{p_{ij}}\right)_k \left(z_k^3 - z_{k-1}^3\right) \end{aligned} \tag{3.64}$$

and

$$N_x^p = \sum_{k=1}^{n} \left(\tilde{e}_{31} E_z\right)_k \left(z_k - z_{k-1}\right) \qquad M_x^p = \tfrac{1}{2} \sum_{k=1}^{n} \left(\tilde{e}_{31} E_z\right)_k \left(z_k^2 - z_{k-1}^2\right)$$

with extensional stiffnesses A_{ij}, coupling stiffnesses B_{ij}, and bending stiffnesses D_{ij} making up the laminate stiffness matrix known as the ABD matrix. The ABD matrix defines the relationship between the stress resultants applied to a laminate, and the reference surface strain and curvatures [29]. Note that the ABD stiffness matrix combines the properties of the material, fiber orientation, thickness, and location of each ply in the laminate [29].

Eq. 3.64 also contains the electrical stress resultant components N_x^p and M_x^p, which show the relation between the stress and the electric field in the PFRC laminate.

3.4.3 Formulation using Variational Principle

Kinetic Energy

Similar to both the FGM and viscoelastic layers, the variation of the kinetic energy of the PFRC laminate is:

$$\delta T_p = \int_{\upsilon} \rho_p \delta u_p \ddot{u}_p \, d\upsilon \tag{3.65}$$

Substituting for u_p from **Eq. (3.41)** yields the following:

$$\delta T_p = \rho_p \int_x \int_y \{\delta \overline{u}_p\}^T [I_p] \{\ddot{\overline{u}}_p\} dy dx = \rho_p b \int_x \{\delta \overline{u}_p\}^T [I_p] \{\ddot{\overline{u}}_p\} dx \tag{3.66}$$

where the matrix $[I_p]$ is given by:

$$[I_p] = \int_z \left([Z_p]^T [Z_p] \right) dz = \int_z \begin{bmatrix} 1 & z & 0 \\ z & z^2 & 0 \\ 0 & 0 & 1 \end{bmatrix} dz$$

Strain Energy

The total variation of strain energy in the PFRC laminate can be described as:

$$\delta \hat{U}_p = \delta U_p + \delta \hat{W}_p \tag{3.67}$$

where U_p denotes the mechanical strain energy and $\hat{W}_p$ represents the work done by the electrical force produced by the applied electrical field E_z.

The variation of the total mechanical strain energy in the PFRC laminate is:

$$\delta U_p = \int_{\upsilon} \sigma_p \delta \varepsilon_p \, d\upsilon \tag{3.68}$$

The stress-strain relation of each ply in the lamina is represented by $\{\sigma_p\}_k = [\tilde{Q}_p]_k \varepsilon_p$, where $[\tilde{Q}_p]_k$ is the reduced transformed matrix of the individual k^{th} ply, such as depicted in **Eq. (3.53)**. Expanding **Eq. 3.68** yields the following:

$$\delta U_p = \int_x \int_y \sum_{k=1}^{n} \int_{z_{k-1}}^{z_k} \delta \varepsilon_p{}^T [\tilde{Q}_p]_k \varepsilon_p \, dz dy dx \tag{3.69}$$

Further expanding the above strain energy equation and substituting with $\varepsilon_p = [1 \quad z] \begin{Bmatrix} \varepsilon_0 \\ \kappa \end{Bmatrix}$ from **Eq. (3.43)**, results in:

$$\delta U_p = \int_x \int_y \sum_{k=1}^{n} \int_{z_{k-1}}^{z_k} \begin{Bmatrix} \delta\varepsilon_0 \\ \delta\kappa \end{Bmatrix}^T \begin{bmatrix} \tilde{Q}_p & z\tilde{Q}_p \\ z\tilde{Q}_p & z^2\tilde{Q}_p \end{bmatrix}_k \begin{Bmatrix} \varepsilon_0 \\ \kappa \end{Bmatrix} dz dy dx \equiv b \int_x \begin{Bmatrix} \delta\varepsilon_0 \\ \delta\kappa \end{Bmatrix}^T \begin{bmatrix} A & B \\ B & D \end{bmatrix} \begin{Bmatrix} \varepsilon_0 \\ \kappa \end{Bmatrix} dx \tag{3.70}$$

where the laminate stiffness ABD matrix is obtained after the integration through the z occurs such as in **Eq. (3.64)**; also, $A = \begin{bmatrix} A_{11} & A_{12} \\ A_{12} & A_{22} \end{bmatrix}$, $B = \begin{bmatrix} B_{11} & B_{12} \\ B_{12} & B_{22} \end{bmatrix}$, and $D = \begin{bmatrix} D_{11} & D_{12} \\ D_{12} & D_{22} \end{bmatrix}$.

Accordingly, substituting with $\begin{Bmatrix} \varepsilon_0 \\ \kappa \end{Bmatrix} = \begin{bmatrix} D_p^0 \\ D_p^1 \end{bmatrix} \{\overline{u}_p\}$ from **Eq. (3.44)**, the final expression of the variational mechanical strain energy becomes:

$$\delta U_p = b \int_x \{\delta \overline{u}_p\}^T \begin{bmatrix} D_p^0 \\ D_p^1 \end{bmatrix}^T \begin{bmatrix} A & B \\ B & D \end{bmatrix} \begin{bmatrix} D_p^0 \\ D_p^1 \end{bmatrix} \{\overline{u}_p\} dx \tag{3.71}$$

The actuator configuration is determined by the method of applying the electric field to the PFRC laminate. The value of the electric field applied is determined by the derivative part of the proportional-derivative (PD) controller through a feedback control system [31]. The feedback signal to the actuator is implemented by specifying a velocity feedback control gain K_v.

As for the virtual work $\delta\hat{W}_p$, the electrical part of the strain energy is expressed as:

$$\delta\hat{W}_p = -\left(\int_{\upsilon} \delta\varepsilon_p{}^T \left[\overline{e}\right]_k^T E \, d\upsilon + \int_{\upsilon} E^T \left[\overline{d}\right]_k^T \delta E \, d\upsilon \right) \tag{3.72}$$

where $E = \begin{Bmatrix} 0 & 0 & E_z \end{Bmatrix}^T$. Since the electrical field E due to the applied voltage is constant and known (i.e., **Eq. 3.46**), the variation of the electrical field is $\delta E = 0$. Substituting the latter into **Eq. 3.72** yields:

$$\delta\hat{W}_p = -\int_{\upsilon} \delta\varepsilon_p{}^T \left[\overline{e}\right]_k^T E \, d\upsilon \tag{3.73}$$

Here, the same process is followed as in the mechanical part of the variation of strain energy. Replacing ε_p with **Eq. 3.44** and substituting the expression $\left[\overline{e}\right]_k^T E = \begin{Bmatrix} \tilde{e}_{31} E_z \\ 0 \end{Bmatrix}_k$ from **Eq. 3.53**, the above virtual work becomes:

$$\delta\hat{W}_p = -b \int_x \left\{\delta\overline{u}_p\right\}^T \begin{bmatrix} D_p^0 \\ D_p^1 \end{bmatrix}^T \begin{Bmatrix} N_x^p \\ 0 \\ M_x^p \\ 0 \end{Bmatrix} dx \tag{3.74}$$

where the electric field resultants N_x^p and M_x^p are obtained and used in a similar way as the ABD matrix from **Eq. 3.64**.

Chapter 4 Finite Element Modeling

The representation of the finite element model utilized in this thesis is shown in **Fig. 4.1** below.

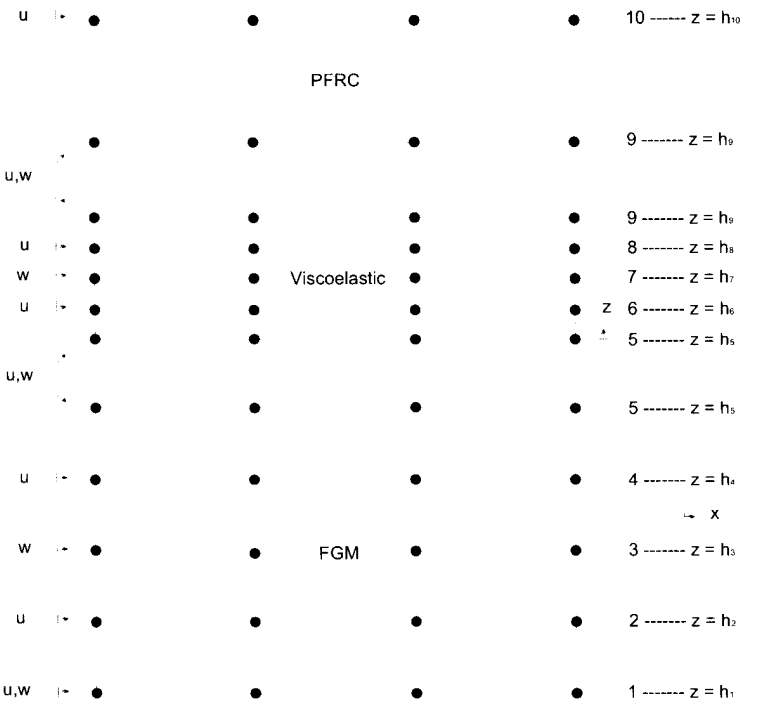

Figure 4.1: Schematic of a finite element

The element consists of four nodes along the span to allow for a cubic Lagrange interpolation of the field variable [32]. Each nodal variable, however, is also interpolated through the thickness with a cubic function for axial displacement and a quadratic function for transverse displacement in the host and viscoelastic layers, and a linear function for axial displacement in the PFRC laminate. As a result, ten points are selected through the thickness for each node, and they are denoted by $h_1, h_2 \ldots, h_{10}$. These points are located relative to the geometric mid-surface of the composite beam structure at $z = 0$.

The global displacement vector of an element is given as:

$$u^T = \{ u_1 \;\; w_1 \;\; u_2 \;\; w_3 \;\; u_4 \;\; u_5 \;\; w_5 \;\; u_6 \;\; w_7 \;\; u_8 \;\; u_9 \;\; w_9 \;\; u_{10} \} \tag{4.1}$$

where u_i and w_i are the axial and transverse displacement magnitudes, respectively, evaluated at the i^{th} position through the thickness.

From the above, it is determined that each node contains 13 degrees of freedom (DOF), resulting in 52 DOF for each element. Hence, the elemental displacement vector q_e can be written as:

$$q_e{}^T = \{q_{ij}\}^T = \{u_{11}\ w_{11}\ u_{21}\ w_{31}\ u_{41}\ u_{51}\ w_{51}\ u_{61}\ w_{71}\ u_{81}\ u_{91}\ w_{91}\ u_{10,1} \cdots \\ \cdots u_{14}\ w_{14}\ u_{24}\ w_{34}\ u_{44}\ u_{54}\ w_{54}\ u_{64}\ w_{74}\ u_{84}\ u_{94}\ w_{94}\ u_{10,4}\} \tag{4.2}$$

where the index $i = 1 \ldots 10$ represents the displacement occurring through the thickness and the index $j = 1 \ldots 4$ signifies the displacement at the node along the span.

As mentioned earlier in this chapter, the field variable is interpolated along the span of the structure using cubic Lagrange interpolation shape functions [32], which are the following:

$$\left.\begin{aligned} N_{1\xi} &= -\frac{(3\xi+1)(3\xi-1)(\xi-1)}{16} \\ N_{2\xi} &= \frac{9(\xi+1)(3\xi-1)(\xi-1)}{16} \\ N_{3\xi} &= -\frac{9(\xi+1)(3\xi+1)(\xi-1)}{16} \\ N_{4\xi} &= \frac{(\xi+1)(3\xi+1)(3\xi-1)}{16} \end{aligned}\right\} \quad for\ -1 \le \xi \le 1 \tag{4.3}$$

4.1 FGM Beam (Bottom Layer)

4.1.1 Mapping

The transformation through the thickness of the axial and transverse displacement is partitioned in the following way.

In terms of the defined coefficients, the transformation is, for the axial displacement:

$$\begin{Bmatrix} u_1 \\ u_2 \\ u_4 \\ u_5 \end{Bmatrix} = \begin{bmatrix} 1 & h_1 & h_1^2 & h_1^3 \\ 1 & h_2 & h_2^2 & h_2^3 \\ 1 & h_4 & h_4^2 & h_4^3 \\ 1 & h_5 & h_5^2 & h_5^3 \end{bmatrix} \begin{Bmatrix} a_0 \\ a_1 \\ a_2 \\ a_3 \end{Bmatrix} \tag{4.4}$$

from which,

$$\begin{Bmatrix} a_0 \\ a_1 \\ a_2 \\ a_3 \end{Bmatrix} = \begin{bmatrix} 1 & h_1 & h_1^2 & h_1^3 \\ 1 & h_2 & h_2^2 & h_2^3 \\ 1 & h_4 & h_4^2 & h_4^3 \\ 1 & h_5 & h_5^2 & h_5^3 \end{bmatrix}^{-1} \begin{Bmatrix} u_1 \\ u_2 \\ u_4 \\ u_5 \end{Bmatrix} = [T_b]_u \begin{Bmatrix} u_1 \\ u_2 \\ u_4 \\ u_5 \end{Bmatrix} \tag{4.5}$$

The transverse displacement is written as:

$$\begin{Bmatrix} w_1 \\ w_3 \\ w_5 \end{Bmatrix} = \begin{bmatrix} 1 & h_1 & h_1^2 \\ 1 & h_3 & h_3^2 \\ 1 & h_5 & h_5^2 \end{bmatrix} \begin{Bmatrix} l_0 \\ l_1 \\ l_2 \end{Bmatrix} \tag{4.6}$$

which implies that,

$$\begin{Bmatrix} l_0 \\ l_1 \\ l_2 \end{Bmatrix} = \begin{bmatrix} 1 & h_1 & h_1^2 \\ 1 & h_3 & h_3^2 \\ 1 & h_5 & h_5^2 \end{bmatrix}^{-1} \begin{Bmatrix} w_1 \\ w_3 \\ w_5 \end{Bmatrix} = [T_b]_w \begin{Bmatrix} w_1 \\ w_3 \\ w_5 \end{Bmatrix} \tag{4.7}$$

Combining **Eqs. 4.5** and **4.7** yields the following transformation matrix:

$$\{\overline{u}_b\} = \begin{Bmatrix} a_0 \\ a_1 \\ a_2 \\ a_3 \\ l_0 \\ l_1 \\ l_2 \end{Bmatrix} = \begin{bmatrix} [T_b]_u & [0] \\ [0]^T & [T_b]_w \end{bmatrix} \begin{Bmatrix} u_1 \\ u_2 \\ u_4 \\ u_5 \\ w_1 \\ w_3 \\ w_5 \end{Bmatrix} \equiv [T_b]\, u_b \tag{4.8}$$

where $[0]$ is a 4x3 zero matrix.

4.1.2 Shape Functions

The displacement vector $u_b^T = \{u_1\ u_3\ u_4\ u_5\ w_1\ w_3\ w_5\}$ can be expanded as:

$$u_b = [N_{b1} \quad N_{b2} \quad N_{b3} \quad N_{b4}]\, q_e = [N_b]\, q_e \tag{4.9}$$

where, for $j = 1 \ldots 4$,

$$[N_{bj}] = \begin{bmatrix} N_{j\xi} & 0 & 0 & 0 & 0 & 0 & 0 & 0 & 0 & 0 & 0 & 0 & 0 \\ 0 & 0 & N_{j\xi} & 0 & 0 & 0 & 0 & 0 & 0 & 0 & 0 & 0 & 0 \\ 0 & 0 & 0 & 0 & N_{j\xi} & 0 & 0 & 0 & 0 & 0 & 0 & 0 & 0 \\ 0 & 0 & 0 & 0 & 0 & N_{j\xi} & 0 & 0 & 0 & 0 & 0 & 0 & 0 \\ 0 & N_{j\xi} & 0 & 0 & 0 & 0 & 0 & 0 & 0 & 0 & 0 & 0 & 0 \\ 0 & 0 & 0 & N_{j\xi} & 0 & 0 & 0 & 0 & 0 & 0 & 0 & 0 & 0 \\ 0 & 0 & 0 & 0 & 0 & 0 & N_{j\xi} & 0 & 0 & 0 & 0 & 0 & 0 \end{bmatrix}$$

Substituting u_b from **Eq. 4.9** into **Eq. 4.8** yields the newly updated vector $\{\overline{u}_b\}$:

$$\{\overline{u}_b\} \equiv [T_b][N_b]\, q_e \tag{4.10}$$

Subsequently, substituting $\{\overline{u}_b\}$ from **Eq. 4.10** into **Eq. 3.11**, the variation of the kinetic energy of the FGM beam is finally given as:

$$\delta T_b = \rho_b b \int_{-1}^{1} \left(\delta q_e^T [N_b]^T [T_b]^T [I_b][T_b][N_b] \ddot{q}_e \right) J(\xi)\, d\xi = \delta q_e^T [M_b] \ddot{q}_e \tag{4.11}$$

where $[M_b] = \rho_b b \int_{-1}^{1} \left([N_b]^T [T_b]^T [I_b][T_b][N_b] \right) |J|\, d\xi$ is the mass matrix of the FGM beam.

In the above mass matrix formulation, $|J|$ is the absolute value of the determinant of the Jacobian matrix used to transform the variables from the global coordinate x to the local coordinate ξ. In other words, to perform finite element analysis, the element of length over which the integration is carried out along the $x-$axis needs to be expressed in terms of the local coordinate ξ with an appropriate change of limits of integration (– 1 and 1) [33].

The same process is followed in formulating the stiffness matrix by substituting $\{\overline{u}_b\}$ from **Eq. 4.10** into **Eq. 3.14**, the expression of the variational strain energy becomes:

$$\delta U_b = b \int_{-1}^{1} \left(\delta q_e^T [B_b]^T [C_b][B_b] \ddot{q}_e \right) |J|\, d\xi = \delta q_e^T [K_b] \ddot{q}_e \tag{4.12}$$

where the stiffness matrix of the FGM beam is $[K_b] = b \int_{-1}^{1} \left([B_b]^T [C_b][B_b] \right) |J|\, d\xi$, in which $[B_b] = [D_b][T_b][N_b]$.

Besides converting the limits of integration from in terms of the global coordinate x to the local coordinate ξ, another transformation has to take place for the stiffness matrix to be evaluated. Since the shape functions matrix $[N_b]$ is defined in terms of the local coordinate, it is necessary to express the global derivative matrix $[D_b]$ in terms of the local derivative.

4.2 Viscoelastic Layer (Core)

4.2.1 Mapping

The transformation through the thickness of the axial and transverse displacement is expressed in a similar form to that of the bottom layer:

For the axial displacement,

$$\begin{Bmatrix} u_5 \\ u_6 \\ u_8 \\ u_9 \end{Bmatrix} = \begin{bmatrix} 1 & h_5 & h_5^2 & h_5^3 \\ 1 & h_6 & h_6^2 & h_6^3 \\ 1 & h_8 & h_8^2 & h_8^3 \\ 1 & h_9 & h_9^2 & h_9^3 \end{bmatrix} \begin{Bmatrix} c_0 \\ c_1 \\ c_2 \\ c_3 \end{Bmatrix} \tag{4.13}$$

Taking inverse of the above equation yields,

$$\begin{Bmatrix} c_0 \\ c_1 \\ c_2 \\ c_3 \end{Bmatrix} = \begin{bmatrix} 1 & h_5 & h_5^2 & h_5^3 \\ 1 & h_6 & h_6^2 & h_6^3 \\ 1 & h_8 & h_8^2 & h_8^3 \\ 1 & h_9 & h_9^2 & h_9^3 \end{bmatrix}^{-1} \begin{Bmatrix} u_5 \\ u_6 \\ u_8 \\ u_9 \end{Bmatrix} = [T_c]_u \begin{Bmatrix} u_5 \\ u_6 \\ u_8 \\ u_9 \end{Bmatrix} \tag{4.14}$$

The transverse displacement is:

$$\begin{Bmatrix} w_5 \\ w_7 \\ w_9 \end{Bmatrix} = \begin{bmatrix} 1 & h_5 & h_5^2 \\ 1 & h_7 & h_7^2 \\ 1 & h_9 & h_9^2 \end{bmatrix} \begin{Bmatrix} m_0 \\ m_1 \\ m_2 \end{Bmatrix} \tag{4.15}$$

from which,

$$\begin{Bmatrix} m_0 \\ m_1 \\ m_2 \end{Bmatrix} = \begin{bmatrix} 1 & h_5 & h_5^2 \\ 1 & h_7 & h_7^2 \\ 1 & h_9 & h_9^2 \end{bmatrix}^{-1} \begin{Bmatrix} w_5 \\ w_7 \\ w_9 \end{Bmatrix} = [T_c]_w \begin{Bmatrix} w_5 \\ w_7 \\ w_9 \end{Bmatrix} \tag{4.16}$$

Eqs. 4.14 and **4.16** are combined and expressed as follows:

$$\{\overline{u}_c\} = \begin{Bmatrix} c_0 \\ c_1 \\ c_2 \\ c_3 \\ m_0 \\ m_1 \\ m_2 \end{Bmatrix} = \begin{bmatrix} [T_c]_u & [0] \\ [0]^T & [T_c]_w \end{bmatrix} \begin{Bmatrix} u_5 \\ u_6 \\ u_8 \\ u_9 \\ w_5 \\ w_7 \\ w_9 \end{Bmatrix} \equiv [T_c]\, u_c \tag{4.17}$$

where $[0]$ is a 4x3 zero matrix.

4.2.2 Shape Functions

Similar to the bottom layer, the displacement vector $u_c^T = \{u_5\ u_6\ u_8\ u_9\ w_5\ w_7\ w_9\}$ is expressed as:

$$u_c = [N_{c1} \quad N_{c2} \quad N_{c3} \quad N_{c4}]\, q_e = [N_c]\, q_e \tag{4.18}$$

where, for $j = 1 \ldots 4$,

$$\left[N_{cj}\right] = \begin{bmatrix} 0 & 0 & 0 & 0 & 0 & N_{j\xi} & 0 & 0 & 0 & 0 & 0 & 0 & 0 \\ 0 & 0 & 0 & 0 & 0 & 0 & 0 & N_{j\xi} & 0 & 0 & 0 & 0 & 0 \\ 0 & 0 & 0 & 0 & 0 & 0 & 0 & 0 & 0 & N_{j\xi} & 0 & 0 & 0 \\ 0 & 0 & 0 & 0 & 0 & 0 & 0 & 0 & 0 & 0 & N_{j\xi} & 0 & 0 \\ 0 & 0 & 0 & 0 & 0 & 0 & N_{j\xi} & 0 & 0 & 0 & 0 & 0 & 0 \\ 0 & 0 & 0 & 0 & 0 & 0 & 0 & 0 & N_{j\xi} & 0 & 0 & 0 & 0 \\ 0 & 0 & 0 & 0 & 0 & 0 & 0 & 0 & 0 & 0 & 0 & N_{j\xi} & 0 \end{bmatrix}$$

Substituting u_c from **Eq. 4.18** into **Eq. 4.17** yields:

$$\{\overline{u}_c\} \equiv [T_c][N_c]\, q_e \tag{4.19}$$

Similarly, the anelastic displacement vector $\{\tilde{u}_c(t)\}$, which depends on the displacement history, can be expressed as:

$$\{\tilde{u}_c\} \equiv [T_c][N_c]\, \tilde{q}_e \tag{4.20}$$

Following Bekuit's thesis [8], and substituting **Eq. 4.20** at a given time t into **Eq. (3.28)**, $\tilde{q}_e(t)$ can be computed to obtain a similar expression as in [8]:

$$\tilde{q}_e(t) = (1-\eta)\frac{E_\infty - E_0}{E_\infty}\overline{q}_e(t) - \eta\sum_{j=1}^{N_t}\left(\prod_{p=1}^{j}\frac{p-\alpha-1}{p}\right)\tilde{q}_e(t - j\Delta t) \tag{4.21}$$

Next, substituting $\{\overline{u}_c\}$ from **Eq. 4.19** into **Eq. 3.33**, the variational kinetic energy of the viscoelastic core is given in its final form as:

$$\delta T_c = \rho_c b \int_{-1}^{1}\left(\delta q_e^T [N_c]^T [T_c]^T [I_c][T_c][N_c]\ddot{q}_e\right)|J|\, d\xi = \delta q_e^T [M_c]\ddot{q}_e \tag{4.22}$$

where $[M_c] = \rho_c b \int_{-1}^{1} \left([N_c]^T [T_c]^T [I_c][T_c][N_c] \right) |J| d\xi$ is the mass matrix of the viscoelastic core and the Jacobian $|J|$ follows the same principle as that of the FGM beam.

Substituting $\{\overline{u}_c\}$ from **Eq. 4.19** into **Eq. 3.37**, the expression of the variational strain energy gives:

$$\delta \bar{U}_c(t) = b \int_{-1}^{1} \left(\delta q_e^T [B_c]^T [C_c][B_c] \ddot{q}_e \right) |J| d\xi = \delta q_e^T [K_c] \ddot{q}_e \tag{4.23}$$

where the stiffness matrix of the viscoelastic layer is $[K_c] = b \int_{-1}^{1} \left([B_c]^T [C_c][B_c] \right) |J| d\xi$, in which $[B_c] = [D_c][T_c][N_c]$. As mentioned before, the same coordinate transformations are followed via the Jacobian as in the FGM beam subsection.

Similarly, the variation of the anelastic strain energy is determined by replacing $\{\overline{u}_c\}$ in **Eq. 3.38** with **Eq. 4.19**. Thus,

$$\delta \tilde{U}_c(t) = b \int_{-1}^{1} \left(\delta q_e^T [B_c]^T \left[\tilde{C}_c \right][B_c] \ddot{q}_e \right) |J| d\xi = \delta q_e^T \left[\tilde{K}_c \right] \ddot{q}_e \tag{4.24}$$

where the anelastic part of the stiffness matrix of the viscoelastic layer can be written as:

$$\left[\tilde{K}_c \right] = b \int_{-1}^{1} \left([B_c]^T \left[\tilde{C}_c \right][B_c] \right) |J| d\xi .$$

From **Eq. 3.38**, it is also concluded that $\left[\tilde{K}_c \right] = \eta \frac{E_\infty - E_0}{E_0} [K_c]$.

Lastly, substituting for $\{\tilde{u}_c(t)\}$ from **Eq. 4.20** into **Eq. 3.39** results in the following final form of the variation of work $\delta\tilde{W}_c(t)$:

$$\delta\tilde{W}_c(t) = \eta\frac{E_\infty}{E_0}\sum_{j=1}^{N_t}\left(\prod_{p=1}^{j}\frac{p-\alpha-1}{p}\right)\times b\int_{-1}^{1}\left(\delta q_e^T[B_c]^T[C_c][B_c]\{\tilde{q}_e(t-j\Delta t)\}\right)|J|d\xi = \delta q_e^T\tilde{F}_c(t) \tag{4.25}$$

where the induced force in the viscoelastic layer is:

$$\tilde{F}_c(t) = \eta\frac{E_\infty}{E_0}[K_c]\sum_{j=1}^{N_t}\left(\prod_{p=1}^{j}\frac{p-\alpha-1}{p}\right)\times\{\tilde{q}_e(t-j\Delta t)\}.$$

4.3 PFRC Laminate (Top Layer)

4.3.1 Mapping

The transformation through the thickness of the displacement vector takes the following form for the top constraining layer:

$$u_p = \begin{Bmatrix} u_9 \\ w_9 \\ u_{10} \end{Bmatrix} = \begin{bmatrix} 1 & h_9 & 0 \\ 0 & 0 & 1 \\ 1 & h_{10} & 0 \end{bmatrix}\begin{Bmatrix} e_0 \\ e_1 \\ n_0 \end{Bmatrix} \tag{4.26}$$

Solving for coefficients e_0, e_1 and n_0 yields:

$$\{\bar{u}_p\} = \begin{Bmatrix} e_0 \\ e_1 \\ n_0 \end{Bmatrix} = \begin{bmatrix} 1 & h_9 & 0 \\ 0 & 0 & 1 \\ 1 & h_{10} & 0 \end{bmatrix}^{-1}\begin{Bmatrix} u_9 \\ w_9 \\ u_{10} \end{Bmatrix} \equiv [T_p]u_p \tag{4.27}$$

Following the same process as for the other two layers, the displacement vector $u_p^T = \{u_9 \; w_9 \; u_{10}\}$ can be expanded in the form:

$$u_p = \begin{bmatrix} N_{p1} & N_{p2} & N_{p3} & N_{p4} \end{bmatrix} q_e = \begin{bmatrix} N_p \end{bmatrix} q_e \tag{4.28}$$

where, for $j = 1 \ldots 4$,

$$\begin{bmatrix} N_{pj} \end{bmatrix} = \begin{bmatrix} 0 & 0 & 0 & 0 & 0 & 0 & 0 & 0 & 0 & 0 & N_{j\xi} & 0 & 0 \\ 0 & 0 & 0 & 0 & 0 & 0 & 0 & 0 & 0 & 0 & 0 & N_{j\xi} & 0 \\ 0 & 0 & 0 & 0 & 0 & 0 & 0 & 0 & 0 & 0 & 0 & 0 & N_{j\xi} \end{bmatrix}$$

Substituting for u_p from **Eq. 4.28** in **Eq. 4.27** produces the following modified vector $\{\overline{u}_p\}$:

$$\{\overline{u}_p\} \equiv \begin{bmatrix} T_p \end{bmatrix} \begin{bmatrix} N_p \end{bmatrix} q_e \tag{4.29}$$

Afterwards, substituting $\{\overline{u}_p\}$ from **Eq. 4.29** into **Eq. 3.66**, the variation of kinetic energy of the PFRC laminate is given as:

$$\delta T_p = \rho_p b \int_{-1}^{1} \left(\delta q_e^T \begin{bmatrix} N_p \end{bmatrix}^T \begin{bmatrix} T_p \end{bmatrix}^T \begin{bmatrix} I_p \end{bmatrix} \begin{bmatrix} T_p \end{bmatrix} \begin{bmatrix} N_p \end{bmatrix} \ddot{q}_e \right) |J| d\xi = \delta q_e^T \begin{bmatrix} M_p \end{bmatrix} \ddot{q}_e \tag{4.30}$$

where $\begin{bmatrix} M_p \end{bmatrix} = \rho_p b \int_{-1}^{1} \left(\begin{bmatrix} N_p \end{bmatrix}^T \begin{bmatrix} T_p \end{bmatrix}^T \begin{bmatrix} I_p \end{bmatrix} \begin{bmatrix} T_p \end{bmatrix} \begin{bmatrix} N_p \end{bmatrix} \right) |J| d\xi$ is the mass matrix of the PFRC laminate and $|J|$ is the Jacobian.

Similarly, replacing $\{\overline{u}_p\}$ in **Eq. 3.71** and **Eq. 3.74** with **Eq. 4.29** yields the following expressions of the variation of strain energy δU_p and virtual work $\delta \hat{W}_p$ in the PFRC laminate:

$$\delta U_p = b\int_{-1}^{1}\left(\delta q_e^T \left[B_p\right]^T \begin{bmatrix} A & B \\ B & D \end{bmatrix} \left[B_p\right] \ddot{q}_e\right)|J|d\xi = \delta q_e^T \left[K_p\right] \ddot{q}_e \tag{4.31}$$

$$\delta \hat{W}_p = -b\int_{-1}^{1} \delta q_e^T \left[B_p\right]^T \begin{Bmatrix} N_x^p \\ 0 \\ M_x^p \\ 0 \end{Bmatrix} |J|d\xi = \delta q_e^T \hat{F}_p \tag{4.32}$$

where the stiffness matrix is $\left[K_p\right] = b\int_{-1}^{1}\left(\left[B_p\right]^T \begin{bmatrix} A & B \\ B & D \end{bmatrix} \left[B_p\right]\right)|J|d\xi$ and the induced force in the top layer is $\hat{F}_p = -b\int_{-1}^{1}\left[B_p\right]^T \begin{Bmatrix} N_x^p \\ 0 \\ M_x^p \\ 0 \end{Bmatrix} |J|d\xi$ with $\left[B_p\right] = \begin{bmatrix} D_p^0 \\ D_p^1 \end{bmatrix}\left[T_p\right]\left[N_p\right]$.

4.4 External Force

Apart from the viscoelastic and PFRC laminate work contributions, the virtual work done by the external force F_e, which is applied at a certain position ξ_f in an element, is written as:

$$\delta W_e = \delta q_e^T F_e \int_{-1}^{1} \left[N\right]^T \mathsf{M}^T \delta(\xi - \xi_f) d\xi \tag{4.33}$$

where $\left[N\right] = \left[N_{1\xi} I \quad N_{2\xi} I \quad N_{3\xi} I \quad N_{4\xi} I\right]$ with a 13x13 identity matrix I and $\mathsf{M} = \left[0 \quad 0 \quad 0 \quad 0 \quad 0 \quad 0 \quad 0 \quad 0 \quad 0 \quad 0 \quad 0 \quad 1 \quad 0\right]$ is a Boolean mapping vector, which shows that the virtual displacement is δw_9.

4.5 Numerical Integration

A standard four point Gauss quadrature has been adopted here to numerically determine the integrals of the above functions of the variable ξ. Specifically,

$$\int_{-1}^{1} f(\xi)\, d\xi = \sum_{1}^{4} H_i f(\xi_i) \tag{4.34}$$

The positions, ξ_i, and weight coefficients, H_i, of the Gaussian quadrature are given in [33]. The integrals from **Eqs. 4.11, 4.12, 4.22, 4.23, 4.30, 4.31, 4.32** and **4.33** are evaluated using this principle.

4.6 Equation of Motion

Following the extended Hamilton's principle from **Eq. 3.9**, the element governing equation of motion can be written as:

$$\left(\left[M_b\right]+\left[M_c\right]+\left[M_p\right]\right)\ddot{q}_e(t)+\left(\left[K_b\right]+\left[K_c\right]+\left[\tilde{K}_c\right]+\left[K_p\right]\right)q_e(t)=F_e(t)+\tilde{F}_c(t)+\hat{F}_p(t) \tag{4.35}$$

where the modified loading $\tilde{F}_c$ in the viscoelastic core becomes negative when moved to the right-hand-side of the equation.

Once the elemental mass and stiffness matrices and force vectors are determined using the Gaussian quadrature, as was mentioned in the previous section, the global equation of motion can be assembled using the finite element technique [32] and may be written as:

$$\left[\boldsymbol{M}\right]\ddot{\boldsymbol{q}}(t)+\left[\boldsymbol{K}\right]\boldsymbol{q}(t)=\boldsymbol{F}(t)+\tilde{\boldsymbol{F}}(t)+\hat{\boldsymbol{F}}(t) \tag{4.36}$$

where $\left[\boldsymbol{M}\right]$, $\left[\boldsymbol{K}\right]$, $\boldsymbol{F}$, $\tilde{\boldsymbol{F}}$ and $\hat{\boldsymbol{F}}$ represent the global mass matrix, stiffness matrix, external force vector, viscoelastic force vector and electrical force vector, respectively.

The Newmark time-integration scheme [32, 34] is used to solve the assembled global equation of motion, **Eq. 4.36**, after applying the boundary conditions. Some modifications are carried out in this classical algorithm to incorporate the viscoelastic property of the core in fractional calculus. The anelastic displacement history is stored as a new parameter in a matrix. The Newmark parameters $\beta = 1/4$ and $\gamma = 1/2$ are used in order to obtain an unconditionally stable and second-order accurate scheme [19] (See Appendix A for flow charts of the algorithm utilized in solving the above equation.) The three-layer model has been simulated using Matlab software (Refer to Appendix C for Matlab codes.) In addition, the explanation on how the matrix B is implemented into the code for all three layers is given in Appendix B.

Chapter 5 Numerical Simulation

A number of simulation tests must be performed in order to verify the resulting global equation assembled in the previous section. First, the current formulation is modified so as to be compared to a problem in the literature, such as a sandwich beam with a viscoelastic core [19] or a cantilever beam with a piezoelectric top layer [8]. Second, the results of the effects of different parameter changes are analyzed and verified for consistency. Note that, in the parametric study, only the current formulation is used: FGM beam with the viscoelastic core and the PFRC laminate top-constraining layer.

5.1 Comparison with Results in the Literature

5.1.1 Viscoelastic-Aluminum Sandwich Beam

As was mentioned earlier, an example from the literature [19] is used in this section to demonstrate the effectiveness of the current Quasi-2D formulation modified to include only an isotropic sandwich beam with a viscoelastic core. In the example, a cantilevered sandwich beam with viscoelastic core and symmetrical aluminum faces is as shown in **Fig. 5.1(a)**. It is discretized along its length with five finite elements and a transverse load is applied to the free end in the form of a triangular impulse as shown in the **Fig. 5.1(b)**.

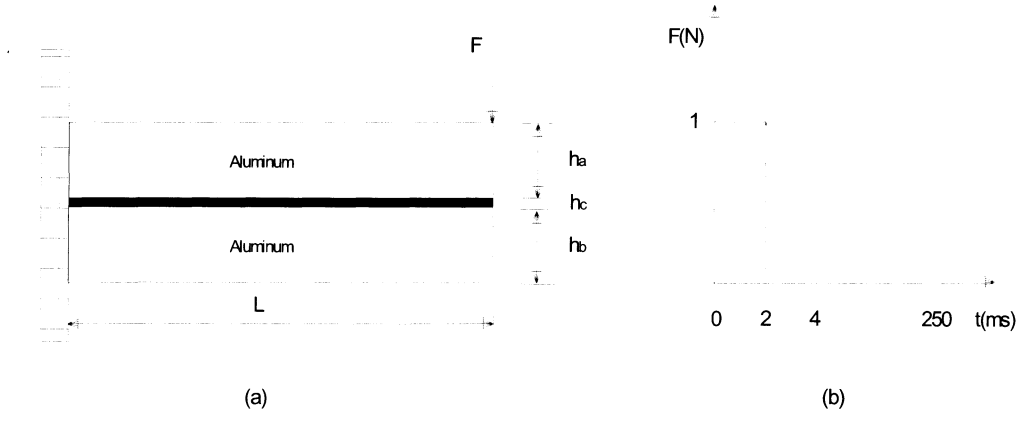

Figure 5.1: Viscoelastic-aluminum sandwich beam

The geometry of the beam comprises: $L = 200$ mm as the length, $b = 10$ mm as the width, $h_a = h_b = 1$ mm as the thickness of the top and bottom layers, and $h_c = 0.2$ mm as

the core thickness. The mechanical properties of the elastic faces and the viscoelastic core along with the fractional derivative model parameters are tabulated in **Table 5.1** below. The time step is taken from the example as $\Delta t = 0.25$ ms and the number of terms in the Grünwald approximation $N = 1000$.

Table 5.1: Mechanical properties of the viscoelastic-aluminum sandwich beam.

ALUMINIUM			ISD112 (at 27° C)					
ρ	ν	E	ρ	ν	E_0	E_∞	α	τ
kg/m^3		GPa	kg/m^3		MPa			ms
2690	0.345	70.3	1600	0.5	1.5	69.9495	0.7915	1.4052×10^{-2}

The transverse displacement history of the beam's tip is depicted in **Fig. 5.2** for the cantilevered fully-clamped case. The dynamic response of the Quasi-2D formulation with constant transverse displacement w in the host (bottom) layer falls between the conventional method [19] and the Quasi-2D with varying w responses. The phase shift between each method is explained by the degree of accuracy each formulation adheres to. The accuracy level can be determined by the number of degrees of freedom chosen for each element in the following order: 8 DOF for the conventional method, 36 DOF for the Quasi-2D with constant w, and 52 DOF for the Quasi-2D with varying w. The greater the number of DOF means the higher the accuracy of the model. The above mentioned phase shift can be decreased by reducing the aspect ratio (height/length) of the host beam and, hence, eliminating the need for quadratic through-the-thickness interpolation of the displacement, as is in the case of the Quasi-2D with constant w.

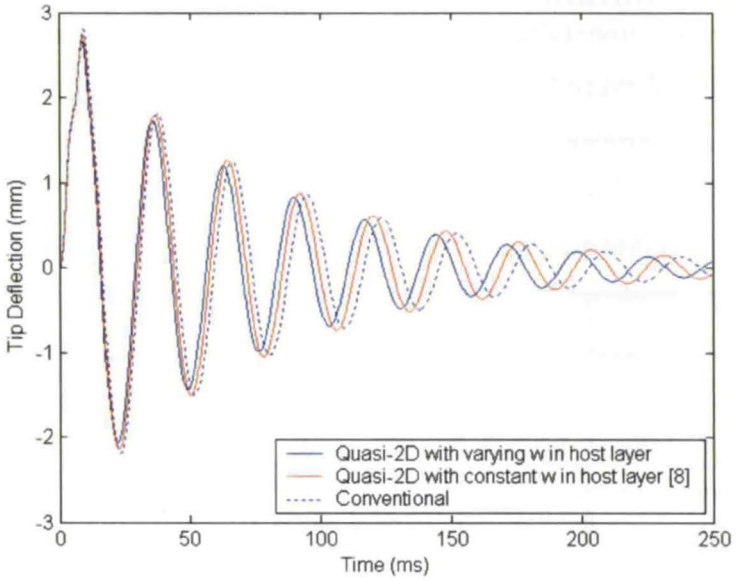

Figure 5.2: Dynamic response of viscoelastic sandwich beam fully-clamped

Fig. 5.3 describes the comparison between the fully-clamped and partially-clamped boundary conditions of the Quasi-2D method with a varying transverse displacement in the host beam. In the fully-clamped case, one end of the beam is fully supported, while in the partially-clamped example, both elastic faces are supported and the viscoelastic core is free at both ends. Both examples depict the same transverse displacement magnitude and phase, which confirms that the beam is not flexible enough to show any dependency on the type of boundary condition where there is a lack of constraint on one end of the viscoelastic core. The reason for the response to overlap could be due to the small thickness of the viscoelastic core relative to the top and bottom sandwich layers.

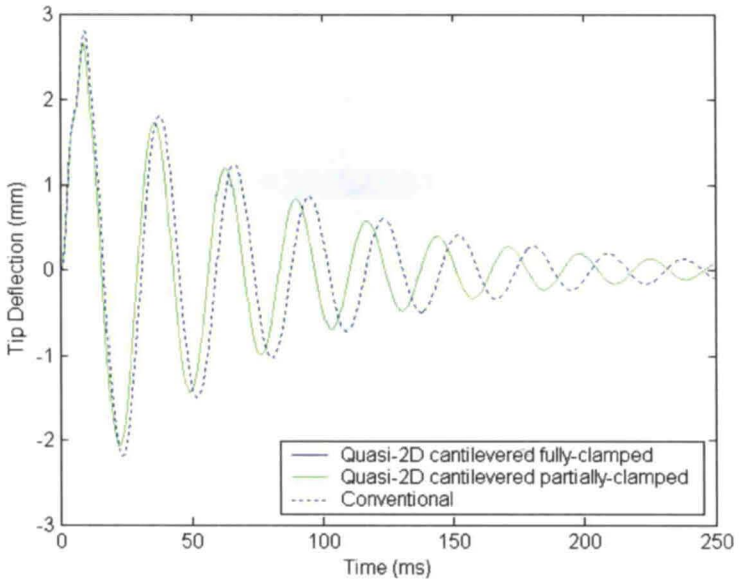

Figure 5.3: Dynamic response of viscoelastic sandwich beam with varying w in host layer

5.1.2 Cantilevered Beam with Viscoelastic Core and Piezoelectric Constraining Layer

Another example is taken from the literature to verify the accuracy of the current Quasi-2D formulation, which is modified to consist of an isotropic bottom layer, a viscoelastic core, and a piezoelectric top constraining-layer, as was the case in the work by Bekuit [8]. This configuration is shown in **Fig. 5.4**. The triangular impulse load applied at the free end is that depicted in **Fig. 5.1(b)**.

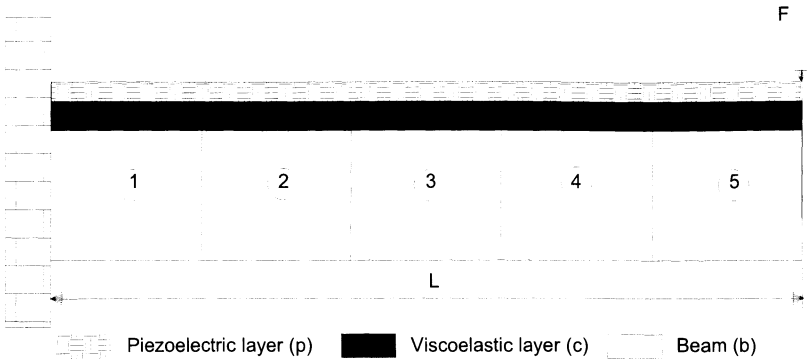

Figure 5.4: Beam with viscoelastic core and piezoelectric constraining layer

The beam has the following geometrical parameters: $L = 300$ mm (length), $b = 15$ mm (width), $h_b = 3$ mm (thickness of host layer), $h_p = 1$ mm (thickness of the piezoelectric layer) and $h_c = 0.2$ mm (core thickness). In the example, the time step is taken as $\Delta t = 0.001$ s and the number of terms in the Grünwald approximation of the fractional derivative $N = 500$. The mechanical properties of the beam are tabulated in **Table 5.2**. The viscoelastic properties of the core are as tabulated in **Table 5.1**.

Table 5.2: Mechanical and piezoelectric characteristics of the cantilever beam.

ALUMINIUM			PZT5H							
ρ	ν	E	ρ	c_{11}	c_{13}	c_{33}	c_{66}	e_{31}	e_{33}	d_{33}
kg/m^3		GPa	kg/m^3	GPa				C/m^2		F/m
2690	0.345	70.3	7500	126	84.1	117	23	−6.5	23.3	1.3×10^{-8}

The results of the controlled tip deflection and the actuation voltage are obtained for both Quasi-2D formulations with constant and varying w in the host beam and are plotted in **Fig. 5.5**. The formulation with constant w is from the work by Bekuit [8]. As seen from the graph, the dynamic responses for both cases are essentially the same, which

establishes the consistency of the current formulation with the published results. To further enhance the phase shift between the two examples, as was observed in the case of viscoelastic-aluminum sandwich beam in **Fig. 5.1**, the gain is set to be $K_v = 0$. Zero gain indicates passive damping of the beam, which results solely from the viscoelastic core. Hence, the difference between the two responses is readily observed in **Fig. 5.6(a)** as the system takes longer time to dampen. Also, in **Fig. 5.6(b)**, the phase shift is even more distinguished due to the greater thickness of the host beam h_b, in which case it is recommended for transverse displacement to be interpolated quadratically to ensure higher accuracy.

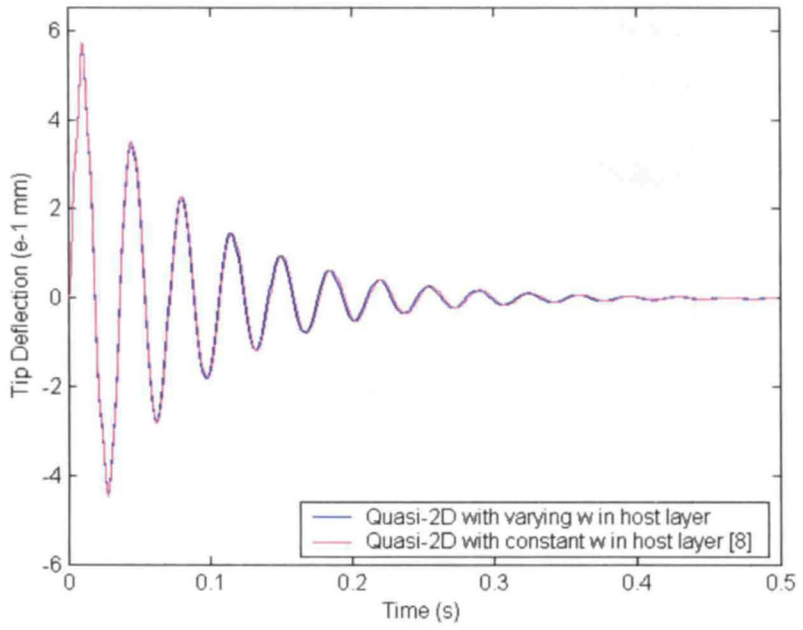

a) Tip deflection controlled with $K_v = 150$ V/(m/s)

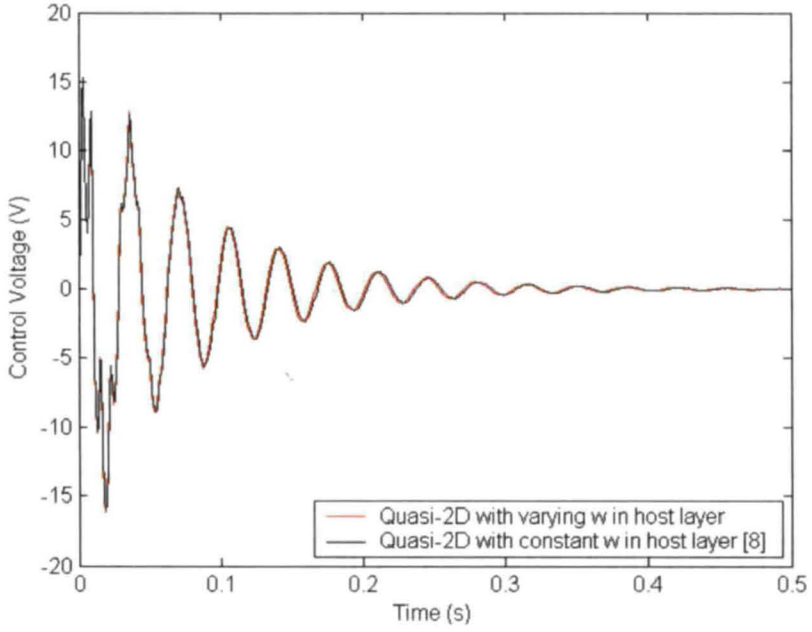

b) Actuator voltage

Figure 5.5: Tip deflection and control voltage of the Quasi-2D formulation with a PZT5H top layer.

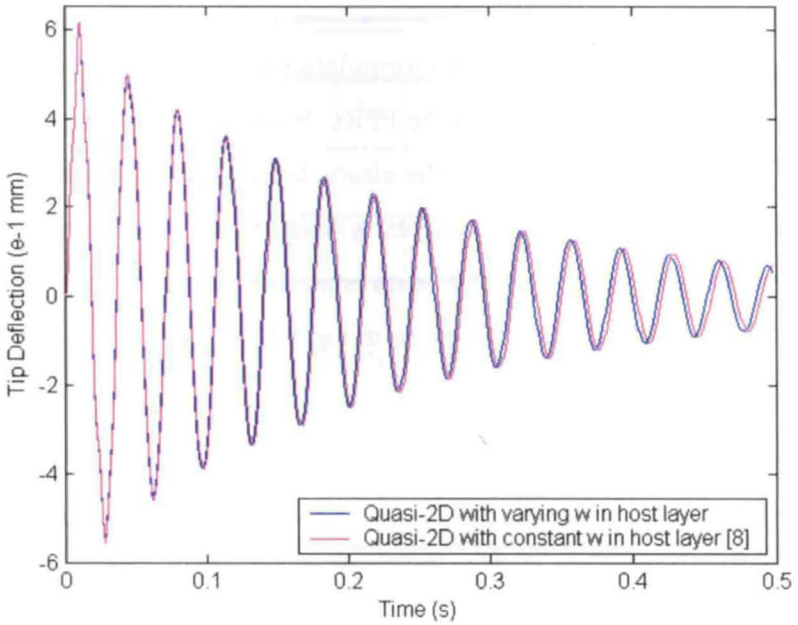

a) Passive damping with $h_b = 3$ mm

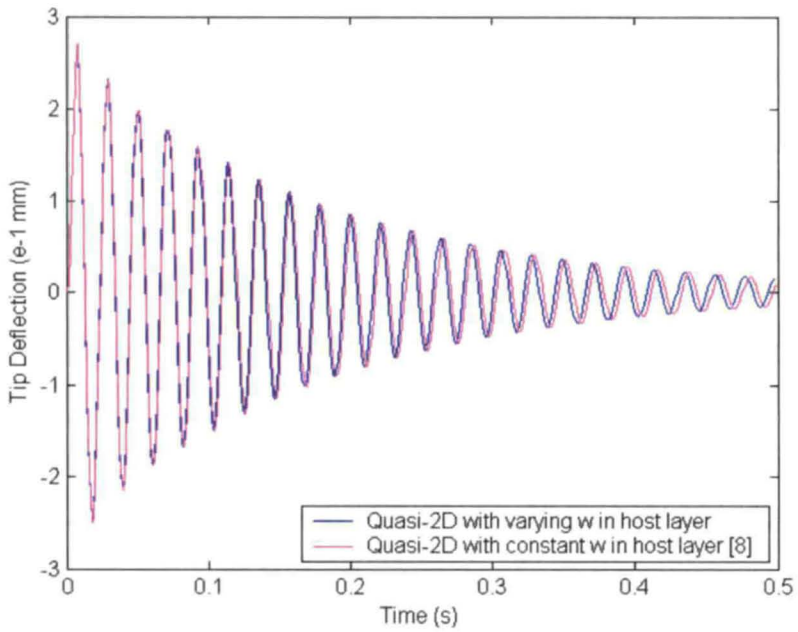

b) Passive damping with $h_b = 5$ mm

Figure 5.6: Tip deflection of the Quasi-2D formulation observed in a shorter time period in a *passive* case.

5.2 *Parametric Study*

In this section, the current Quasi-2D formulation is used in a parametric study. The parameters of interest are ply angle θ in the PFRC laminate and Young's modulus E in the host beam. As mentioned previously, the elastic layer or the host beam is made of FGM and is treated with the viscoelastic layer, which, in turn, is covered by the PFRC laminate, as seen in **Fig. 5.7(a)** below. The beam is meshed with five finite elements along the span. The triangular impulse load is given in **Fig. 5.7(b).**

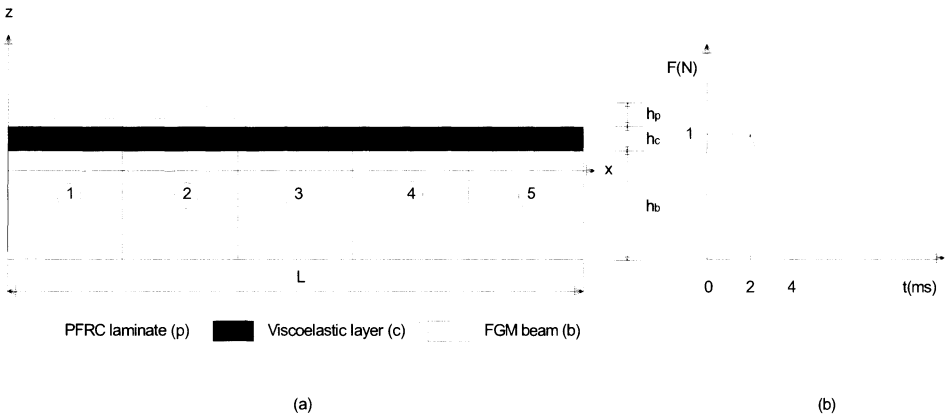

Figure 5.7: Beam with viscoelastic core and PFRC laminate top constraining layer

The geometric characteristics of the composite beam are the following: $L = 300$ mm (length), $b = 15$ mm (width), $h_b = 3.75$ mm (thickness of host layer), $h_p = 1$ mm (thickness of the PFRC layer) and $h_c = 0.25$ mm (core thickness). The mechanical and piezoelectric properties of the host beam and top-constraining layer, respectively, are given in the **Table 5.3** below, and the viscoelastic parameters of ISD112 are listed in **Table 5.1** in the previous section. The piezoelectric fibers and the matrix of the PFRC laminate are made of PZT5H and epoxy, respectively. The effective coefficients of PFRC employed in this thesis were predicted using the micromechanical analysis performed by Mallik and Ray in [25], while considering the 40% fiber volume fraction.

Table 5.3: Elastic and PFRC properties of the beam.

FGM			PZT5H/EPOXY							
ρ	ν	E_{avg}	ρ	c_{11}	c_{12}	c_{22}	c_{44}	$c_{55}=c_{66}$	e_{31}	d_{33}
kg/m^3		GPa	kg/m^3	GPa					C/m^2	F/m
2690	0.345	70.3	3640	32.6	4.3	7.2	1.05	1.29	−6.76	10.64×10^{-9}

Note from the above table that Young's modulus is chosen as an average value, which is achieved by integrating the varying elastic modulus through the thickness of the host beam. The average E in this case is the elastic modulus of the aluminum material. However, the elastic modulus is varied across the thickness of the beam by manipulating the functional gradient λ. The greater the gradient indicates the higher the increase or decrease of stiffness from the bottom to the top surface of the host layer.

With regard to the support mechanism, three types of supports are studied in each subsection, including the cantilevered, fixed-end and simply-supported beams. For each case, the effects of ply orientation in the PFRC laminate and functional gradient λ in the host layer are examined. A simple velocity feedback is adopted for the controlled vibration. See the algorithm flow chart in Appendix A for further explanation.

5.2.1 Effect of Ply Orientation

In order to examine the effect of ply orientation on the dynamic response of the beam, parameters, like the Young's modulus in the host layer and the number of plies in the top layer are fixed or unchanged. A six-ply quasi-isotropic PFRC laminate with the stacking sequence $[0°/\theta/-\theta/-\theta/\theta/0°]$, where angle θ is the fiber angle relative to the $+x$ axis of each layer, is used. The sequence may be abbreviated to its short form notation of $[0°/\pm\theta]_S$, where subscript S denotes symmetry. The shorthand notation is to be used in the subsequent investigations of different ply angles.

As mentioned earlier, the functional gradient $\lambda = 0$ in the FGM beam, which indicates that the elastic modulus is constant throughout the host beam and its material is homogeneous isotropic.

5.2.1.1 Cantilevered Beam Case

The cantilevered beam is supported at the left-hand end and free at the other as seen in the **Fig. 5.8**.

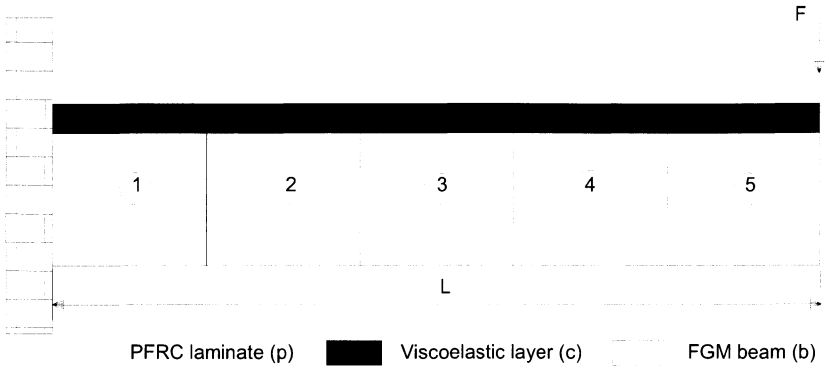

Figure 5.8: Schematic of a cantilevered beam fully-clamped and entirely covered with ACLD treatment.

The gain is set to $K_v = 350$ V/(m/s) , which is chosen only to best represent the effects, since the use of higher gain is permitted given that the resulting actuation voltage is not in the breakdown voltage range, which is approximately 200 V for most piezoelectric ceramics. The observation time of the beam subjected to an impulse load is taken to be 1 second. According to fast Fourier Transform (FFT) analysis, the time step is chosen to be $\Delta t = 0.001$ s and the resulting number of terms in the Grünwald approximation of the fractional derivative $N = 1000$. The load is the triangular impulse force applied at the free tip of the beam and given in **Fig. 5.7(b).**

For various ply orientations, **Fig. 5.9** shows the plot of uncontrolled transverse displacement of the node on the tip of the beam for the case of only passive damping. **Figs. 5.10** and **5.11** depict the controlled tip deflection and the corresponding actuation voltage, respectively, for each angle θ arrangement. Comparing **Figs. 5.9** and **5.10**, the effectiveness of the active-passive combination of damping is readily noted over the employment of only a passive element. The responses are independent of the boundary conditions (i.e., fully-clamped or partially-clamped). This could be due to a very small

thickness of the viscoelastic layer, which would not be thick enough to increase flexibility of the beam in the case of partially-clamped boundary conditions.

The PFRC laminate acts as one layer with longitudinal piezoelectric fibers when the angle θ is zero for each ply (See **Figs. 5.9(a), 5.10(a)** and **5.11(a).**) **Figs. 5.9(b), 5.9(c)** and **5.9(d)** depict the results for the following angle orientation: $[0°/\pm 90°]_S$, $[0°/\pm 60°]_S$ and $[0°/\pm 45°]_S$ respectively. The same ply orientation order and stacking sequence are followed in **Figs. 5.10(b), 5.10(c)** and **5.10(d)** for actively controlled deflection and in **Figs. 5.11(b), 5.11(c)** and **5.11(d)** for actuator voltage response. The response in **Fig. 5.10(b)** shows a faster damping of the transverse displacement magnitude with a bit of higher initial response than in **Fig. 5.10(a).** In the passive case of **Fig. 5.9**, the better result in terms of damping occurs with a zero angle θ in each ply, as the fibers with zero degree orientation fully contribute to the bending resistance, while fibers with $\theta = 90°$ do not. However, since piezoelectric fibers in **Fig. 5.10** act as actuators by manipulating the PFRC laminate, the above observation no longer applies and a better damping result occurs, instead, in **Fig. 5.10(b).** In this response, fibers with $\theta = 90°$ increase the flexibility of the beam, which, in turn, enables the constraining layer to be more apt for control.

The response in **Fig. 5.10(c)** is worse than in **Fig. 5.10(a)** in terms of attenuation, while the result of **Fig. 5.10(d)** exhibits the least damping and does not reasonably attenuate the vibration with the observation time of 1 second. The reason could be due to the relatively low contribution to the bending stiffness matrix D. The actuator voltage responses in **Fig. 5.11** correspond to the deflection responses in **Fig. 5.10** because of their linear relationship to response velocity. It can be noted that the magnitudes of the voltages are well below the breakdown value of 200V.

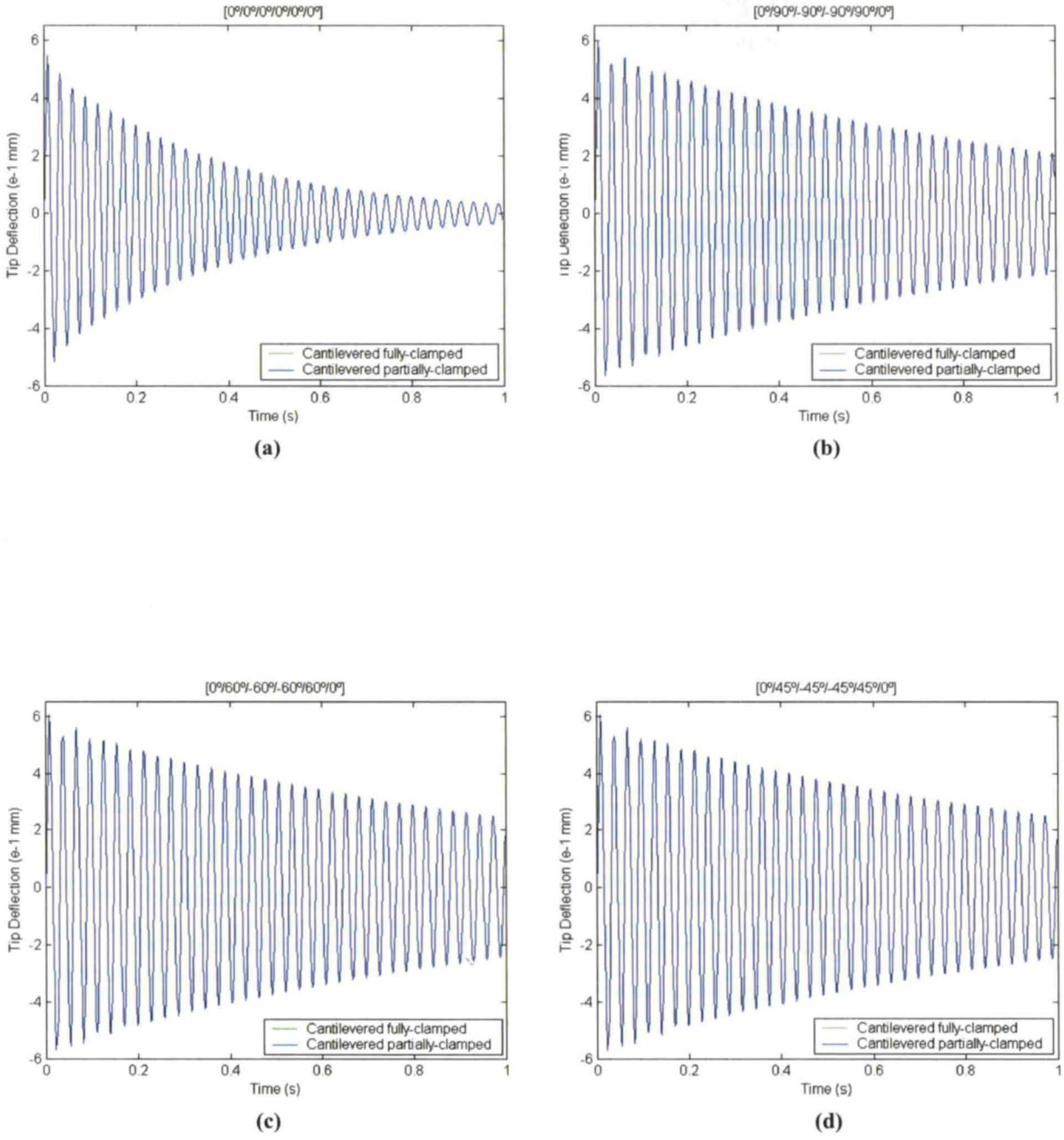

Figure 5.9: Effect of ply angle θ on the transverse displacement of a tip in a *passive* cantilevered beam under fully- and partially-clamped conditions.

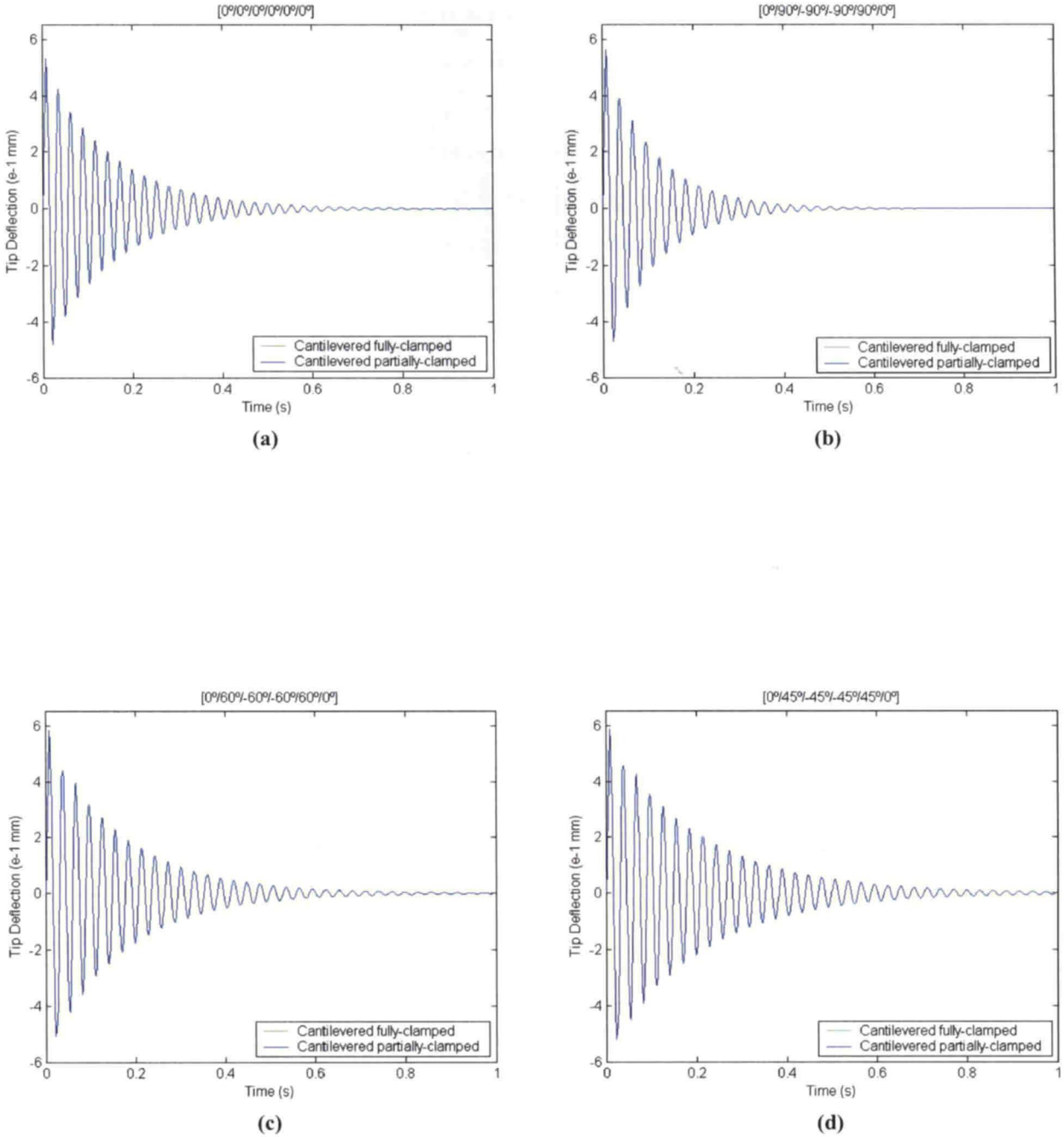

Figure 5.10: Effect of ply angle θ on the transverse displacement of a tip in a cantilevered beam under fully- and partially-clamped conditions with *active* control.

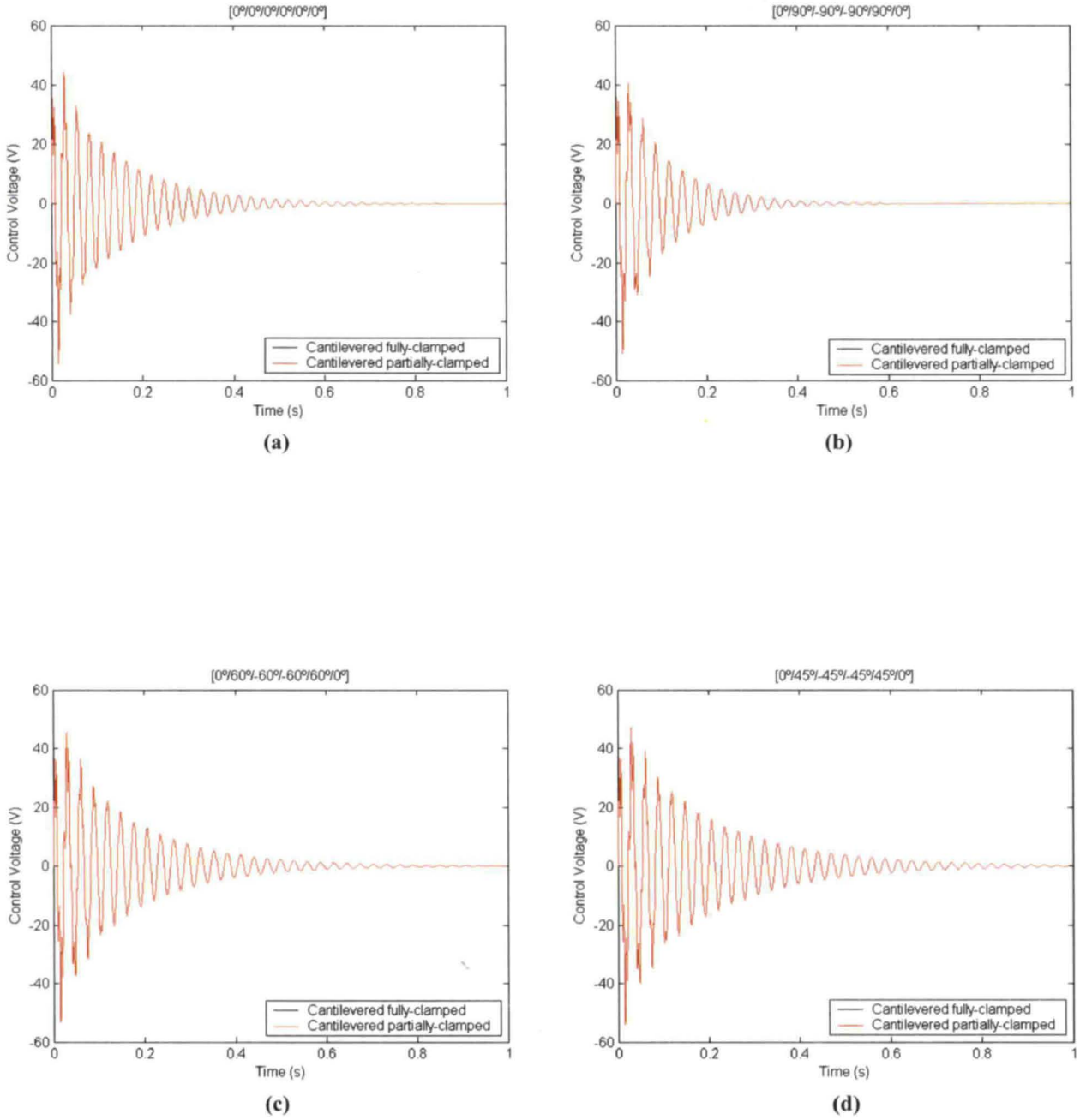

Figure 5.11: Effect of ply angle θ on the actuator voltage of a cantilevered beam under fully- and partially-clamped conditions.

The response is independent of the stacking sequence for any ply angle in a quasi-isotropic laminate if active damping is activated. However, **Fig. 5.12** indicates that when only passive damping is considered, that is, the piezoelectric fibers in the laminate contribute only to the stiffness matrix, the $0°$ layers are less efficiently located near the reference surface of the laminate. This is because the stiffness and strength of longitudinal fibers are not fully utilized if they are located near the reference surface when bending is the primary response. It is further observed from **Fig. 5.12(a)** that the response with $[0°/\pm 90°]_S$ stacking sequence dampens faster than the response with $[\pm 90°/0°]_S$ sequence, which supports the earlier assertion. **Fig. 5.12(b)** shows a phase change in the responses beyond 1 second. Note that the thickness of the host beam has been changed to $h_b = 1.75$ mm to best illustrate this behavior/observation.

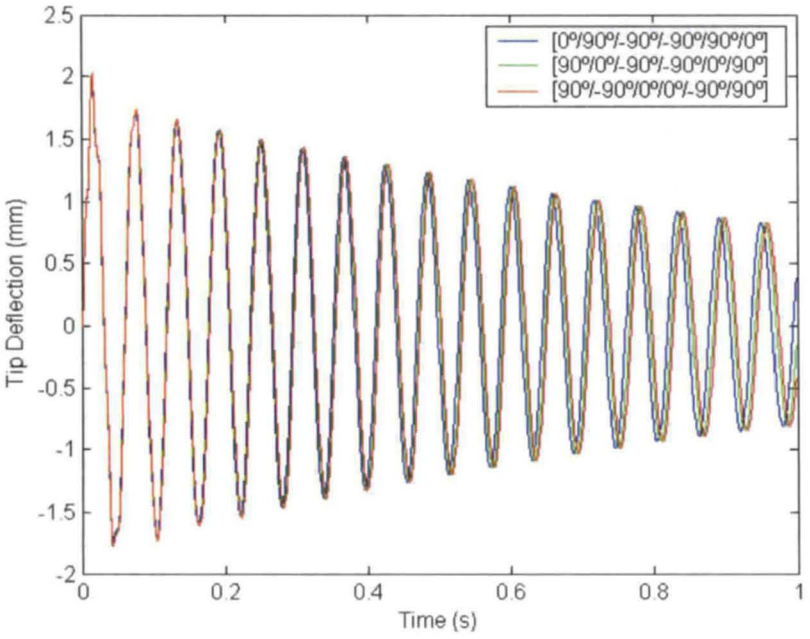

(a) Observation time between 0 and 1 second

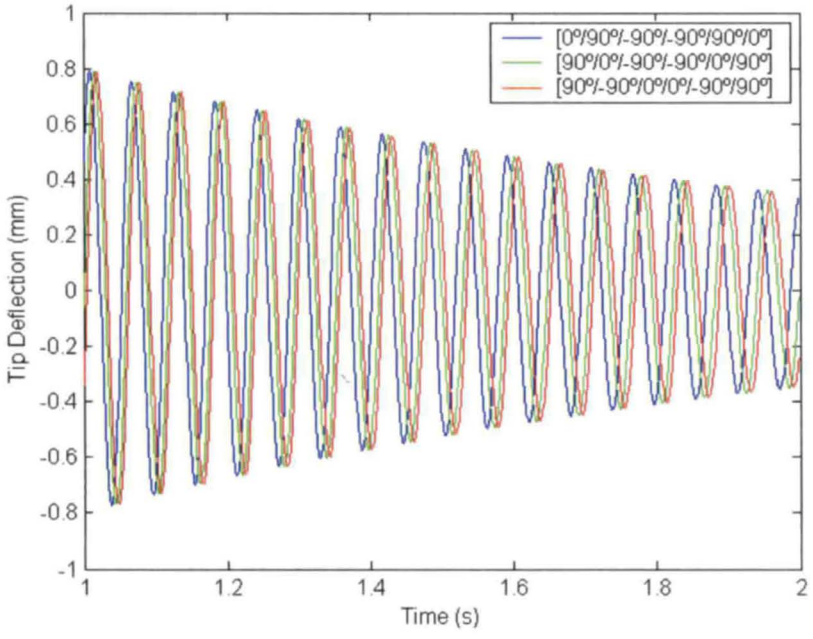

(b) Observation time between 1 and 2 seconds

Figure 5.12: Passive damping response of a cantilevered fully-clamped beam with a thin host layer for varying stacking sequence.

5.2.1.2 Fixed-End Partially-Constrained Beam Case

A fixed-end beam refers to a beam with both ends clamped as shown in **Fig. 5.13** below. Also, the fixed-end beam is only partially constrained in order to take advantage of the actuation of the PFRC laminate. As seen from the figure, elements 2, 3, and 4 are constrained with both viscoelastic and PFRC laminate layers, while elements 1 and 5 remain unconstrained. The triangular impulse load (see **Fig. 5.7(b)**) is applied to the middle upper node of the element 3 in the transverse direction.

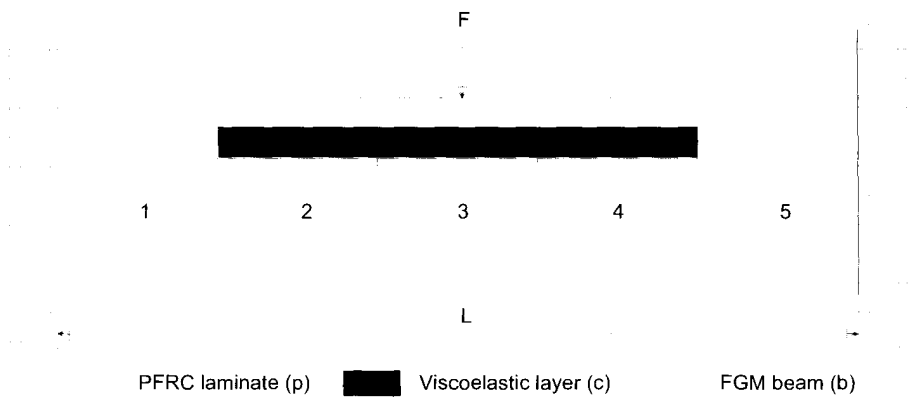

Figure 5.13: Schematic of a partially-constrained fixed-end beam

The gain used in this scenario is the same ($K_v = 350$ V/(m/s)) as is in the cantilevered case. The only changes made to the parameter specifications include the thickness of the host beam, which is reduced to $h_b = 2.5$ mm , and the time period is set to 0.5 seconds instead of 1 second as in the previous example, which results in $N = 500$ terms. Note that modifications are solely made for enhanced presentation and are not necessarily optimal. Though this case is considered as a different problem from the cantilever case, one can observe the decreased deflection and higher frequency of vibration, which are consistent with the form of the boundary conditions.

The deflection is observed at the middle node of the composite beam in the direction of the applied load. **Figs. 5.14** and **5.15** depict the passive and active damping responses of the transverse displacement at the middle node, respectively. **Fig. 5.16** shows the actuator voltage corresponding to the response in **Fig. 5.15**. Ply angle orientation is

illustrated in the same order and form of $[0°/\pm\theta]_S$ notation as in the previous case. In general, **Figs. 5.14, 5.15,** and **5.16** follow the same pattern of response as the **Figs. 5.9, 5.10,** and **5.11** of the cantilevered beam, respectively.

Fig. 5.14(a) shows the best result in terms of faster damping, which can be explained by the same reasoning as was done regarding **Fig. 5.9**. The response with $[0°/\pm 90°]_S$ from **Fig. 5.15(b)** also shows a slightly greater damping pattern than in **Fig. 5.15(a)** due to the enhancement of actuation control in a more flexible PFRC laminate. **Fig. 5.15(d)** shows the worst damping response, since only a horizontal component of the fibers contributes to the bending stiffnesses, while, at the same time, the flexibility of the PFRC laminate is not increased in the bending direction as in the case of **Fig. 5.15(b). Fig. 5.16** shows the control voltage response in direct proportionality with the derivative of the response of **Fig. 5.15.**

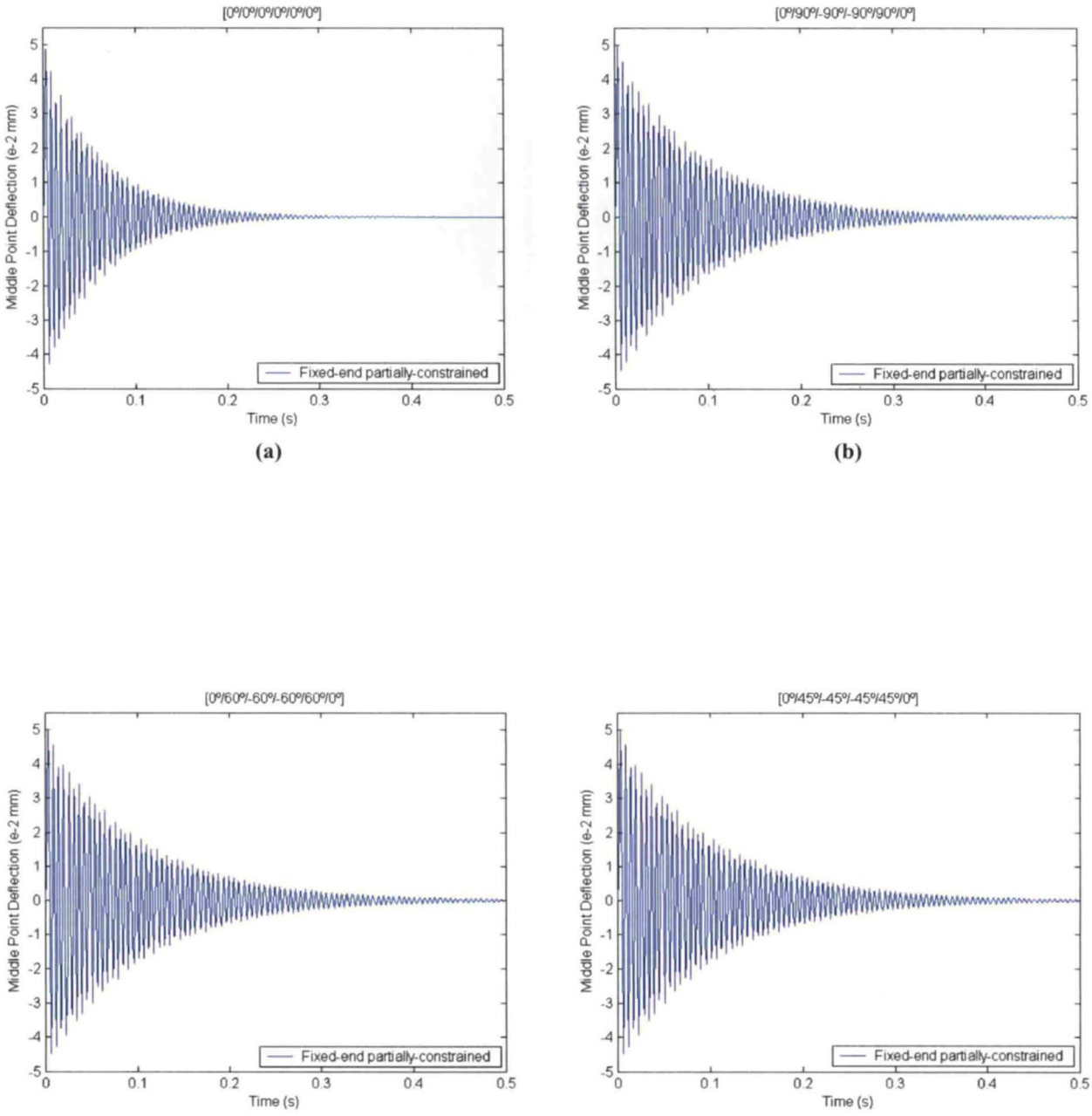

Figure 5.14: Effect of ply angle θ on the transverse displacement of a middle point in a *passive* fixed-end beam under partially-constrained condition.

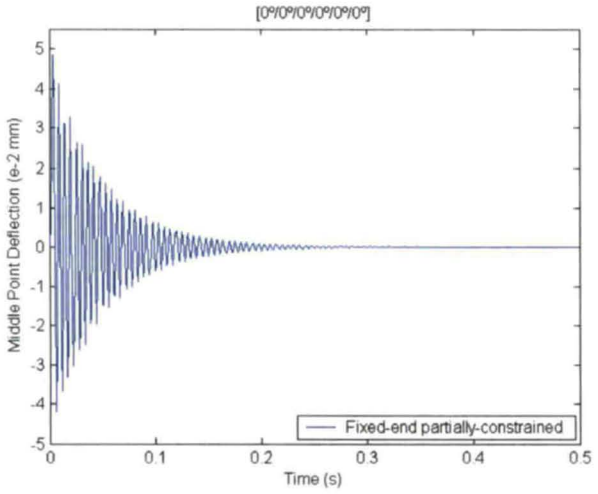

(a)

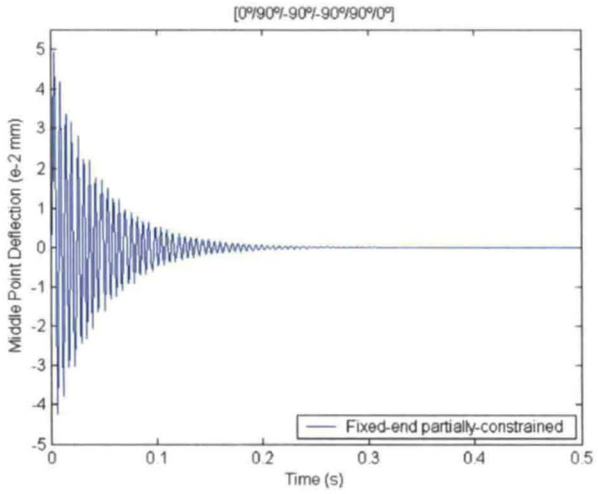

(b)

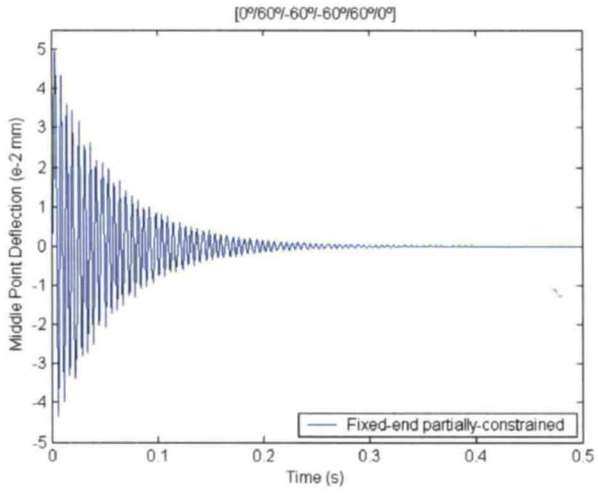

(c)

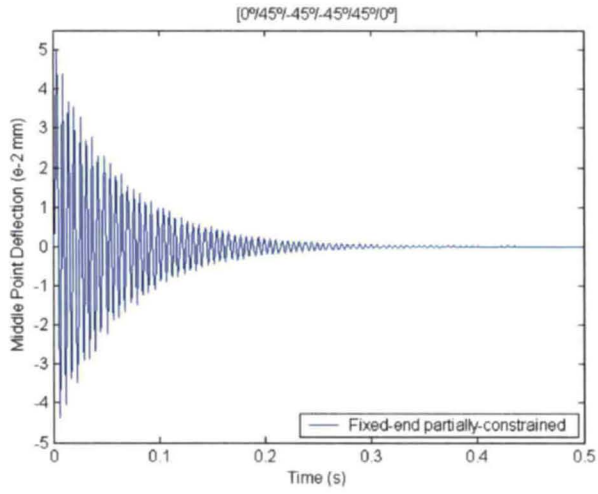

(d)

Figure 5.15: Effect of ply angle θ on the transverse displacement of a middle node in a fixed-end beam under partially-constrained condition with *active* control.

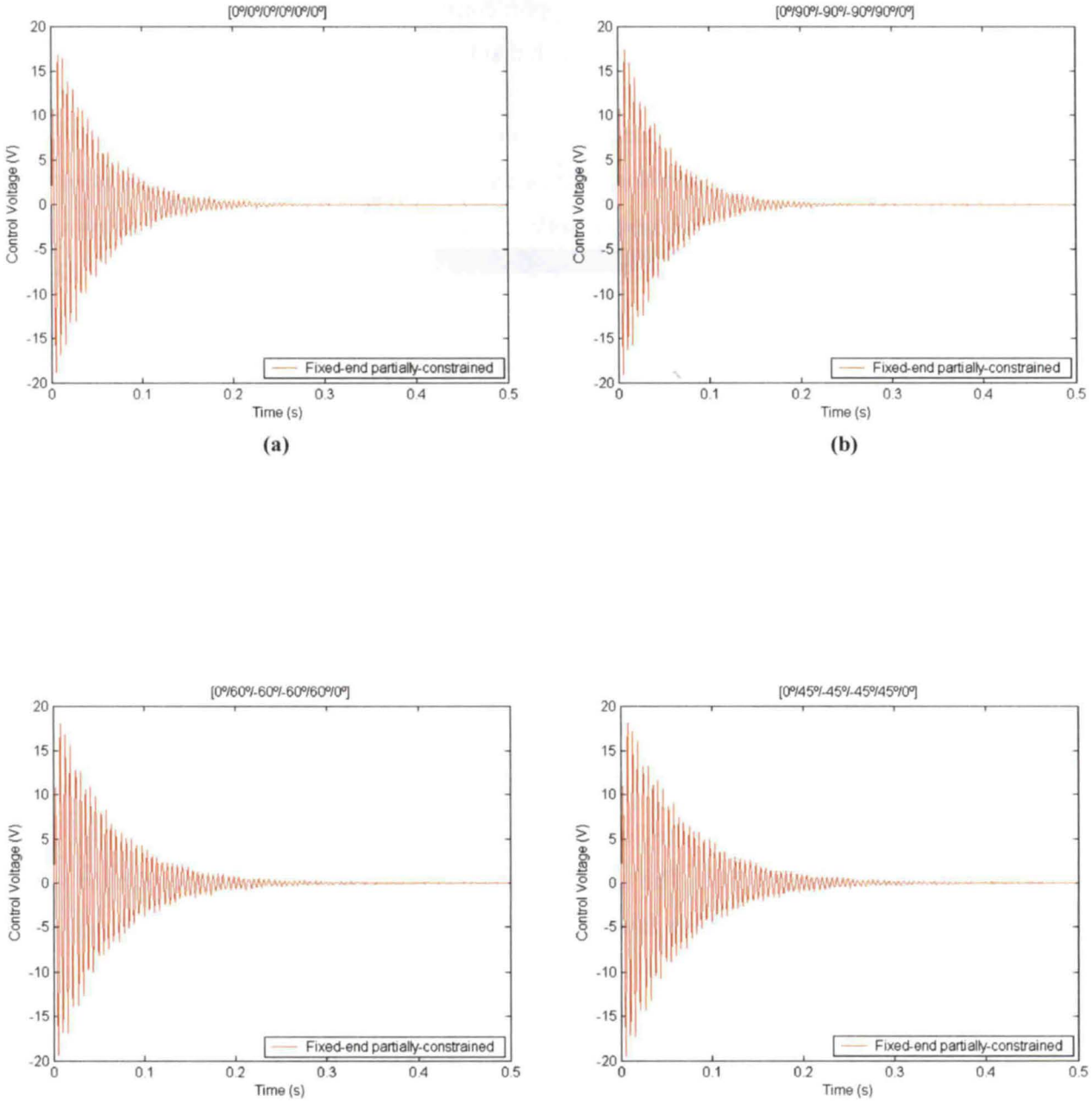

Figure 5.16: Effect of ply angle θ on the actuator voltage of a fixed-end beam under partially-constrained condition.

5.2.1.3 Simply-Supported Beam Case

The configuration of this type of support consists of two point supports at each end of the beam and is shown in **Fig. 5.17** such that both axial and transverse displacements are constrained.

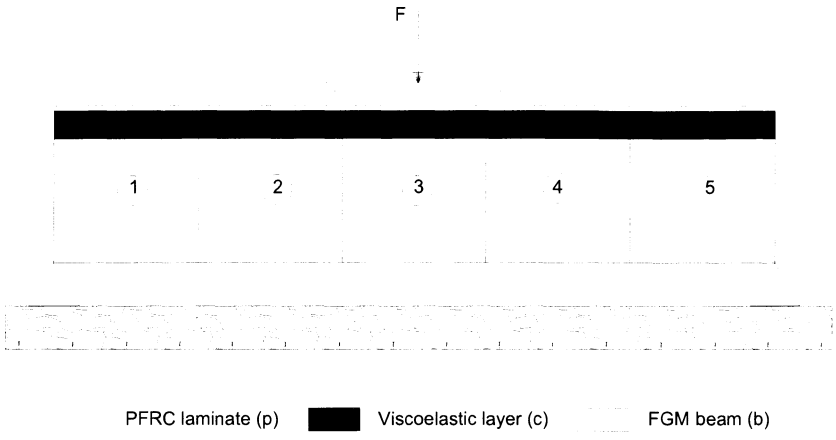

Figure 5.17: Schematic of a simply-supported beam.

The gain $K_v = 350$ V/(m/s) as in the previous cases and the host beam thickness is also reduced to $h_b = 2.5$ mm as in the fixed-end beam case. The observation time period is 0.5 seconds, as in the previous example, and the number of Grünwald approximation terms $N = 500$. The triangular impulse load (see **Fig. 5.7(b)**) is applied to the middle node in the transverse direction in the same manner as in the fixed-end beam case.

Figs. 5.18, 5.19, and **5.20** depict the passive damping, active damping, and actuator voltage responses, respectively, of the simply-supported beam. Based on these figures, it is noted that the deflection is higher in the simply-supported beam than in the fixed-end partially-constrained beam case. This result is compatible with the form of support at both ends, which is characterized by the number of displacement points clamped. For this particular case, the lesser number indicates the greater flexibility of the beam and, thus, higher deflection.

Different ply angle arrangements follow the same order as in the previous cases. **Fig. 5.18(a)** shows the fastest damping and **Fig. 5.18(c)** and **5.18(d)** describe very slow attenuation rate due to the same reasons given in the previous subsections. However, in **Fig 5.19**, the best damping response is observed in **Fig. 5.19(a)** rather than **5.19(b)**, as was the case in the previous examples. Here, the beam is already flexible enough to enable a successful actuation of the PFRC laminate with the addition of longitudinal plies amplifying the bending resistance as well. In **Fig. 5.19(b)**, it is interesting to note a slight fluctuation of the deflection response even after the most damping is achieved at around 0.2 s. This could be accounted for with the higher frequencies dominating the response. Since the beam is already flexible enough with only two point supports, the ply orientation $[0°/\pm 90°]_S$ does not contribute to attenuation of the higher frequency vibration response.

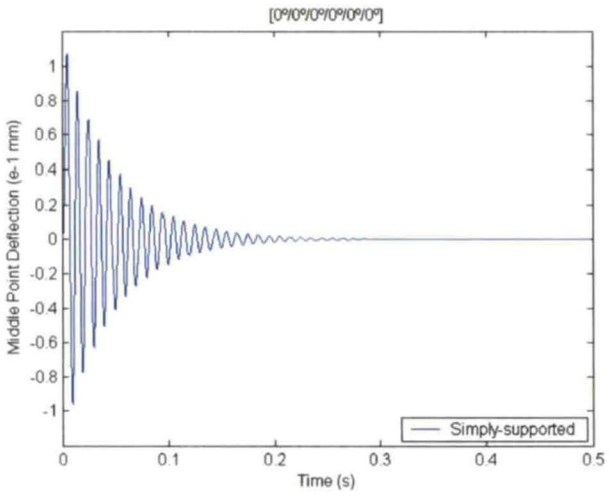

(a)

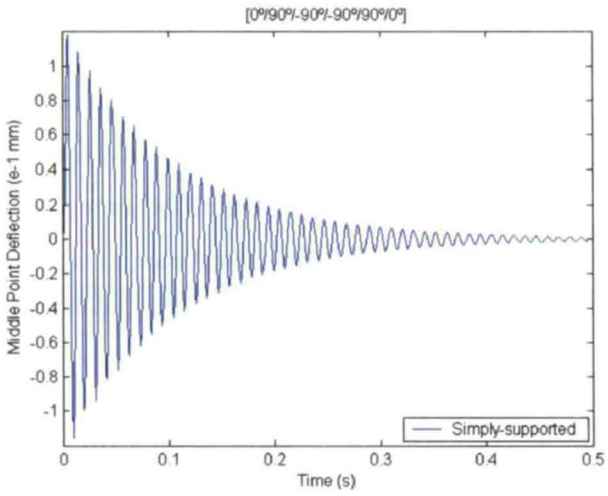

(b)

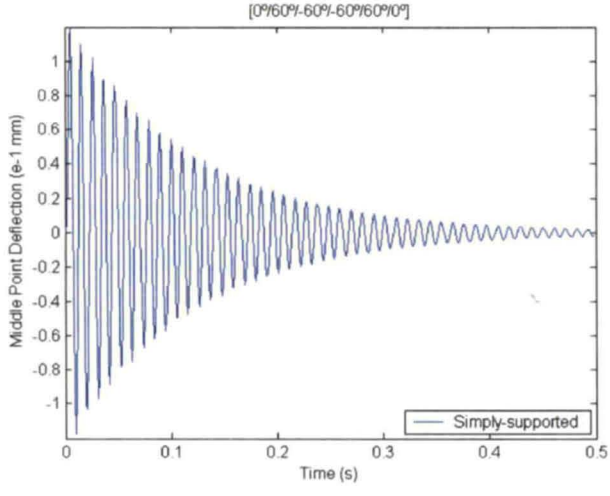

(c)

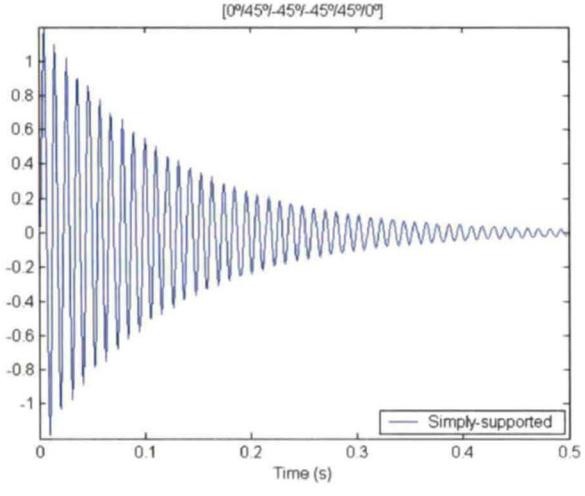

(d)

Figure 5.18: Effect of ply angle θ on the transverse displacement of a middle node in a *passive* simply-supported beam.

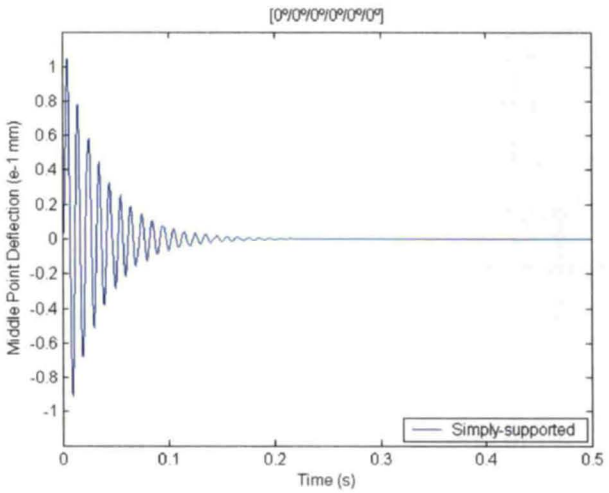

(a)

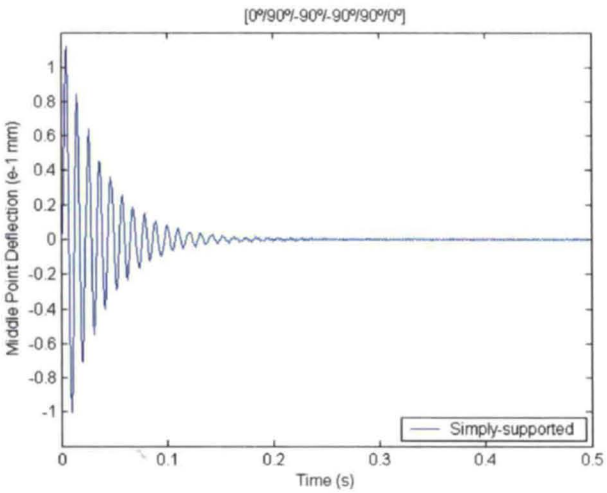

(b)

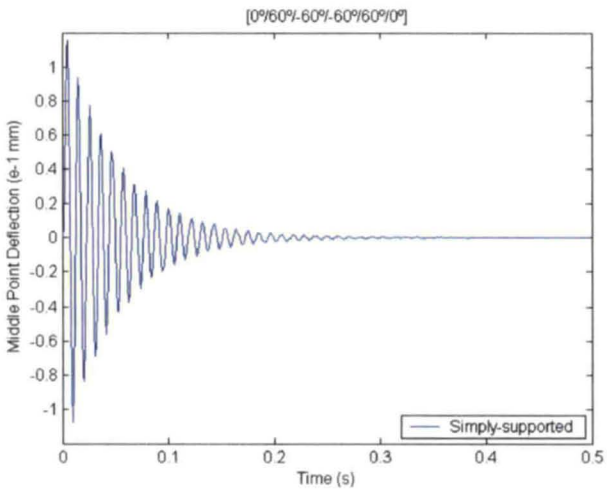

(c)

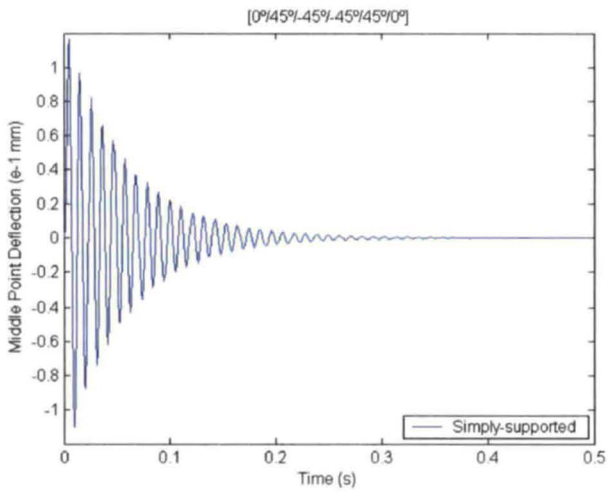

(d)

Figure 5.19: Effect of ply angle θ on the transverse displacement of a middle node in a simply-supported beam with *active* control.

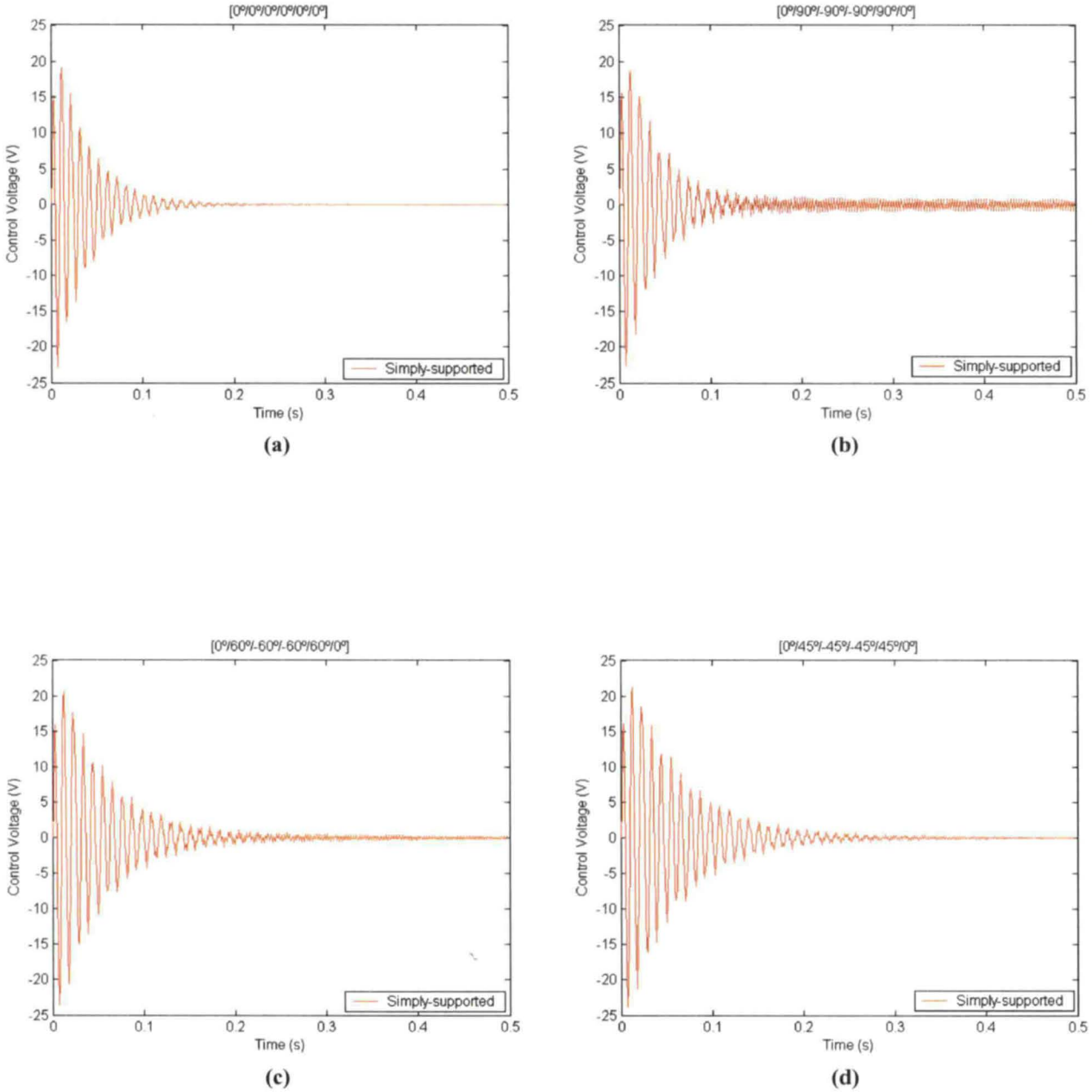

Figure 5.20: Effect of ply angle θ on the actuator voltage of a simply-supported beam.

5.2.2 Effect of FGM Properties

The effect of functional grade in a host beam is studied by fixing each ply orientation at $\theta = 0°$ in the PFRC laminate. The host beam stiffness either increases or decreases with height by varying Young's modulus E across its thickness. In the case of stiffness decreasing (increasing) with height, the higher stiffness is at the bottom (top) of the host beam. In order to have a varying elastic modulus, one must manipulate the functional gradient λ, which is a function of the top and bottom surface Young's moduli, E_b^1 and E_b^0, respectively, and thickness of the FGM beam h_b as seen in Section 3.2.2. **Table 5.4** shows how the elastic moduli vary for a given λ. Note that a constant average E, the elastic modulus of aluminum ($E_{avg} = 70.3$ GPa), is used for each λ. This is done to permit reasonable comparison.

Table 5.4: Variation of Young's modulus with respect to functional gradient λ.

$\lambda = 500$		$\lambda = 0$		$\lambda = -500$	
E_b^0	E_b^1	E_b^0	E_b^1	E_b^0	E_b^1
GPa		GPa		GPa	
23.876	155.69	70.3	70.3	155.69	23.876

5.2.2.1 Cantilevered Beam Case

The cantilever beam problem remains the same with the parameter specifications mentioned in Section 5.2.1 and illustrated in **Fig. 5.8**. The dynamic response is observed for both fully- and partially-clamped boundary conditions. As seen from **Figs. 5.21, 5.22** and **5.23**, the response for the two conditions coincide, as was the case in the previous section.

Figs. 5.21 and **5.22** correspond to the response of the system in the passive and active states, respectively. **Fig. 5.23** represents the actuation voltage response when the gain of $K_v = 350$ V/(m/s) is applied to the composite beam. In **Figs. 5.21(a), 5.21(b),** and **5.21(c)** the passive damping response is shown for the following functional gradients: $\lambda = 500$, $\lambda = 0$, and $\lambda = -500$, respectively. The corresponding elastic moduli for the

bottom and top surfaces of the host layer are as tabulated in **Table 5.4**. Comparing **Figs. 5.21(a)** and **5.21(b)**, one observes a better damping response when the beam is homogeneously isotropic than in the case of gradual increase of stiffness with height in the host beam. A functional gradient of 500, as in **Fig. 5.21(a)**, yields lower elastic modulus at the bottom of the beam and higher Young's modulus at the interface between the host and viscoelastic layers. **Fig. 5.21(c)**, however, shows a better result with greater damping than **Fig. 5.21(b)**, where the host beam stiffness is gradually decreasing from the bottom to the top. The lack of effectiveness of the greater stiffness at the top surface of the host layer results because the top surface is located near the reference surface of the total beam, that is, near what would have been the "neutral axis" if the beam was completely isotropic. In other words, the greater stiffness and strength of the FG material is not utilized completely if it is located near the reference surface and if the primary response is the bending response. Another reason for this trend comes from the increased passive damping in the vibration of the system, as seen in **Fig. 5.21(c)**. The top surface of the host beam, being lower in stiffness than the bottom surface and bonded to the viscoelastic core, increases the shear deformation of the viscoelastic core and, in turn, increases the passive damping of the beam.

Fig. 5.22 emphasizes the effectiveness of active-passive damping over the sole use of passive damping in **Fig. 5.21**. Similar to the passive case, **Fig. 5.22(c)** also shows a faster damping with a lower initial response than in **Fig. 5.22(a)**. In spite of the reasons mentioned above regarding passive damping, the application of negative functional gradient to the host beam affects active damping as well. This is because the PFRC laminate/viscoelastic combination layer is now attached to a more flexible surface of the beam, which can enhance the control by the actuator. The actuator voltage responses in **Fig 5.23** are proportional to the rate of the deflection responses in **Fig. 5.22**.

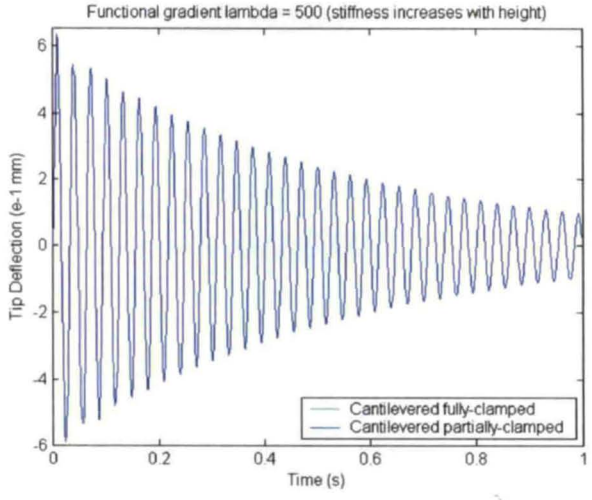

(a)

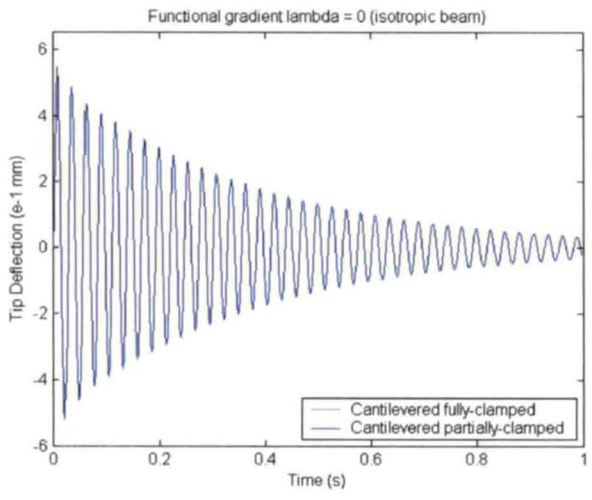

(b)

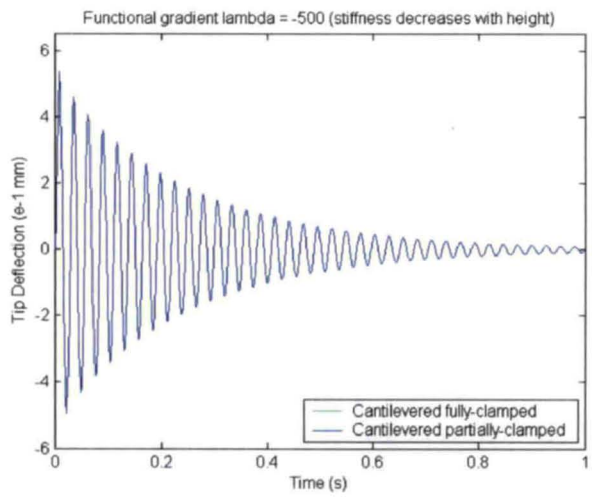

(c)

Figure 5.21: Effect of functional gradient λ on the transverse displacement of a tip in a *passive* cantilevered beam under fully- and partially-clamped conditions.

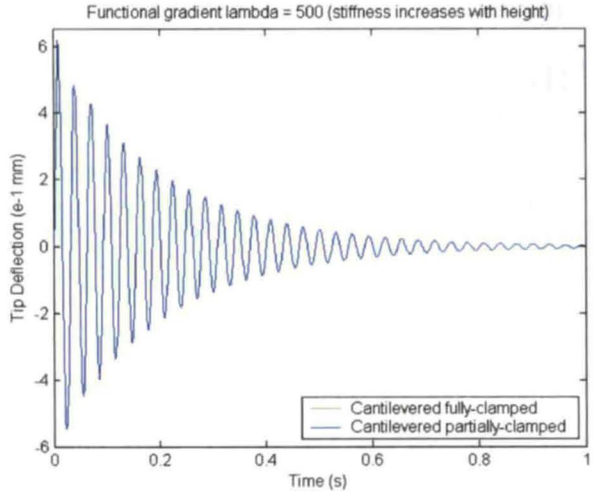

(a)

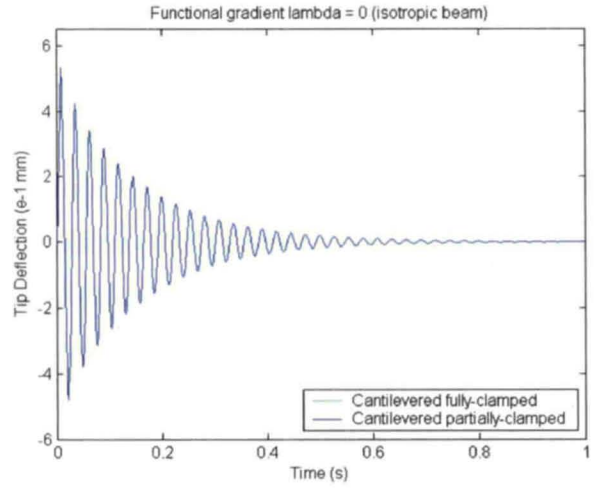

(b)

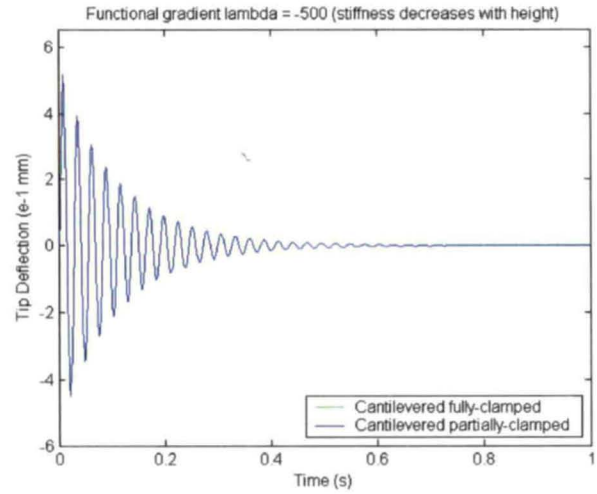

(c)

Figure 5.22: Effect of functional gradient λ on the transverse displacement of a tip in a cantilevered beam under fully- and partially-clamped conditions with *active* control.

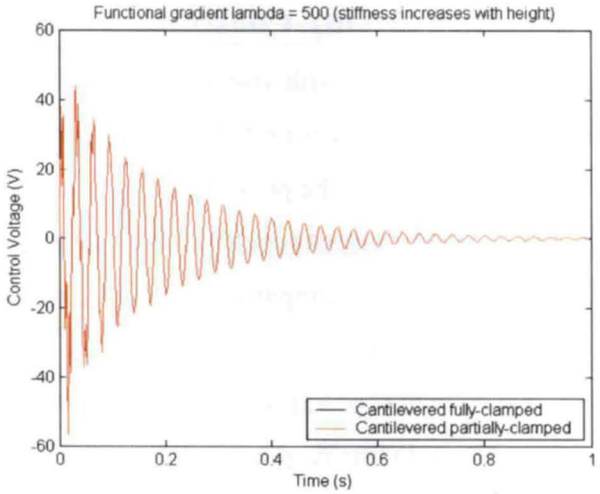

(a)

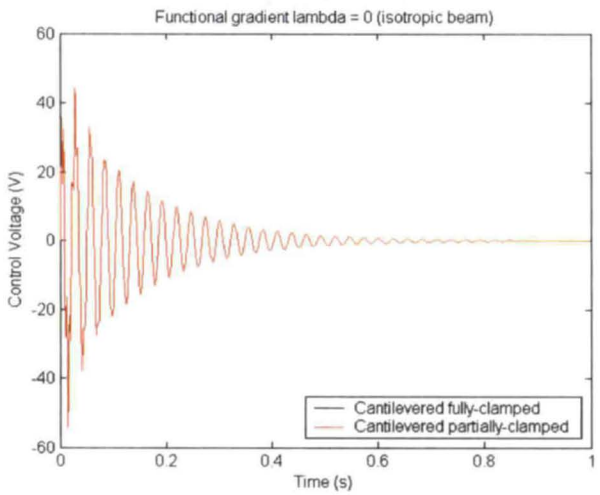

(b)

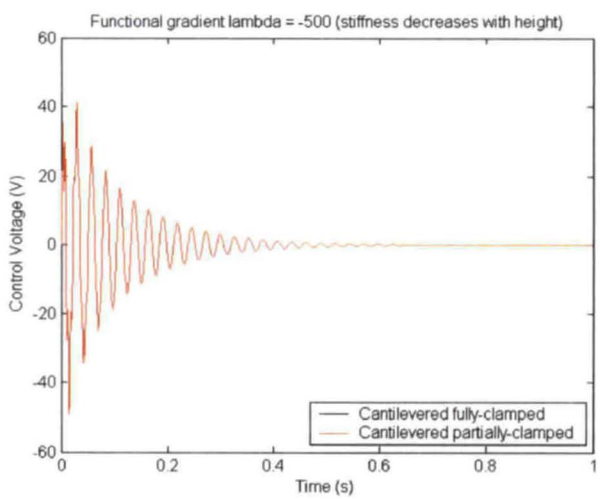

(c)

Figure 5.23: Effect of functional gradient λ on the actuator voltage of a cantilevered beam under fully- and partially-clamped conditions.

5.2.2.2 Fixed-End Partially-Constrained Beam Case

A fixed-end beam partially covered with viscoelastic and PFRC laminate constraining layers is shown in **Fig. 5.13** in Section 5.2.1. The parameters remain the same. The same response pattern is repeated as in the previous case, featuring the response due to only passive damping in **Fig. 5.24**, the response with active damping in **Fig. 5.25**, and the control voltage response in **Fig. 5.26**. When comparing **Figs. 5.24** and **5.25**, note that incorporation of actuation in the composite beam does not have as significant an effect on the damping of the system as it does in **Figs. 5.21** and **5.22** of the cantilever beam case.

Similar to the previous example, the responses in **Figs. 5.24(c)** and **5.25(c)** highlight a faster damping trend than in **Figs. 5.24(a)** and **5.25(a)**, respectively. The reasoning for this occurrence is the same as that of the cantilever case. However, in this scenario, the figures with $\lambda = -500$ show a slightly higher initial response magnitude than with $\lambda = 0$ in **Figs. 5.24** and **5.25**. This observation reflects the type of support, which, in this case, constrains two ends of the beam. In **Figs. 5.24(c)** and **5.25(c)**, the beam becomes more flexible as it has more concentrated stiffness in the bottom part and less in the upper part of the host layer. In **Figs. 5.24(b)** and **5.25(b)**, however, the beam is homogeneously isotropic and hence flexibility of the beam is not increased. This flexibility issue explains the slightly higher initial response in **Figs. 5.24(c)** and **5.25(c)**. The same pattern can also be seen when comparing **Figs. 5.26(b)** and **5.26(c)**.

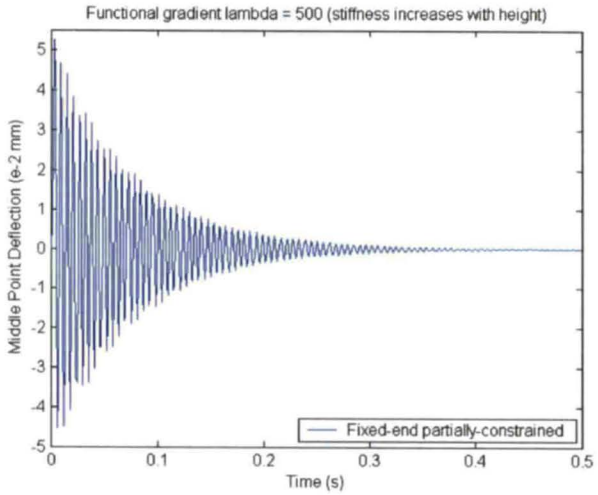

(a)

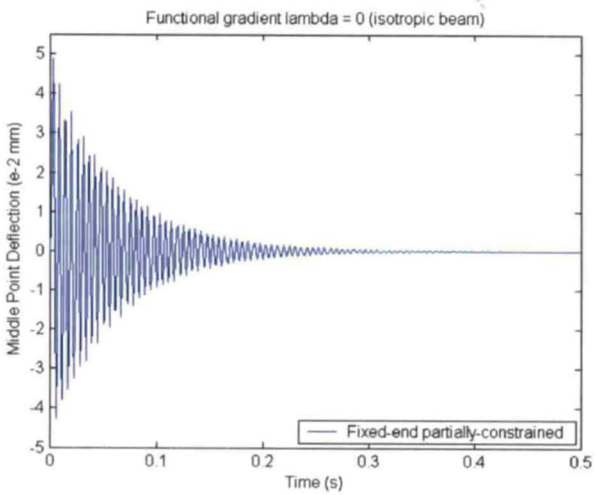

(b)

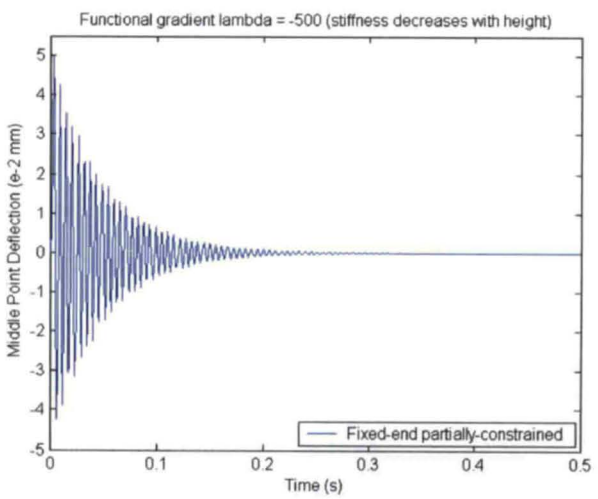

(c)

Figure 5.24: Effect of functional gradient λ on the transverse displacement of a middle node in a *passive* fixed-end beam under partially-constrained condition.

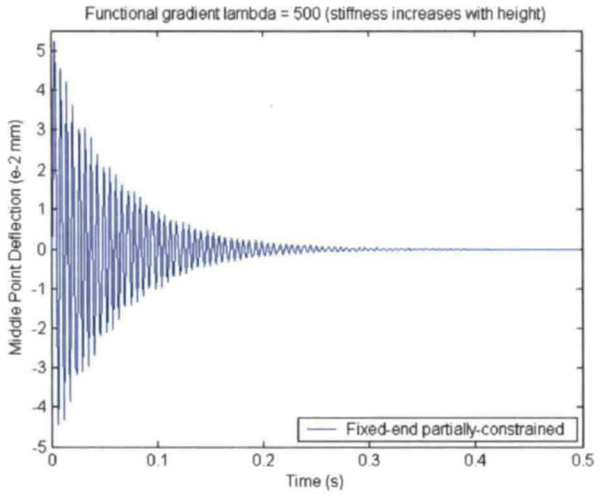

(a)

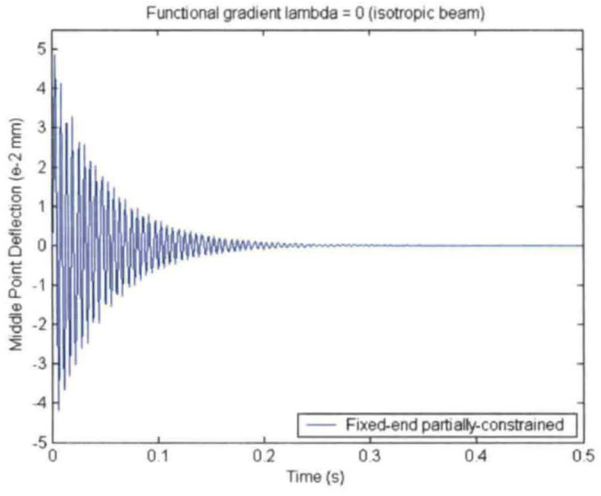

(b)

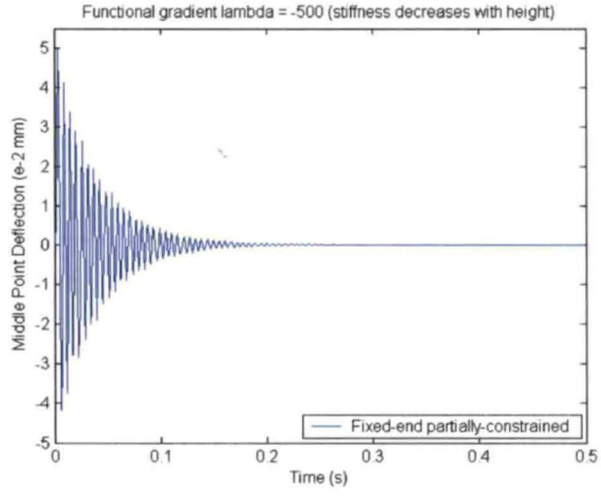

(c)

Figure 5.25: Effect of functional gradient λ on the transverse displacement of a middle node in a fixed-end beam under partially-constrained condition with *active* control.

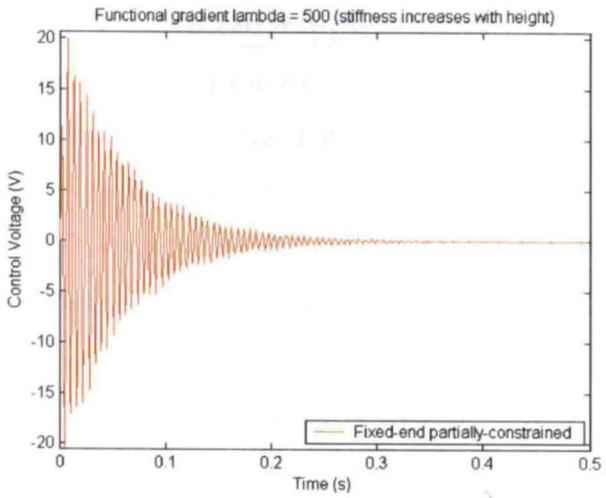

(a)

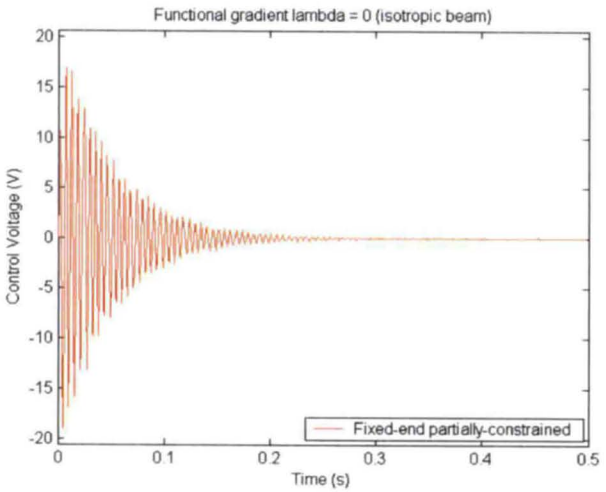

(b)

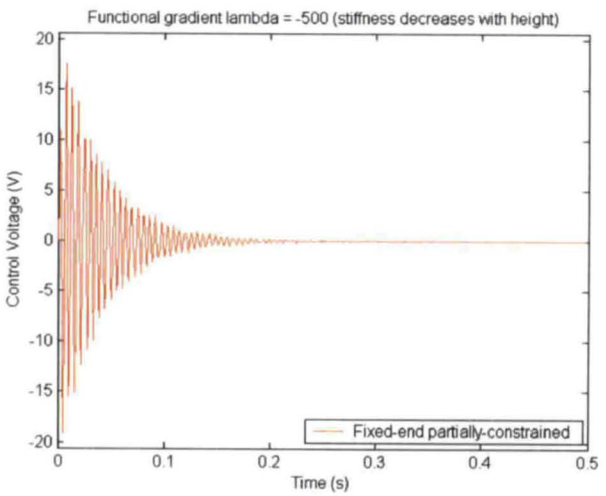

(c)

Figure 5.26: Effect of functional gradient λ on the actuator voltage of a fixed-end beam under partially-constrained condition.

5.2.2.3 Simply-Supported Beam Case

The same simply-supported beam shown in **Fig. 5.17** and explained in Section 5.2.1 is used in this section. **Figs. 5.27** and **5.28** depict the effects of functional gradient λ on the middle node deflection when the beam is damped passively and actively, respectively. **Fig. 5.29** shows the actuator voltage response when the system's gain $K_v = 350\ \text{V/(m/s)}$, as in the previous sections. **Figs. 5.27(c)** and **5.28(c)** also show the best results in terms of damping rate. However, as observed in the case of fixed-end beam, **Figs. 5.27(c)** and **5.28(c)** (for $\lambda = -500$) show slightly higher initial response than **Figs. 5.27(b)** and **5.28(b)** ($\lambda = 0$). The reason for this is explained in the previous case, and it is compatible with the above explanation on the importance of the support mechanism. In this case, unlike in the cantilevered beam, two opposite corners are constrained thus limiting much movement in the transverse direction. Making the host beam stiffer at the bottom rather than at the top surfaces, most likely, enhances the initial flexibility of the system; however, it reduces the flexibility once the stiffnesses located farther from the reference axis start contributing to the vibration suppression. Since the flexibility of the system is greatly limited considering its support mechanism, this type of beam does not yield to actuation as well as the cantilevered beam does. **Fig. 5.29(c)** shows the least voltage required to suppress the vibration of the beam, as observed in the other cases.

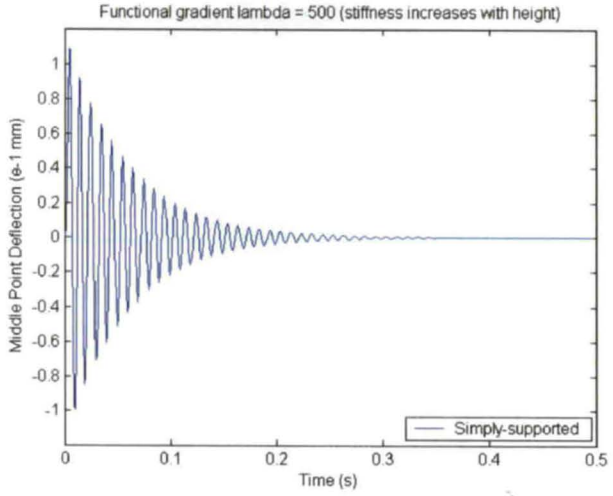

(a)

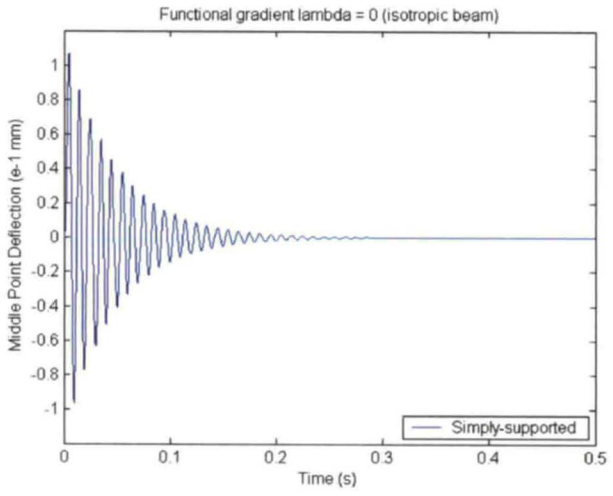

(b)

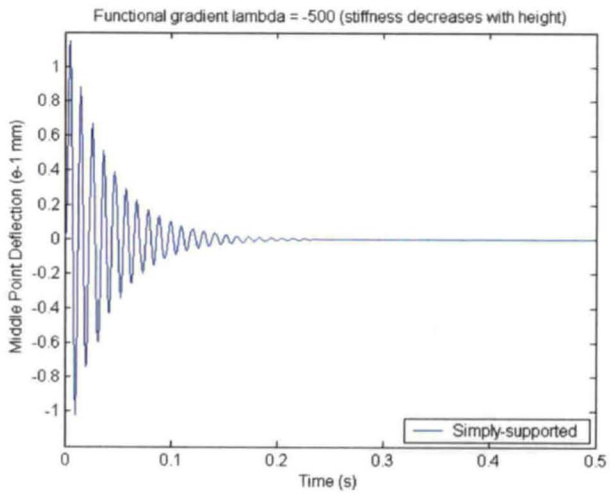

(c)

Figure 5.27: Effect of functional gradient λ on the transverse displacement of a middle node in a *passive* simply-supported beam.

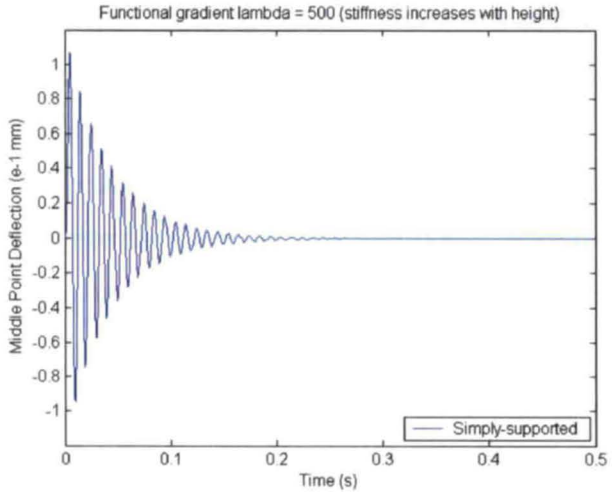

(a)

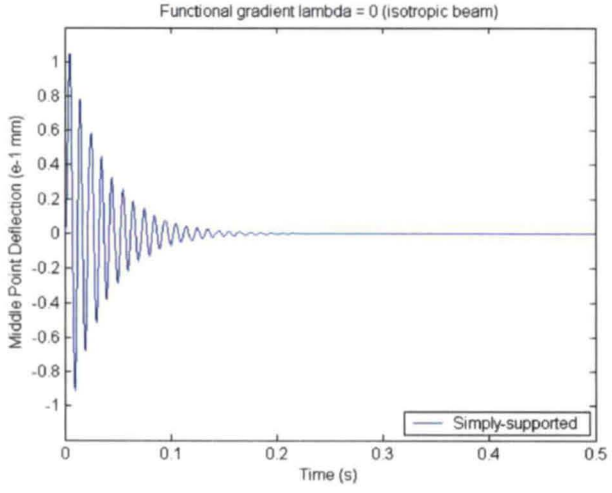

(b)

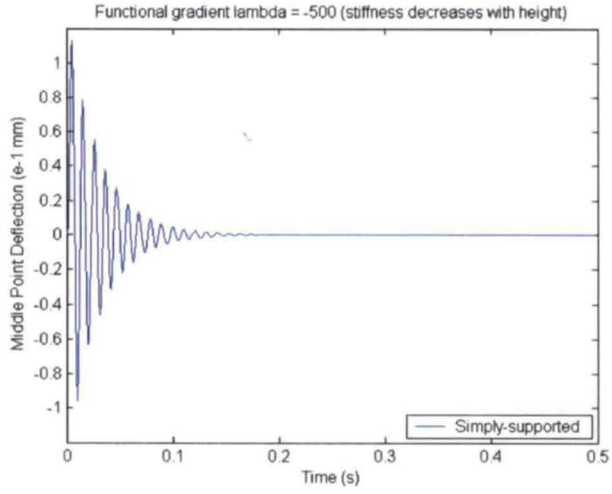

(c)

Figure 5.28: Effect of functional gradient λ on the transverse displacement of a middle node in a simply-supported beam with *active* control.

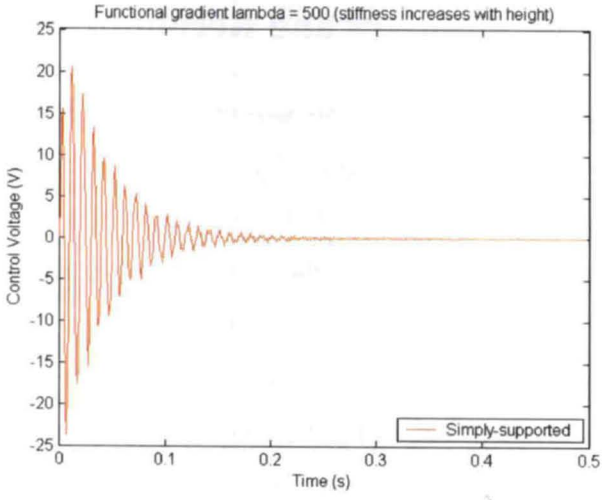

(a)

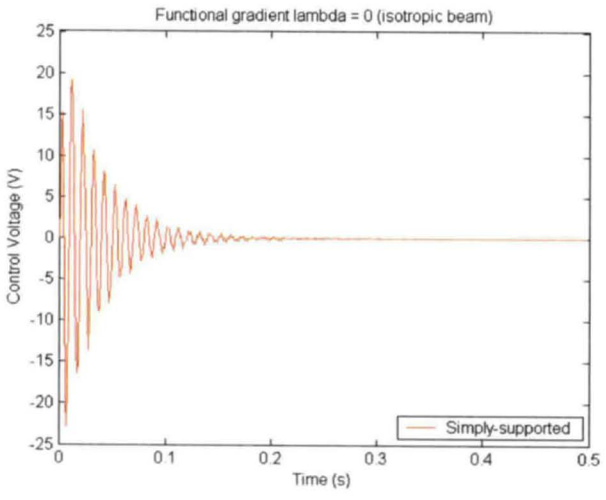

(b)

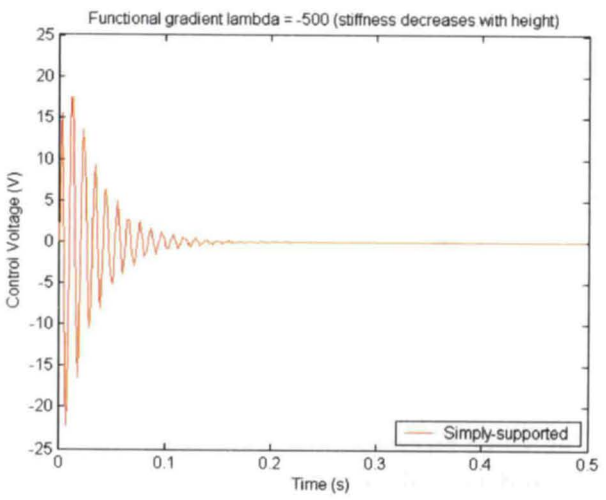

(c)

Figure 5.29: Effect of functional gradient λ on the actuator voltage of a simply-supported beam.

Chapter 6 Summary and Recommendations

The preceding chapters presented a quasi-two-dimensional finite element formulation for vibration analysis of a functionally graded (FG) beam with active-passive constrained layer damping (ACLD) treatment. The viscoelastic layer, as part of ACLD treatment, contributes to passive damping of the structure, while the piezoelectric fiber-reinforced composite (PFRC) laminate acts as an active constraining layer.

The piezoelectric fibers in the PFRC act as the actuator of the system by means of a velocity feedback control system. The PFRC laminate comprises six plies, each of which is orientated at a ply angle θ in the reference plane of the system. Classical laminate theory is used to determine the ABD constitutive matrix relating force and moment resultants with strains and curvatures. The Young's modulus of the FG beam is assumed to vary exponentially along the thickness of the host beam, while the Poisson's ratio is constant over the domain of the beam. A four-parameter fractional derivative model is used in describing the time-dependent behavior of the viscoelastic material.

The three-layer beam model is built assuming the Timoshenko hypothesis for all layers. The deformation of the top constraining layer follows the same assumption of a basic three-layer theory, where the axial displacement is linear through the thickness and the transverse displacement is constant. In the host beam and the core, however, the axial displacement varies cubically, while the transverse displacement varies quadratically through the thickness. The field variables are interpolated through the thickness of the composite beam using the polynomial expansion, while cubic Lagrange finite elements are used to interpolate along the span. This formulation results in a smaller number of degrees of freedom than in other more conventional two-dimensional models, which use many elements through the thickness to avoid an aspect ratio problem. However, this model still produces highly accurate results. The formulation is suitable only for small deformations.

The formulation was compared with two examples from the literature: a viscoelastic-aluminum sandwich beam and a cantilever beam with viscoelastic and piezoelectric constraining layers. The parametric study showed superior performance of the active-passive combination constraining layer over the sole use of passive damping. Three

different cases were simulated; namely, the cantilevered, fixed-end partially-constrained and simply-supported beams. When analyzing the effect of ply orientation, it was noted that the active cantilevered beam, with $[0°/\pm 90°]_S$ stacking sequence (i.e., cross-ply), showed the fastest attenuation rate. However, for passive damping, the best result in terms of damping rate was observed when the ply angles are all equal to zero. For the fixed-end beam, a similar vibration pattern was followed, though with smaller amplitude and higher frequency. In the simply-supported scenario, however, both the actively controlled and the uncontrolled deflection results showed higher damping rate in the instance of all longitudinal plies. During the study of the effects of FGM properties on the vibration suppression, the response with negative functional gradient (i.e., stiffness decreases with height) yielded the best damping result. This is true in each support case and during both the active and passive treatments.

Though the current study encompasses several issues, from the development of quasi-two-dimensional model to the utilization of various materials to enhance the structure, there are numerous opportunities for further development. The extension of this work might contribute to the solution of a problem of noise and vibration reduction, which is increasing rapidly with the introduction of new components and machines in today's industrial world. The future steps to take include the following:

a. Since optimization usually follows the design and development part of the component process, it must be considered in the future work. In the current formulation and analysis the geometrical parameters were chosen only for the purpose of presenting the results with a higher quality of observation. Also, the control gain chosen for each simulation was again based on the need to increase readability of the results and did not represent the optimum solution. As mentioned previously, the gain is selectable as long as it does not destabilize the system and yields control voltage in the safe range of the piezoelectric material. Determination of control gains can be achieved by using the linear quadratic regulator (LQR) optimal control theory [3].

b. With regard to the previous point, optimum location of the active constraining layer must also be considered as it may enhance the actuation capability of the structure. For instance, the PFRC laminate would fully contribute to the damping of the system if it is located close to the clamped part of the beam, since, at that point, the flexural moment is the greatest and hence must be counterbalanced with the moment created by the electrical force induced in the PFRC laminate.

c. The current formulation can be extended to accommodate dynamic analysis of plates and/or shells. Using a quasi-three-dimensional finite element model as in [9], the FG plate with bonded viscoelastic layer and PFRC laminate can be formulated and analyzed. Bicubic trial functions would have to be incorporated to model both in-plane (x, y) displacement characteristics. Compared to three-dimensional finite element analysis, in the quasi-three-dimensional model, numerical errors associated with element aspect ratio would be avoided [9].

d. The use of different viscoelastic models can be researched. The four-parameter fractional derivative model utilized in this thesis is not readily available in the commercial finite element analysis software, such as ANSYS. The Prony series method or plotting master curves can be incorporated into the viscoelastic layer modeling in the future.

e. Considering the effectiveness of varying elastic modulus such that the active-passive constraining layer comes in contact with the "softer" side of the host beam, the viscoelastic core can also be extended to being functionally graded. This could prove effective as the active constraining layer would be bonded to the surface of the viscoelastic layer with minimum stiffness and, hence, increase actuation of the beam.

f. Furthermore, the current formulation can be verified by experimental study. Vibration simulation tests can be performed and the deflection of the beam may be measured via a sensor and compared to the numerical simulation results.

References

1. Stanway, R., Rongong, J.A., and Sims, N.D., "Active constrained-layer damping: state-of-the-art review," *Proc. of the Institution of Mechanical Engineers – Journal of Systems and Control Engineering*, 2003, 217(16), 437-456.
2. Trindade, M.A., and Benjeddou, A., "Hybrid active-passive damping treatments using viscoelastic and piezoelectric materials: review and assessment," *Journal of Vibration and Control*, 2002, 8, 699-745.
3. Balamurugan, V., and Narayanan, S., "Finite element formulation and active vibration control study on beams using smart constrained layer damping (SCLD) treatment," *Journal of Sound and Vibration*, 2002, 249(2), 227-250.
4. Frostig, Y., and Baruch, M., "Bending of sandwich beams with transversely flexible core". *AIAA Journal*, 1990, 28(3), 523-531.
5. Shi, Y., Hua, H., and Sol, H., "The finite element analysis and experimental study of beams with active constrained layer damping treatments," *Journal of Sound and Vibration*, 2004, 278, 343-363.
6. Ma, B.-A., and He, J.-F., "A finite element analysis of viscoelastically damped sandwich plates," *Journal of Sound and Vibration*, 1992, 152(1), 107-123.
7. Banerjee, J.R., and Sobey, A.J., "Dynamic stiffness formulation and free vibration analysis of a three-layered sandwich beam," *International Journal of Solids and Structures*, 2005, 42, 2181-2197.
8. Bekuit, J.-J.R.B., "A quasi-two-dimensional finite element formulation for analysis of active-passive constrained layer beams," *M.A.Sc. Thesis. Ryerson University*, 2006.
9. Nabarrete, A., de Almeida, S.F.M., and Hansen, J.S., "Sandwich-plate vibration analysis: three-layer quasi-three-dimensional finite element model," *AIAA Journal*, 2003, 41(8), 1547-1555.
10. Gao, J.X., and Liao, W.H., "Vibration analysis of simply supported beams with enhanced self-sensing active constrained layer damping treatments," *Journal of Sound and Vibration*, 2005, 280, 329-357.

11. Vasques, C.M.A., Mace, B.R., Gardonio, P., and Rodrigues, J. D., "Arbitrary active constrained layer damping treatments on beams: Finite element modeling and experimental validation," *Computers and Structures*, 2006, 84, 1384-1401.
12. Crawley, E.G., and de Luis, J., "Use of piezoelectric actuators as elements of intelligent structures," *AIAA Journal,* 1987, 25(10), 1373-1385.
13. Ray, M.C., and Sachade, H.M., "Exact solutions for the functionally graded plates integrated with a layer of piezoelectric fiber-reinforced composite," *ASME Transactions on Applied Mechanics*, 2006, 73, 622-632.
14. Sankar, B.V., "An elasticity solution for functionally graded beams," *Journal of Composites Science and Technology*, 2001, 61, 689-696.
15. Sankar, B.V., and Tzeng, J.T., "Thermal stresses in functionally graded beams," *AIAA Journal*, 2002, 40(6), 1228-1232.
16. Ray, M.C., and Sachade, H.M., "Finite element analysis of smart functionally graded plates," *International Journal of Solids and Structures*, 2006, 43, 5468-5484.
17. Liew, K.M., Sivashanker, S., He, X.Q., and Ng, T.Y., "The modeling and design of smart structures using functionally graded materials and piezoelectric sensor/actuator patches," *Journal of Smart Materials and Structures*, 2003, 12, 647-655.
18. Chi, S.-H., and Chung, Y.-L., "Mechanical behavior of functionally graded material plates under transverse load – Part I: Analysis," *International Journal of Solids and Structures*, 2006, 43, 3657-3674.
19. Galucio, A.C., Deü, J.-F., and Ohayon, R., "Finite element formulation of viscoelastic sandwich beams using fractional derivative operators," *Journal of Computational Mechanics*, 2004, 33, 282-291.
20. Galucio, A.C., Deü, J.-F., and Ohayon, R., "A fractional derivative viscoelastic model for hybrid active-passive damping treatments in time domain – Application to sandwich beams," *Journal of Intelligent Material Systems and Structures*, 2005, 16, 33-45.
21. Golla, D.F., and Hughes, P.C., "Dynamics of viscoelastic – a time domain, finite element formulation," *Journal of Applied Mechanics*, 1985, 52, 897-906.

22. Welch, S.W.J., Rorrer, R.A.L., and Duren, Jr., R.G., "Application of time-based fractional calculus methods to viscoelastic creep and stress relaxation of materials," *Journal of Mechanics of Time-Dependent Materials*, 1999, 3, 279-303.
23. Ray, M.C., and Mallik, N., "Performance of smart damping treatment using piezoelectric fiber-reinforced composites," *AIAA Journal*, 2005, 43(1), 184-193.
24. Ray, M.C., "Hybrid damping of smart, functionally graded plates using piezoelectric, fiber-reinforced composites," *IEEE Transactions on Ultrasonics, Ferroelectrics, and Frequency Control*, 2006, 53(11), 2152-2165.
25. Mallik, N., and Ray, M.C., "Effective coefficients of piezoelectric fiber-reinforced composites," *AIAA Journal*, 2003, 41(4), 704-710.
26. Zhang, X.D., and Sun, C.T., "Formulation of an adaptive sandwich beam," *Journal of Smart Materials and Structures*, 1996, 5(6), 814-823.
27. Sun, B., and Huang, D., "Vibration suppression of laminated composite beams with a piezo-electric damping layer," *Composite Structures*, 2001, 53, 437-447.
28. Boresi, A.P., and Schmidt, R.J., "Advanced Mechanics of Materials (6th Edition)," *John Wiley & Sons*, 2003, 61-62.
29. Hyer, M.W., "Stress Analysis of Fiber-Reinforced Composite Materials," *McGraw-Hill*, 1998, 276-327.
30. Jones, R.M., "Mechanics of Composite Materials," *Taylor & Francis*, 1975, 152-155.
31. Kuo, B.C., "Automatic Control Systems," *Prentice-Hall*, 1982, 471-479.
32. Logan, D.L., "A First Course in the Finite Element Method (3rd Edition)," *Brooks & Cole*, 2002, 271-277, 399-405.
33. Zienkiewicz, O.C., and Taylor, R.L., "Finite Element Method (5th Edition) Volume 1 - The Basis," *Elsevier*, 2000, 208-209, 219-220.
34. Bathe, K.J., and Wilson, E.L., "Numerical Methods in Finite Element Analysis," *Prentice-Hall*, 1976, 125-128.

Appendix A – Flow Charts

A-1 Algorithm Flow Chart for Entire Program

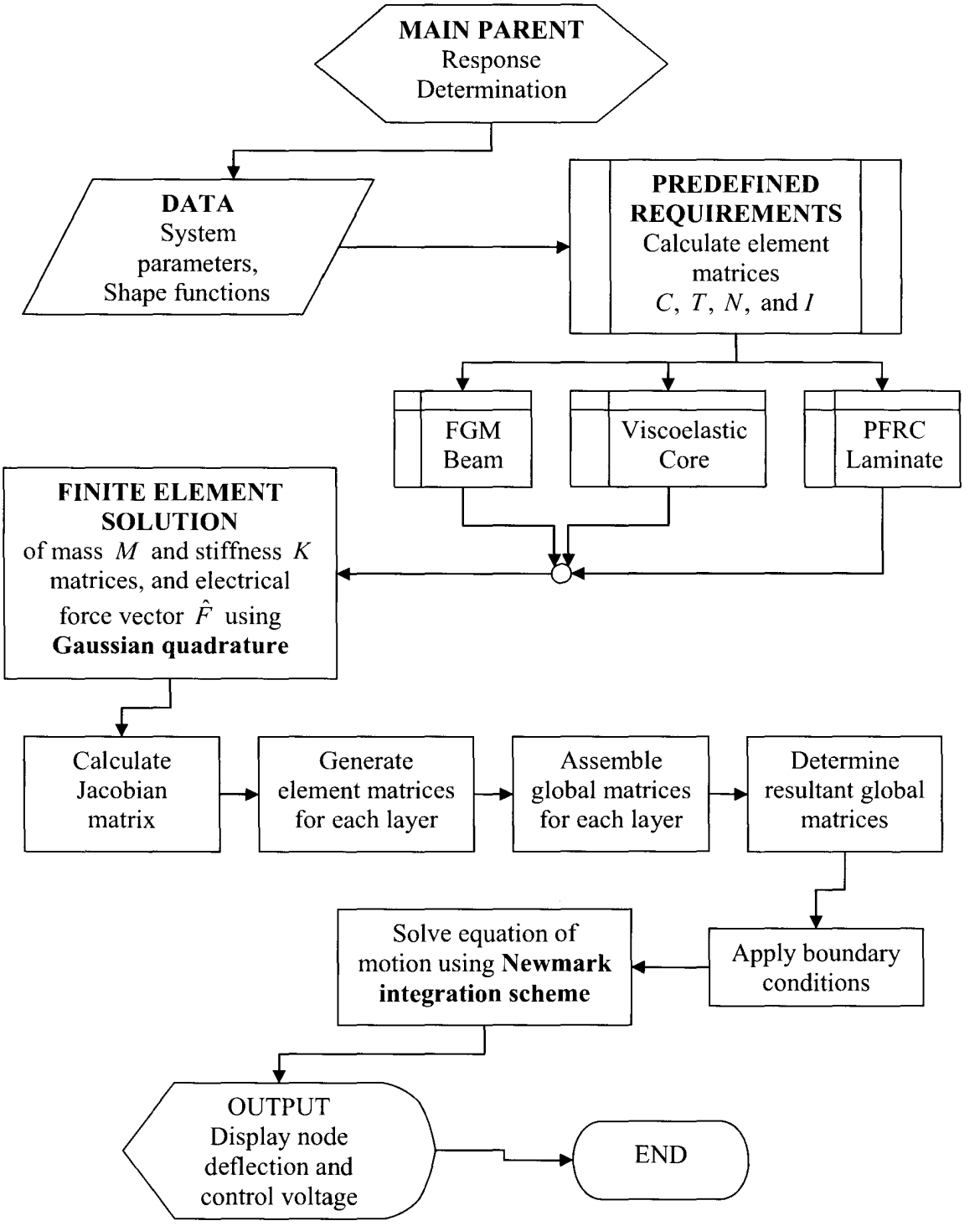

A-2 Algorithm Flow Chart for Newmark Integration Scheme

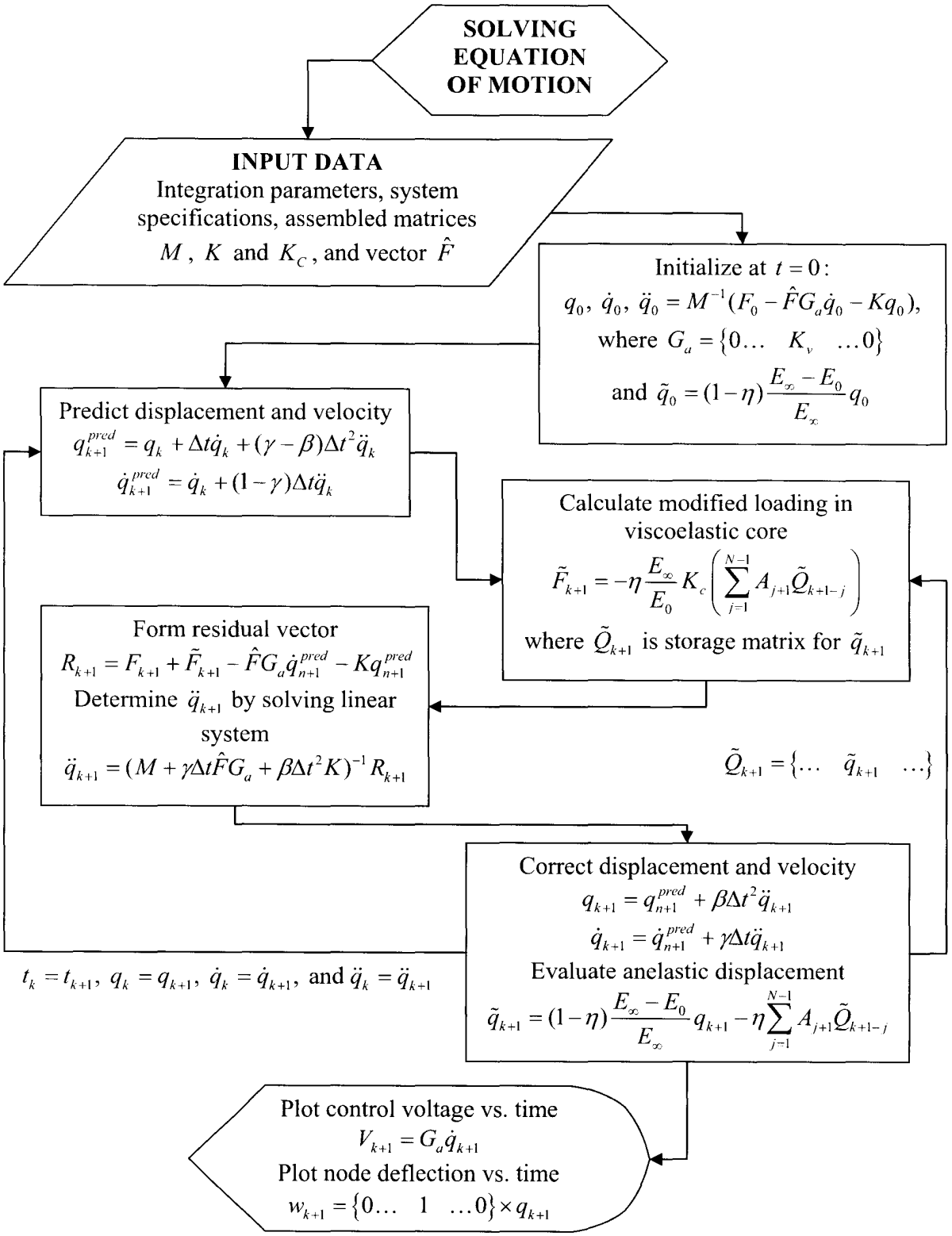

Appendix B – Implementation of Matrix B

To incorporate the derivative operator D into the Matlab code the following adjustments to matrix B are suggested for easier implementation.

For the host beam:

With reference to **Eqs. 3.3** and **3.4**, the strain vector ε_b can be written as:

$$\varepsilon_b = \begin{Bmatrix} \varepsilon_x \\ \varepsilon_z \\ \gamma_{xz} \end{Bmatrix} = \begin{bmatrix} 0 & 0 & 0 & 1 & z & z^2 & z^3 & 0 & 0 & 0 & 0 & 0 \\ 0 & 0 & 0 & 0 & 0 & 0 & 0 & 1 & 2z & 0 & 0 & 0 \\ 1 & 2z & 3z^2 & 0 & 0 & 0 & 0 & 0 & 0 & 1 & z & z^2 \end{bmatrix} \begin{Bmatrix} a_1 \\ a_2 \\ a_3 \\ a_{0,x} \\ a_{1,x} \\ a_{2,x} \\ a_{3,x} \\ l_1 \\ l_2 \\ l_{0,x} \\ l_{1,x} \\ l_{2,x} \end{Bmatrix} \qquad \textbf{[B - 1]}$$

This permits the partitioning of the derivative operator $[D_b]$ as follows:

$$[D_b] = \begin{bmatrix} \boxed{\begin{matrix} 0 & 1 & 0 & 0 \\ 0 & 0 & 1 & 0 \\ 0 & 0 & 0 & 1 \end{matrix}} & \begin{matrix} 0 & 0 & 0 \\ 0 & 0 & 0 \\ 0 & 0 & 0 \end{matrix} \\ \boxed{\begin{matrix} \partial/\partial x & 0 & 0 & 0 \\ 0 & \partial/\partial x & 0 & 0 \\ 0 & 0 & \partial/\partial x & 0 \\ 0 & 0 & 0 & \partial/\partial x \end{matrix}} & \begin{matrix} 0 & 0 & 0 \\ 0 & 0 & 0 \\ 0 & 0 & 0 \\ 0 & 0 & 0 \end{matrix} \\ \begin{matrix} 0 & 0 & 0 & 0 \\ 0 & 0 & 0 & 0 \end{matrix} & \boxed{\begin{matrix} 0 & 1 & 0 \\ 0 & 0 & 1 \end{matrix}} \\ \begin{matrix} 0 & 0 & 0 & 0 \\ 0 & 0 & 0 & 0 \\ 0 & 0 & 0 & 0 \end{matrix} & \boxed{\begin{matrix} \partial/\partial x & 0 & 0 \\ 0 & \partial/\partial x & 0 \\ 0 & 0 & \partial/\partial x \end{matrix}} \end{bmatrix} \qquad \textbf{[B - 2]}$$

The through-the-thickness mapping matrix is $[T_b]=\begin{bmatrix}[T_b]_u & [0]\\ [0]^T & [T_b]_w\end{bmatrix}$ from **Eq. 4.8** (where $[0]$ is a 4x3 zero matrix) and the shape functions matrix $[N_{bj}]$ from **Eq. 4.9** can be written as follows:

$$[N_{bj}]=\left[\begin{array}{cccccccccccc} N_{j\xi} & 0 & 0 & 0 & 0 & 0 & 0 & 0 & 0 & 0 & 0 & 0\\ 0 & 0 & N_{j\xi} & 0 & 0 & 0 & 0 & 0 & 0 & 0 & 0 & 0\\ 0 & 0 & 0 & 0 & N_{j\xi} & 0 & 0 & 0 & 0 & 0 & 0 & 0\\ 0 & 0 & 0 & 0 & 0 & N_{j\xi} & 0 & 0 & 0 & 0 & 0 & 0 \end{array}\right]=\begin{bmatrix}[N_{bj}]_u\\ [N_{bj}]_w\end{bmatrix} \quad \textbf{[B - 3]}$$

$$\left[\begin{array}{cccccccccccc} 0 & N_{j\xi} & 0 & 0 & 0 & 0 & 0 & 0 & 0 & 0 & 0 & 0\\ 0 & 0 & 0 & N_{j\xi} & 0 & 0 & 0 & 0 & 0 & 0 & 0 & 0\\ 0 & 0 & 0 & 0 & 0 & 0 & N_{j\xi} & 0 & 0 & 0 & 0 & 0 \end{array}\right]$$

where $j=1\ldots4$.

Since the matrix $[T_b]$ is not a function of x, the derivative components of operator $[D_b]$ do not affect the matrix $[T_b]$. Hence, combining **Eqs. [B - 2]** and **[B - 3]** for an element yields the newly formulated matrix $[B_b]$ of **Eq. 4.12** with implemented operator $[D_b]$ components:

$$[B_b]=\begin{bmatrix}\begin{bmatrix}0 & 1 & 0 & 0\\ 0 & 0 & 1 & 0\\ 0 & 0 & 0 & 1\end{bmatrix}[T_b]_u[N_b]_u\\ [T_b]_u\dfrac{\partial[N_b]_u}{\partial x}\\ \begin{bmatrix}0 & 1 & 0\\ 0 & 0 & 1\end{bmatrix}[T_b]_w[N_b]_w\\ [T_b]_w\dfrac{\partial[N_b]_w}{\partial x}\end{bmatrix} \quad \textbf{[B - 4]}$$

The matrix $[B_c]$ for the core is formulated in the same manner as for the host beam, given that the axial and transverse displacements are also expressed through the thickness by cubic and quadratic functions, respectively.

For the top layer:

The local displacement vector $\{\bar{u}_p\}$ is rearranged in such a way as to obtain modified derivative operator matrices $[D_p^0]$ and $[D_p^1]$. Consequently, the displacement vector can be written as:

$$u_p = \begin{bmatrix} 1 & 0 & z \\ 0 & 1 & 0 \end{bmatrix} \begin{Bmatrix} e_0 \\ n_0 \\ e_1 \end{Bmatrix} \equiv [Z_p]\{\bar{u}_p\} \qquad \textbf{[B – 5]}$$

In accordance with **Eq. 3.44**, the derivative operator matrices can be combined and partitioned in the following way:

$$\begin{bmatrix} D_p^0 \\ D_p^1 \end{bmatrix} = \left[\begin{array}{ccc} \hat{\partial}/\partial\hat{x} & 0 & 0 \\ 0 & \hat{\partial}/\partial\hat{x} & 1 \\ \hline 0 & 0 & \hat{\partial}/\partial\hat{x} \\ 0 & 0 & 0 \end{array}\right] = \left[\begin{bmatrix} \hat{\partial}/\partial\hat{x} & 0 & 0 \\ 0 & \hat{\partial}/\partial\hat{x} & 0 \\ 0 & 0 & \hat{\partial}/\partial\hat{x} \end{bmatrix} + \begin{bmatrix} 0 & 0 & 0 \\ 0 & 0 & 1 \\ 0 & 0 & 0 \end{bmatrix}\right] \qquad \textbf{[B – 6]}$$

$$[0 \quad 0 \quad 0]$$

The mapping matrix $[T_p]$ from **Eq. 4.27** is also adjusted in agreement with the local displacement vector change and is given as:

$$[T_p] = \begin{bmatrix} 1 & 0 & h_9 \\ 0 & 1 & 0 \\ 1 & 0 & h_{10} \end{bmatrix}^{-1} \qquad \textbf{[B – 7]}$$

As mentioned previously for the host beam, the matrix $\left[T_p\right]$ does not depend on the variable x. Hence, using **Eqs. [B – 6]** and **[B – 7]** with addition of the shape functions matrix $\left[N_p\right]$ from **Eq. 4.28**, the modified matrix $\left[B_p\right]$ from **Eq. 4.31** is as follows for the PFRC layer:

$$\left[B_p\right]=\begin{bmatrix}\left[T_p\right]\dfrac{\partial\left[N_p\right]}{\partial x}+\begin{bmatrix}0&0&0\\0&0&1\\0&0&0\end{bmatrix}\left[T_p\right]\left[N_p\right]\\ \left[0\quad 0\quad 0\right]\left[T_p\right]\left[N_p\right]\end{bmatrix} \qquad \textbf{[B – 8]}$$

Appendix C – Matlab Codes

C-1 Main File

Main file collects information about system parameters, as well as matrices required for determination of mass and stiffness matrices for host beam, viscoelastic core, and PFRC laminate. Then, this program uses a numerical integration function to calculate global mass and stiffness matrices. Global resultant matrices are attained and boundary conditions are applied. The code below features the cantilevered fully-clamped boundary conditions only. Main code also solves the governing equation using the Newmark integration method and plots the transverse displacement of a node and control voltage required for actuation.

main_file.m

```
clear all
%----------------------------Determination of mass (M)-----------------------------------------------------%
%----------------------------and stiffness  (K) matrices---------------------------------------------------%

global F_ext n DOF Theta ply b rho_b rho_c rho_p lambda  % global variables

shape_functions(0);  % introduces shape functions for the beam
system_parameters(0);  % outlines beam's parameters for all three layers

%----------------------------FGM Host Beam (Bottom Layer)---------------------------------------------------%

global Cb Tb_u Tb_w Nb_u Nb_w Ib  % element matrices

host_beam(0);  % returns C_b, T_b, I_b and N_b matrices
boolean=0;
[Mb_temp,Kb_temp,dummy]=num_integration(Nb_u,Nb_w,Tb_u,Tb_w,Ib,Cb,0,boolean);

Mb=rho_b.*b*Mb_temp;  % Mass matrix of the host beam
Kb=b*Kb_temp;   % Stiffness matrix of the host beam

%----------------------------Viscoelastic Layer (Core)-----------------------------------------------------%

global Cc Tc_u Tc_w Nc_u Nc_w Ic eta E_inf E_0  % element matrices

viscoelastic_core(0);  % returns C_c, T_c, I_c and N_c matrices
boolean=0;
[Mc_temp,Kc_temp,dummy]=num_integration(Nc_u,Nc_w,Tc_u,Tc_w,Ic,Cc,0,boolean);

Mc=rho_c.*b*Mc_temp;   % Mass matrix of the viscoelastic layer
Kc=b*Kc_temp;   % Stiffness matrix of elastic portion of the core
K_c=(eta.*(E_inf-E_0)./E_0)*Kc;  % Stiffness matrix of anelastic portion of the core
```

```
%-----------------------------PFRC Laminate (Top Layer)-----------------------------------------------%

global ABD NM Tp Np Ip  % element matrices

piezo_laminate(0); % returns ABD, N_xp, M_xp, T_p, I_p and N_p matrices
boolean=1;
[Mp_temp,Kp_temp,Fp_temp]=num_integration(Np,0,Tp,0,Ip,ABD,NM,boolean);

Mp=rho_p.*b*Mp_temp;   % Mass matrix of the piezoelectric laminate
Kp=b*Kp_temp;   %Stiffness matrix of the piezoelectric laminate
Fp=b*Fp_temp;  % Electric force caused by the applied electrical field E_z

%-----------------------------Global resultant matrices-----------------------------------------------%

M=Mb+Mc+Mp;  % resultant mass matrix
K=Kb+Kc+K_c+Kp;  % resultant stiffness matrix

%-------------------------Boundary conditions (cantilevered fully-clamped)-------------------------%

M(:,1:DOF)=[]; % deleting column 1 to 13 of the mass matrix
K(:,1:DOF)=[]; % deleting column 1 to 13 of the stiffness matrix
Kc(:,1:DOF)=[]; % deleting column 1 to 13 of the core elastic stiffness matrix
M(1:DOF,:)=[]; % deleting row 1 to 13 of the mass matrix
K(1:DOF,:)=[]; % deleting row 1 to 13 of the stiffness matrix
Kc(1:DOF,:)=[]; % deleting row 1 to 13 of the core elastic stiffness matrix

F_ext(1:DOF)=[]; % deleting row 1 to 13 of the external force vector
Fp(1:DOF)=[]; % deleting row 1 to 13 of the electrical force vector

sprintf('Natural frequencies with %d elements and %d ply(ies) used; lambda=%d',n,ply,lambda)
freq=sort(sqrt(eig(K,M))/(2*pi));
fprintf(1,'%6.0f\n',freq(1:10));
disp(' ');


%-----------------------------Solving the governing equation-----------------------------------------%
%-----------------------------using Newmark integration scheme---------------------------------------%

global Kv N alpha dt

Hw = subs([zeros(1,39) zeros(1,6) 1 zeros(1,6)]); % specifies node w_54
w(1)=0;

Ga=zeros(1,3*DOF*n);
Ga(1,3*DOF*n-6)=Kv; % assigns gain value of K_v to node w_54 in the last element

% initializing displacement, velocity and acceleration, respectively, at t=0
t=0;
q=zeros(3*DOF*n,1);
q_vel=zeros(3*DOF*n,1);
q_accel=inv(M)*(F_ext-Fp*Ga*q_vel-K*q); % isolates q_accel in a governing equation
```

```
% anelastic displacement at t=0
q_=(1-eta)*((E_inf-E_0)/E_inf)*q;

Q_=zeros(3*DOF*n,N);  % storage matrix of the anelastic displacement history
Q_(:,1)=q_; % stores initial q_ vector as a column in the matrix Q_

% integration parameters
gamma=0.5;
beta=0.25*(0.5+gamma)^2;

A(1) = 1;

for k=1:N  % counts number of terms
   t=t+dt;

   % chooses load type
   F_ext=load_type(1,t);  % 1- impulse load; 2-impact load; 3-harmonic load;

   % predicts displacement and velocity
   q_pred=q+dt*q_vel+(gamma-beta)*dt^2*q_accel;
   q_vel_pred=q_vel+(1-gamma)*dt*q_accel;

   % calculates the modified loading in the viscoelastic core
   sum=0;

   for j = 1:N-1
      A(j+1) = ((j-alpha-1)/j)*A(j);
      if (k+1-j) > 0 % truncation terms
         sum = sum + A(j+1)*Q_(:,k+1-j);
      else
         break
      end
   end

   F_c=-eta*(E_inf/E_0)*Kc*sum; % loads in the core

   R=F_ext+F_c-Fp*Ga*q_vel_pred-K*q_pred;  % forms residual
   q_accel=(M+(0.5*Fp*Ga)*dt+beta*dt^2*K)\R;  % evaluates acceleration by solving linear system

   % corrects displacement and velocity
   q=q_pred+beta*dt^2*q_accel;
   q_vel=q_vel_pred+gamma*dt*q_accel;

   % evaluates and stores the anelastic displacement history
   q_=(1-eta)*((E_inf-E_0)/E_inf)*q-eta*sum;
   Q_(:,k+1)=q_; % stores every q_ vector as a column in the matrix Q_

   voltage(k+1) = Ga*q_vel; % calculates voltage by multiplying velocity with gain control
   w(k+1) = Hw*q(3*DOF*n-51:3*DOF*n,1)*1e+3; % determines transverse displacement of the node w54
in the last element

end
```

```
%--------------------------------Results-----------------------------------------------------------------%
%--------------------------------------------------------------------------------------------------------%

T=[0:dt:N*dt];
figure;plot(T(1:1:N),10*w(1:1:N),'-b') % plots transverse displacement node w54 in the last element
axis([0,1,-6,6.5]);
xlabel('Time (s)'); ylabel('Tip Deflection (e-1 mm)');
legend('Cantilevered fully-clamped',1);
title('[0°/0°/0°/0°/0°/0°]');
hold on

figure;plot(T(1:1:N),voltage(1:1:N),'-r') % plots control voltage node w54 in the last element
axis([0,1,-60,60]);
xlabel('Time (s)'); ylabel('Control Voltage (V)');
legend('Cantilevered fully-clamped',1);
title('[0°/0°/0°/0°/0°/0°]');grid off
hold on
```

C-2 Introduction of Parameters and General Functions

shape_functions.m

```
% This function introduces cubic Lagrange interpolation shape functions

function shape_functions(dummy)
global xi Nxi
syms xi  % global variable xi

Nxi=[-(3*xi+1)*(3*xi-1)*(xi-1)/16;
   9*(xi+1)*(3*xi-1)*(xi-1)/16;
   -9*(xi+1)*(3*xi+1)*(xi-1)/16;
   (xi+1)*(3*xi+1)*(3*xi-1)/16];

return
```

system_parameters.m

```
% This function stores parameters of the beam

function system_parameters(dummy)
global L b Eb_0 Ec E_0 E_inf vb vc rho_b rho_c rho_p scf eta N dt alpha
global h h1 h2 h3 h4 h5 h6 h7 h8 h9 h10 hp hb hc Kv lambda

syms z
N = 1000; t = 1; dt = t/N;  % time parameters, time step dt

%-----------------FGM Host Beam (Bottom Layer)-----------------%

L = 300e-3; b = 15e-3; hb = 3.75e-3;  % geometrical parameters
Eb_avg = 70.3e+9; vb = 0.345; rho_b = 2690; scf = 5/6;  % mechanical characteristics
(aluminum)
lambda=0; % functional gradient (lambda=ln(Eh/E0)/hb)
```

```
%------------------Viscoelastic Layer (Core)-----------------------%

Lc = 100e-3; hc = 0.25e-3; % geometrical parameters
%-------elastic properties--------%
Ec=1.5e+6;  vc = 0.499;
%--------viscoelastic properties---------%
E_0 = Ec; E_inf = 69.9495e+6; rho_c = 1600;  % mechanical characteristics
tau = 1.4052e-5; alpha = 0.7915; eta = tau^alpha/(tau^alpha+dt^alpha); % anelastic characteristics

%----------------------PFRC Laminate (Top Layer)-----------------%

Lp = 100e-3; hp = 1e-3; % geometrical parameters
Kv=350; %feedback control gain
rho_p=3640; % PFRC

%-------------------------Z-Coordinates--------------------------------%

h=hb+hc+hp;
% positions relative to geometric mid-surface of h
h1=-h/2; h2=hb/4-h/2; h3=hb/2-h/2; h4=3*hb/4-h/2; h5=hb-h/2;  % FGM beam
h5; h6=hb+hc/4-h/2; h7=hb+hc/2-h/2; h8=hb+3*hc/4-h/2; h9=hb+hc-h/2;  % viscoelastic core
h9; h10=h/2;  % PFRC-laminate layer

% E_b at the bottom of the beam found from the averaged E_b
Eb_0=eval(Eb_avg*hb/(exp(lambda*h/2)*int(exp(lambda*z),z,h1,h5)));
% E_b at the top of the FGM layer
Eb_h=Eb_0*exp(lambda*hb);
```

cubic_interpolation.m

```
% This function returns reference displacement matrices Z and Z_(bar)

function [Z,Z_]=cubic_interpolation(dummy)
global z

syms z
Z=[1 z z^2 z^3 0 0 0;0 0 0 0 1 z z^2];
Z_=[0 0 0 1 z z^2 z^3 0 0 0 0 0;0 0 0 0 0 0 0 1 2*z 0 0 0;1 2*z 3*z^2 0 0 0 0 0 0 1 z z^2];
```

kinetic_energy.m

```
% This function accepts the input of Z matrix and the limits of integration and returns matrix I for each
layer

function I=kinetic_energy(Z,z1,z2)
global z

I=eval(int(transpose(Z)*Z,z1,z2));
```

C-3 Functions for Calculation of Elemental Matrices in each Layer

host_beam.m

```
% This function calculates the constitutive, mapping and interpolation matrices of the FGM host beam

function host_beam(dummy)
global Eb_0 vb scf h h1 h2 h3 h4 h5 Cb Tb_u Tb_w Nb_u Nb_w Nb5_u Nb5_w Ib Nxi xi lambda

syms z
%----------------------kinematic assumptions----------------------%
[Zb,Z_b]=cubic_interpolation(0);

%----------------------constitutive equations---------------------%
% Determines compliance matrix C_b for FGM

Cb_0=(Eb_0./(1+vb)./(1-2*vb)).*[1-vb vb 0;vb 1-vb 0;0 0 (1-2*vb)./2];  % plane strain assumption
Qb=exp(lambda*h/2)*Cb_0; % elastic coefficients vary exponentially
Cb=eval(int((transpose(Z_b)*Qb*Z_b)*exp(lambda*z),h1,h5));  % integrates from h1 to h5 through the
host beam's thickness

%--------------------------mapping----------------------------------%
Tb_u=[1 h1 h1^2 h1^3;1 h2 h2^2 h2^3;1 h4 h4^2 h4^3;1 h5 h5^2 h5^3]^(-1);  % axial displacement
Tb_w=[1 h1 h1^2;1 h3 h3^2;1 h5 h5^2]^(-1);  % transverse displacement

%-------------------------shape functions---------------------------%
for i=1:4

   % Determines N_b matrix for each shape function
   Nbi_u=[Nxi(i) 0 0 0 0 0;0 0 Nxi(i) 0 0 0;0 0 0 0 Nxi(i) 0;0 0 0 0 0 Nxi(i)];
   Nbi_w=[0 Nxi(i) 0 0 0 0 0;0 0 0 Nxi(i) 0 0 0;0 0 0 0 0 0 Nxi(i)];
   Nb_u=[Nbi_u zeros(4,7)];
   Nb_w=[Nbi_w zeros(3,6)];

  if i==1
     Nb1_u=Nb_u; Nb1_w=Nb_w;
  elseif i==2
       Nb2_u=Nb_u; Nb2_w=Nb_w;
    elseif i==3
         Nb3_u=Nb_u; Nb3_w=Nb_w;
      elseif i==4
          Nb4_u=Nb_u; Nb4_w=Nb_w;
        end
end
% allocates shape functions in the final N_b matrix
Nb_u=[Nb1_u Nb2_u Nb3_u Nb4_u];
Nb_w=[Nb1_w Nb2_w Nb3_w Nb4_w];

Ib=kinetic_energy(Zb,h1,h5);  % moment of inertia

return
```

viscoelastic_core.m

```
% This function determines constitutive, mapping, and interpolation matrices of the viscoelastic core

function viscoelastic_core(dummy)
global Ec vc h5 h6 h7 h8 h9 eta E_inf E_0 Cc Tc_u Tc_w Nc_u Nc_w Ic Nxi xi

syms z
%----------------------kinematic assumptions-------------------------%
[Zc,Z_c]=cubic_interpolation(0);

%-----------------------constitutive equations-----------------------%

elastic properties
qtype = 1; % 0-plane stress 1-plane strain
if qtype == 1  % elastic coefficients under plane strain assumption
   c11=(1-vc)*Ec/(1-2*vc)/(1+vc);
   c13=vc*Ec/(1-2*vc)/(1+vc);
else  % elastic coefficients under plane stress assumption
   c11 = Ec/(1-vc^2);
   c13 = vc*Ec/(1-vc^2);
end
c33=c11;
c55=Ec/(2*(1+vc));
Qc=[c11 c13 0;c13 c33 0;0 0 c55];  % constitutive relation
Cc=eval(int(transpose(Z_c)*Qc*Z_c,h5,h9));  % elastic compliance matrix of the core

%-------------------------mapping---------------------------------------%
Tc_u=[1 h5 h5^2 h5^3;1 h6 h6^2 h6^3;1 h8 h8^2 h8^3;1 h9 h9^2 h9^3]^(-1);  % axial displacement
Tc_w=[1 h5 h5^2;1 h7 h7^2;1 h9 h9^2]^(-1);  % transverse displacement

%-------------------------shape functions-------------------------------%
for i=1:4
   % Determines N_c matrix for each shape function
   Nci_u=[Nxi(i) 0 0 0 0 0;0 0 Nxi(i) 0 0 0;0 0 0 0 Nxi(i) 0;0 0 0 0 0 Nxi(i)];
   Nci_w=[Nxi(i) 0 0 0 0 0;0 0 Nxi(i) 0 0 0;0 0 0 0 0 Nxi(i)];
   Nc_u=[zeros(4,5) Nci_u zeros(4,2)];
   Nc_w=[zeros(3,6) Nci_w zeros(3,1)];

  if i==1
     Nc1_u=Nc_u; Nc1_w=Nc_w;
  elseif i==2
        Nc2_u=Nc_u; Nc2_w=Nc_w;
     elseif i==3
          Nc3_u=Nc_u; Nc3_w=Nc_w;
        elseif i==4
           Nc4_u=Nc_u; Nc4_w=Nc_w;
          end
end
% allocates shape functions in the final N_c matrix
Nc_u=[Nc1_u Nc2_u Nc3_u Nc4_u];
Nc_w=[Nc1_w Nc2_w Nc3_w Nc4_w];

Ic=kinetic_energy(Zc,h5,h9);  % moment of inertia
return
```

piezo_laminate.m

```
% This function returns constitutive, mapping and interpolation matrices of the PFRC laminate

function piezo_laminate(dummy)
global hp h h9 h10 Tp Nxp Mxp NM ABD Np Ip Nxi xi ply Theta scf Eb_0 vb
syms c13 c23 c33
syms z m d

% PZT5H and epoxy combined properties of fiber-reinforced matrix layer
c11=32.6e+9; c12=4.3e+9; c22=7.2e+9; c44=1.05e+9; c55=1.29e+9; c66=c55;  % mechanical
characteristics
e31=-6.76; % electric constant

V=1; % initial value of voltage
Ez=V/hp; % electric field

ply=6;  % determines number of plies in the laminate
if ply==3
   Theta=[0 pi 0];  % symmetric cross-ply laminate
   z_=[-hp/6 hp/6 hp/2];
elseif ply==4
%    Theta=[0 0 0 0];  % symmetric cross-ply laminate
   Theta=[pi/6 pi/3 pi/3 pi/6];
   z_=[-hp/4 0 hp/4 hp/2];
elseif ply==6
%    Theta=[0 pi/2 -pi/2 -pi/2 pi/2 0]; % symmetric cross-ply laminate
%    Theta=[0 pi/3 -pi/3 -pi/3 pi/3 0];
%    Theta=[0 pi/4 -pi/4 -pi/4 pi/4 0];
   Theta=[0 0 0 0 0 0];
   z_=[-hp/3 -hp/6 0 hp/6 hp/3 hp/2];
end

zk=z_+(h-hp)/2;

%--------------------------kinematic assumptions---------------------%
Zp=[1 0 z;0 1 0]; % modified from formulation in order to rearrange the derivative operators for the top
layer only

%-------------------------constitutive equations-------------------------%
A=0; B=0; D=0; Nxp=0; Mxp=0;
z_0=-hp/2;
z0=z_0+(h-hp)/2;

for k=1:ply

   %-----------------------mechanical-----------------------------------%

   % constitutive relation of the k layer in the laminate
   Cp=[c11 c12 c13 0 0 0;c12 c22 c23 0 0 0;c13 c23 c33 0 0 0;0 0 0 c44 0 0;0 0 0 0 c55 0;0 0 0 0 0 c66];
   R=[1 0 0 0 0 0;0 1 0 0 0 0;0 0 1 0 0 0;0 0 0 2 0 0;0 0 0 0 2 0;0 0 0 0 0 2];

   % transformation matrix from principal to global coordinates through a
```

```
   % counterclockwise rotation Theta about z-axis
   T=[m^2 d^2 0 0 0 2*d*m;d^2 m^2 0 0 0 -2*d*m;0 0 1 0 0 0;0 0 0 m -d 0;0 0 0 d m 0;-d*m d*m 0 0 0
m^2-d^2];
   Qp=simple(T^(-1)*Cp*R*T*R^(-1));
   Qp=subs(Qp,(d^2+m^2),1);  % cos(Theta)^2+sin(Theta)^2=1
   Qp=subs(Qp,{m,d},{cos(Theta(k)),sin(Theta(k))});

   % transformed stiffness constants
   Q11=Qp(1,1); Q12=Qp(1,2); Q16=Qp(1,6); Q22=Qp(2,2); Q26=Qp(2,6);
   Q44=Qp(4,4); Q45=Qp(4,5); Q55=Qp(5,5); Q66=Qp(6,6);

   % transformed and reduced stiffness constants
   Q_11=Q11 + (Q16*Q26-Q12*Q66)/(Q22*Q66-Q26^2)*Q12 + (Q12*Q26-Q16*Q22)/(Q22*Q66-
Q26^2)*Q16;
   Q_55=Q55-Q45^2/Q44;
   Qp_k=eval([Q_11 0;0 scf*Q_55]);  % transformed reduced constitutive matrix

   %----------------------------electrical-------------------------------------%
   e_31=eval((1-(Q12*Q66-Q16*Q26)/(Q22*Q66-Q26^2))*e31);

   % Determination of resultant stiffness matrices
   A=A+(zk(k)-z0)*Qp_k;
   B=B+(zk(k)^2-z0^2)*Qp_k;
   D=D+(zk(k)^3-z0^3)*Qp_k;
   Nxp=Nxp+(zk(k)-z0)*(e_31*Ez);
   Mxp=Mxp+(zk(k)^2-z0^2)*(e_31*Ez);
   z0=zk(k);
end

B=(1/2)*B;
D=(1/3)*D;
Mxp=(1/2)*Mxp;
ABD=[A B; B D];  % ABD matrix of the PFRC laminate
NM=[Nxp 0 Mxp 0];  % Resultant electric force stiffness vector

%-----------------------------mapping-----------------------------------%
Tp=[1 0 h9;0 1 0;1 0 h10]^(-1);  % transformation through the thickness
% modified from formulation in order to rearrange the derivative operators for the top layer only

%----------------------------shape functions----------------------------%
for i=1:4
   % Determines N_p matrix for each shape function
   Npi=[Nxi(i) 0 0;0 Nxi(i) 0;0 0 Nxi(i)];
   Np=[zeros(3,10) Npi];

  if i==1
     Np1=Np;
  elseif i==2
        Np2=Np;
     elseif i==3
           Np3=Np;
        elseif i==4
             Np4=Np;
           end
```

```
end
Np=[Np1 Np2 Np3 Np4];  % allocates shape functions in the final N_p matrix

Ip=kinetic_energy(Zp,h9,h10);  % moment of inertia

return
```

C-4 Numerical Integration Function

num_integration.m

```
% This function uses gauss quadrature to calculate the Jacobian and numerically integrate mass and
stiffness matrices

% It also outputs electric force vector for the PFRC laminate layer only

function [M,K,Fp]=num_integration(Nu,Nw,Tu,Tw,I,C,NMp,boolean)
global Nxi xi L DOF F_ext n

syms xi
%------------------Defining the number of elements-----------------%
n=5;  % number of elements
Le=L/n;  % element length
DOF=13;  % degrees of freedom per node

%---------------------Setting parameters-------------------------------%
p=0;  % counter for each element increment
M=zeros(DOF*(3*n+1),DOF*(3*n+1));  % allocating space for mass matrix
K=zeros(DOF*(3*n+1),DOF*(3*n+1));  % allocating space for stiffness matrix
Fp=zeros(DOF*(3*n+1),1);  % allocating space for electrical force vector
F_ext=zeros(DOF*(3*n+1),1);  % allocating space for external force vector

if boolean==1  % if the input matrices are of the PFRC laminate
   N_temp=Nu; T=Tu;
   dNdxi=diff(N_temp,xi);  % takes derivative of N with respect to xi

else  % input matrices of the host beam or visco core
   N_temp=[Nu;Nw];
   O=zeros(4,3);
   T=[Tu O; O' Tw];  % combined transformation through the thickness matrix
end

%-----------------------Gauss Quadrature-----------------------------%
for element=1:n

   % four positions located along the span distance Le of each element according to xi values at {-1 -1/3 1/3
1}
   x1=(element-1)*Le; x2=x1+Le/3; x3=x2+Le/3; x4=x3+Le/3;
   xs=[x1;x2;x3;x4];
   jx=transpose(Nxi)*xs;
   djxdxi=diff(jx,xi);  % (dN_xi/d_xi)*x, calculates the jacobian at each node

   Npts=4;
```

```
guasspts=zeros(Npts,1); wghts=zeros(Npts,1);

%-------------------------Gauss points-----------------------------%
guasspts(1)=-0.861136311594953; wghts(1)=0.347854845137454;
guasspts(2)=-0.339981043584856; wghts(2)=0.652145154862546;
guasspts(3)=0.339981043584856; wghts(3)=0.652145154862546;
guasspts(4)=0.861136311594953; wghts(4)=0.347854845137454;

Msum=0; Ksum=0; Fpsum=0;

for gp=1:Npts

   cxi=guasspts(gp);
   J=subs(djxdxi,xi,cxi); % takes the jacobian at each node and replaces it with gauss points
   N_m=subs(N_temp,xi,cxi);

   M_temp=N_m'*T'*I*T*N_m;
   Msum=Msum+wghts(gp)*M_temp*abs(J);  % numerically integrates mass matrix including the
jacobian

   if boolean==1  % if the input matrices are of the PFRC laminate
      dN=subs(dNdxi,xi,cxi)*inv(J);  % converts dN_xi/d_x to dN_xi/d_xi

       B=[T*dN+[0 0 0;0 0 1;0 0 0]*T*N_m; zeros(1,3)*T*N_m]; % incorporates derivative operators
into the B matrix; hence, the modified kinematic assumptions and mapping matrices with respect to
original formulations

      Fp_temp=B'*NMp';
      Fpsum=Fpsum+wghts(gp)*Fp_temp*abs(J);  % numerically integrates electric force vector
including the jacobian

   else  % input matrices of the host beam or visco core
      dNu=subs(diff(Nu,xi),xi,cxi)*inv(J);  % converts dN_xi/d_x to dN_xi/d_xi
      dNw=subs(diff(Nw,xi),xi,cxi)*inv(J);  % converts dN_xi/d_x to dN_xi/d_xi
      Nu_temp=subs(Nu,xi,cxi); Nw_temp=subs(Nw,xi,cxi);

      B=[[0 1 0 0;0 0 1 0;0 0 0 1]*Tu*Nu_temp; Tu*dNu; [0 1 0;0 0 1]*Tw*Nw_temp; Tw*dNw];
        % incorporates derivative operator into the B matrix without modification of kinematic
        assumptions and mapping matrices with respect to original formulations
   end

   K_temp=B'*C*B;
   Ksum=Ksum+wghts(gp)*K_temp*abs(J);  % numerically integrates stiffness matrix including the
jacobian

end

%---------------------Determines global matrices---------------------%

for k=1:4*DOF
   for j=1:4*DOF
      M(k+p,j+p)=M(k+p,j+p)+Msum(k,j);
      K(k+p,j+p)=K(k+p,j+p)+Ksum(k,j);
```

```
      end
      if boolean==1
        Fp(k+p,1)=Fp(k+p,1)+Fpsum(k,1);
      end
    end

  p=p+3*DOF; % element increment in terms of DOF
end % end of element loop
```

C-5 Load Function

load_type.m

```
% This function chooses loadtype

function F_ext=load_type(loadtype,t)
global F_ext DOF n
% load is applied to the transverse displacement node w94 in the last element
  if loadtype == 1  % impulse load
    if t <= 2e-3
      F_ext(3*DOF*n-1,1) = 500*t;
    else
      if t <= 4e-3
        F_ext(3*DOF*n-1,1) = -500*t + 2;
      else
        F_ext(3*DOF*n-1,1) = 0;
      end
    end
  else
    if loadtype == 2  % impact load
      if t <= 1e-3
        F_ext(3*DOF*n-1,1) = 1;
      else
        F_ext(3*DOF*n-1,1) = 0;
      end
    else  % harmonic load
      if t <= 41.8888e-3
        F_ext(3*DOF*n-1,1) = 0.1*sin(150*t); % initial harmonic load
      else
        F_ext(3*DOF*n-1,1) = 0*0.1*sin(150*t); % constant zero or harmonic load
      end
    end
  end

  return
```